Reservoir Methane Monitoring and Mitigation - Little Nerang and Hinze Dam Case Study

Bradford Sherman, Phillip Ford, Danny Hunt and Chris Drury

November 2012

Urban Water Security Research Alliance
Technical Report No. 96

Queensland Government
National Research FLAGSHIPS Water for a Healthy Country
CSIRO
Griffith UNIVERSITY
The University Of Queensland AUSTRALIA

Urban Water Security Research Alliance Technical Report ISSN 1836-5566 (Online)
Urban Water Security Research Alliance Technical Report ISSN 1836-5558 (Print)

The Urban Water Security Research Alliance (UWSRA) is a $50 million partnership over five years between the Queensland Government, CSIRO's Water for a Healthy Country Flagship, Griffith University and The University of Queensland. The Alliance has been formed to address South East Queensland's emerging urban water issues with a focus on water security and recycling. The program will bring new research capacity to South East Queensland tailored to tackling existing and anticipated future issues to inform the implementation of the Water Strategy.

For more information about the:

UWSRA - visit http://www.urbanwateralliance.org.au/
Queensland Government - visit http://www.qld.gov.au/
Water for a Healthy Country Flagship - visit www.csiro.au/org/HealthyCcountry.html
The University of Queensland - visit http://www.uq.edu.au/
Griffith University - visit http://www.griffith.edu.au/

Enquiries should be addressed to:

The Urban Water Security Research Alliance
PO Box 15087
CITY EAST QLD 4002

Ph: 07-3247 3005
Email: Sharon.Wakem@qwc.qld.gov.au

Project Leader – Shiroma Maheepala
CSIRO Land and Water
HIGHETT VIC 3190

Ph: 03-9252 6072
Email: Shiroma.Maheepala@csiro.au

Authors: 1 – CSIRO

Sherman, B., Ford, P., Hunt, D. and Drury, C. (2012). *Reservoir Methane Monitoring and Mitigation - Little Nerang and Hinze Dam Case Study*. Urban Water Security Research Alliance Technical Report No. 96.

Copyright

Disclaimer

Cover Photograph:

Description: Bubble emission of methane at Hinze Dam
Photographer: Bradford Sherman

ACKNOWLEDGEMENTS

This research was undertaken as part of the South East Queensland Urban Water Security Research Alliance, a scientific collaboration between the Queensland Government, CSIRO, The University of Queensland and Griffith University.

Special thanks to the Seqwater rangers (Laurie Fairall and Leigh Brown) and water quality specialists (Deb Gale and James Udy) whose assistance in accessing the reservoirs, storing equipment and collecting data were instrumental to the successful execution of this project. Thanks also to Alistair Grinham (University of Queensland) for sharing data, photos and many useful conversations about Little Nerang Dam.

Thanks are also provided to Michael Bartkow, Seqwater, for his review and comments on this report.

FOREWORD

Water is fundamental to our quality of life, to economic growth and to the environment. With its booming economy and growing population, Australia's South East Queensland (SEQ) region faces increasing pressure on its water resources. These pressures are compounded by the impact of climate variability and accelerating climate change.

The Urban Water Security Research Alliance, through targeted, multidisciplinary research initiatives, has been formed to address the region's emerging urban water issues.

As the largest regionally focused urban water research program in Australia, the Alliance is focused on water security and recycling, but will align research where appropriate with other water research programs such as those of other SEQ water agencies, CSIRO's Water for a Healthy Country National Research Flagship, Water Quality Research Australia, eWater CRC and the Water Services Association of Australia (WSAA).

The Alliance is a partnership between the Queensland Government, CSIRO's Water for a Healthy Country National Research Flagship, The University of Queensland and Griffith University. It brings new research capacity to SEQ, tailored to tackling existing and anticipated future risks, assumptions and uncertainties facing water supply strategy. It is a $50 million partnership over five years.

Alliance research is examining fundamental issues necessary to deliver the region's water needs, including:

- ensuring the reliability and safety of recycled water systems.
- advising on infrastructure and technology for the recycling of wastewater and stormwater.
- building scientific knowledge into the management of health and safety risks in the water supply system.
- increasing community confidence in the future of water supply.

This report is part of a series summarising the output from the Urban Water Security Research Alliance. All reports and additional information about the Alliance can be found at http://www.urbanwateralliance.org.au/about.html.

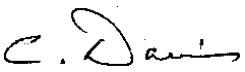

Chris Davis
Chair, Urban Water Security Research Alliance

CONTENTS

LIST OF FIGURES

LIST OF TABLES

EXECUTIVE SUMMARY

Extensive measurements of methane emissions were undertaken at Little Nerang and Hinze Dams during November 2009 - August 2010. A combination of operational issues at the Gold Coast desalination plant and construction work on the outlet tower at Hinze Dam required a significant increase in water abstraction from Little Nerang Dam in June 2010. The resultant drawdown of Little Nerang Dam prevented access to the water and, as a consequence, project field operations were shifted from Little Nerang Dam to Hinze Dam in June 2010 so that the effect of seasonal overturn (complete mixing) of the water column on methane dynamics could be investigated.

This project used, for the first time from a small boat without mains power, a highly sensitive and accurate gas analyser, a Picarro G1301 cavity ringdown spectrometer (CRDS). The project team built all the necessary ancillary hardware based on the floating chamber and air recirculation system designs used by Hydro Quebec and Environment Illimite (Tremblay *et al*. 2005).

A total of 202 flux chamber measurements and 36 vertical profiles of dissolved methane concentrations were collected during the project.

Methane emissions from both dams exhibited high spatial and short-term temporal variability arising from the frequent occurrence of bubble events. Methane emissions from Little Nerang Dam measured during summer, autumn and winter did not exhibit major seasonal variability. Hinze Dam measurements focused mainly on winter 2010 overturn and do not allow any conclusions to be drawn regarding seasonal variability of emissions.

Both reservoirs exhibited strong longitudinal gradients of methane fluxes along arms of the reservoirs that received fresh inputs of sediment and detritus direct from the catchment. Methane fluxes were orders of magnitude greater at the upstream ends of these arms relative to the deeper regions of the reservoirs near the dam walls. Methane fluxes of 100-1,000 mg-CH_4 m^{-2} d^{-1} were routinely observed at the upstream ends of these arms. In contrast, the Little Nerang River arm of Hinze Dam, which receives water and suspended material which have previously passed through Little Nerang Dam, showed no pronounced longitudinal gradient of fluxes.

The areal mean flux[1] of methane from Little Nerang Dam was in the range 61 – 135 mg-CH_4 m^{-2} d^{-1} and for Hinze Dam the range was 28 – 44 mg-CH_4 m^{-2} d^{-1}. Bubble fluxes occurring over a relatively small proportion of each reservoir account for the major part of each reservoir's emission. In Little Nerang Dam, 80% of the total flux was emitted from 10% of the reservoir's surface area. In Hinze Dam 60% of the total flux came from 6% of the total area.

The observed fluxes were consistent with the assumed emissions used by the Life Cycle Analysis project for estimating methane emissions from other water supply reservoirs in SEQ.

Bubble fluxes were frequently so large that they caused the methane concentration in the floating chamber to exceed the gas analyser's maximum limit of detection before the 15-minute deployment period had elapsed. To provide a consistent basis for reporting, the emissions are presented as a range incorporating 'scaled' and 'instantaneous' fluxes. The lower estimates have been scaled from the instantaneous flux measurements by assuming no further emission of methane occurred between the time the gas analyser's maximum limit of detection was exceeded and the end of a 15-minute deployment: they are the absolute minimum value consistent with the measured data. The upper value of the range uses the 'instantaneous' flux values and is equivalent to assuming that the flux would have continued for the duration of a 15-minute deployment at the same rate measured as of the time the gas analyser's maximum limit of detection was exceeded.

[1] The areal mean flux is computed as $\left(\sum_{i=1}^{n} A_i F_i\right) / \sum_{i=1}^{n} A_i$

where F_i is the flux measured at site i and A_i is the surface area represented by site i. n is the total number of measurement sites.

The floating chamber method of measuring air-water gas fluxes is well suited to examining the methane emission process at small spatial and time scales but it has limitations when it comes to estimating fluxes from an entire large reservoir. The method allows direct observation of the effects wind and water turbulence exert on diffusive fluxes of dissolved gases. It also allows examination of emissions arising from individual bubble events. However, the time-consuming nature of a deployment limits the number of sites that can be measured in a day and therefore reduces the ability to resolve spatial gradients in fluxes and quantify responses to meteorological events.

The system proved to be robust in the field but its application in regions with high bubble fluxes was constrained by methane concentrations building up to levels greater than the maximum limit of detection during the nominal 15-minute deployment time. This necessitated development of a conservative calculation procedure for estimating the flux when a deployment was shortened from the normal protocol. Flux calculations presented in this report are the most conservative values consistent with the measured data.

The observed high spatial variability of fluxes, the consistent presence of longitudinal gradients with fluxes increasing upstream in arms receiving fresh catchment organic matter, and the dominant contribution of bubbles to the total reservoir methane flux imply that future methane emission studies:

- Focus on resolving areas of high emission - a logical starting point is to examine those regions expected to receive high catchment organic matter loads
- Quantify and qualify the catchment organic matter load to the reservoir
- Adopt measurement strategies that accommodate the temporal variability of bubble fluxes, e.g.
  - Deploy adequate numbers of bubble traps for sufficient durations to allow discrimination between short-term temporal variability in flux at a site and small-scale spatial variability between sites.
  - Use long-term, continuous floating chamber measurements to build up enough data to establish a probability density function for the occurrence of bubble events.

1. INTRODUCTION

Greenhouse gas (GHG) emissions from reservoirs has been a topic of high interest to the hydropower industry since the 1990's (Anonymous 1996; Fearnside 1995), when the need to quantify the GHG emissions became apparent in order to more objectively evaluate the environmental cost of hydroelectric facilities. In the case of some Amazonian reservoirs, hydroelectric production has been estimated to emit more GHGs than equivalent fossil fuel generation (e.g., Fearnside 2005).

GHG emissions from Australian reservoirs are not well quantified. Sherman *et al*. (2001) presented measurements from Dartmouth and Chaffey Dams that illustrated the wide range of potential emissions. Additional measurements have been made for some hydropower reservoirs in Tasmania and the Snowy Hydro project (Bastien *et al*. 2009, pers. comm.).

As part of the Life Cycle Analysis Project, Hall *et al*. (2009; 2011) estimated that GHG emissions from SEQ water supply reservoirs comprised nearly 45% of total current GHG emissions associated with the urban water supply cycle. This estimate assumed an emission rate of 80 mg-CH_4 m^{-2} d^{-1} based on observations of methane (CH_4) emissions in some SEQ storages (Little Nerang, Wivenhoe, Borumba) by Grinham (pers. comm.). The range of estimates for SEQ storages varied from 1/2 to 10 times this amount.

This report presents results of direct measurements of methane emissions from Little Nerang and Hinze Dams performed between December 2009 and August 2010. The measurements were structured to examine both the spatial and temporal variability of methane emissions.

The focus of this study is on methane emissions because this represents the principal modification to the global warming potential (GWP) arising from the construction of water reservoirs. Emissions of carbon dioxide (CO_2) do not necessarily represent a net greenhouse contribution if one assumes that the origin of the organic carbon is from photosynthesis, i.e. atmospheric CO_2 is converted to organic carbon and subsequently degraded back to CO_2 and CH_4. The high global warming potential of CH_4 (roughly 20 times that of CO_2) means that if just 5% of the organic carbon load is outgassed as CH_4 rather than CO_2, then the global warming impact of the reservoir will double.

2. THEORY - A CONCEPTUAL MODEL OF RESERVOIR GHG EMISSIONS

A basic conceptual model of the important sources, sinks and fluxes of greenhouse gases is shown in Figure 1. Nitrous oxide (N_2O) is not considered here because its contribution from reservoirs to global warming is typically very small compared to carbon dioxide and methane (Tremblay *et al*. 2005).

Most Australian reservoirs more than 6 or 7 m deep are persistently thermally stratified during spring-autumn – absorption of solar radiation in the water column causes the surface waters to warm more than the deep waters. This stratification suppresses vertical transport in the water column to the extent that the interior of most reservoirs are quiescent with effective vertical diffusivities, κ_z, only 10-100 times greater than molecular levels (Sherman *et al*. 2000). A consequence of this stratification is that dissolved oxygen becomes depleted rapidly in deeper waters (the hypolimnion) due to respiratory demands and CO_2 accumulates.

Methane is generated typically within or close to the sediments of a reservoir where anoxic conditions prevail. Organic carbon, supplied from the catchment (allochthonous) and from local production of phytoplankton within the reservoir (autochthonous), is degraded by anaerobic bacteria which release the methane as a by-product of their metabolic processes. As the concentration of dissolved methane increases beyond the solubility limit in water it forms bubbles. The rate at which the bubbles grow in volume depends particularly upon the depth of the water column (hydrostatic pressure) and the local rate of methane generation. Eventually, the bubbles detach and rise through the water column to the surface. As the bubbles rise through the water column they constantly exchange their gases with the surrounding water to approach an equilibrium governed by Henry's Law (McGinnis *et al*. 2006); the bubbles lose methane to the surrounding water where the water is under saturated and the bubbles may gain other dissolved gases such as nitrogen where the water contains relatively higher concentrations of a gas than exists in the bubble.

Because the methane is mainly produced near the bottom of the water column, a dissolved methane concentration gradient results with concentrations in the surface layer typically just a little greater than equilibrium conditions with the atmosphere rising to concentrations up to 1,000 times greater at depth. There is a diffusive flux of dissolved methane along the concentration gradient towards the surface. Typically, one observes very low methane concentrations in the surface layer ([CH4]) because of consumption of methane, largely by aerobic methanotrophic bacteria, that concentrate near the top of the gradient where they receive methane diffusing from below and oxygen supplied from above.

2.1. Carbon Dioxide (CO_2)

CO_2 is produced by oxidation of organic matter by bacteria, both in the water column and (predominantly) the sediments. Respiration by larger organisms is a minor source. The organic carbon is contained in living and dead phytoplankton and macrophytes (autochthonous carbon) produced within the dam, or dissolved and particulate organic material brought in by stream flow and groundwater percolation (allochthonous carbon).

Oxygen is the principal oxidant but different consortia of organic matter-consuming bacteria utilize nitrate, manganese oxides, iron oxides, and sulphate sequentially to produce CO_2. Once all electron acceptors/oxidants are used up, fermentation processes set in converting any remaining reactive organic matter to a mixture of CO_2 and CH_4. CO_2 can be removed from the water by photosynthesis, by pelagic or benthic phytoplankton. Part of the organic carbon produced *in situ*, or entering the dam, will be buried in the sediments.

The concentration of CO_2 increases with depth in the water column in the presence of stable density stratification. Density stratification is virtually always due to thermal stratification.

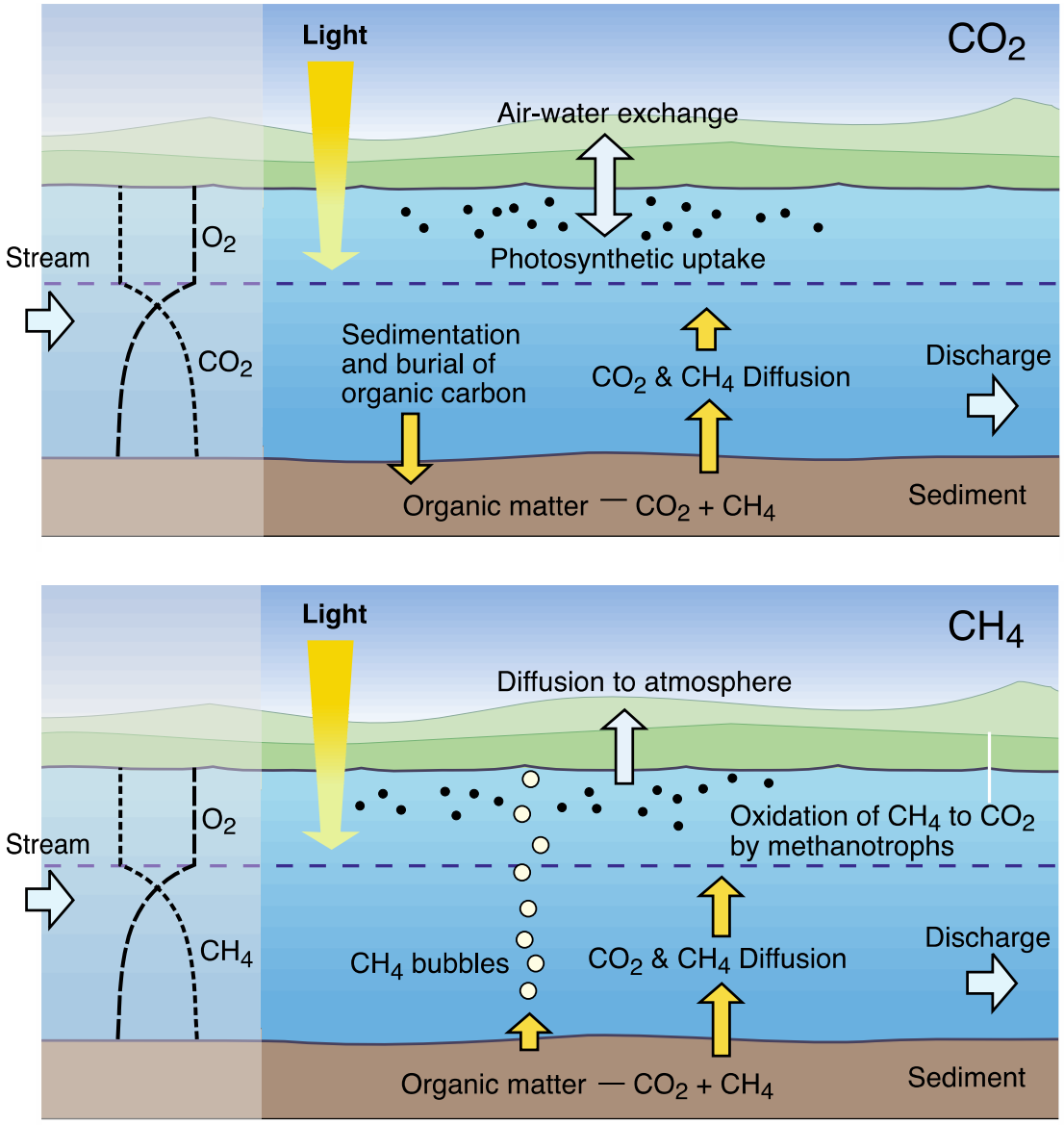

Figure 1: Conceptual model CO_2 and CH_4 cycles in reservoirs. (Figure from Sherman *et al*. 2001).

2.2. Methane (CH_4)

CH_4 is produced exclusively by bacterial fermentation processes in anoxic parts of the water column and (predominantly) sediments in stratified water bodies. It is removed by methanotrophic bacteria inhabiting a narrow oxygenated zone immediately above the ox cline in stratified systems. On a molecule for molecule basis, CH_4 has a much greater GWP than CO_2. The current value for greenhouse analyses considering a time horizon of 100 years is accepted as 25 times the CO_2 equivalent (4th Assessment of the IPCC, Solomon *et al*. 2009), however, more recent analyses suggest a higher GWP of 33 would be more appropriate (Shindell *et al*. 2009).

2.3. Nitrous Oxide (N_2O)

Nitrous oxide is produced in small amounts as a byproduct of oxidation of ammonia in the water column (Downes 1988), and through coupled nitrification/denitrification just beneath the sediment surface (Mengis *et al*. 1996). Once formed, N_2O appears to be fairly stable under both oxic and anoxic conditions. Molecule for molecule, this has about 310 times the CO_2 GWP. However, it is not generally found in significant quantities in reservoirs.

2.4. GHG Emissions Paths

The dominant GHG flux paths between the water and the atmosphere are due to diffusion, ebullition, and storage. Methane emission also occurs from littoral plants (Bastviken *et al*. 2004) and becomes more significant as the percentage cover of littoral vegetation increases for a lake or reservoir.

A simple conceptual model of methane flux pathways that neglects inflow and outflow effects is shown in Figure 2. Here, the reservoir is considered as consisting principally of two layers: an oxygenated surface layer (epilimnion) and an anoxic bottom layer (hypolimnion) adjacent to the sediments. Methane is produced in the reservoir's sediments (even if the water column is saturated with oxygen, the sediments will be anoxic a short distance below their surface). A portion, (1 - α), of the sediment methane flux, F_{sed}, is emitted directly to the atmosphere as bubbles, F_{bubble}, and the remainder dissolves into the anoxic bottom water where the concentration of dissolved methane $[CH4]_{hypo}$ generally increases with time during seasonal stratification. This produces a concentration gradient (dCH_4/dz) and the methane diffuses along this gradient towards the surface layer of the reservoir with flux, $F_{gradient} = k\ dCH_4/dz$, where k is the turbulent diffusivity. Methane consuming bacteria are typically found near the top of the gradient where they receive oxygen from above and methane from below and consume (at a rate F_{biota}) a large proportion of the diffusive flux. Some of the gradient flux makes it to the surface layer, where the concentration $[CH4]_{epi}$ changes with time to reflect the supply of methane from below and the diffusive flux of methane from the water to the atmosphere, F_{atm}.

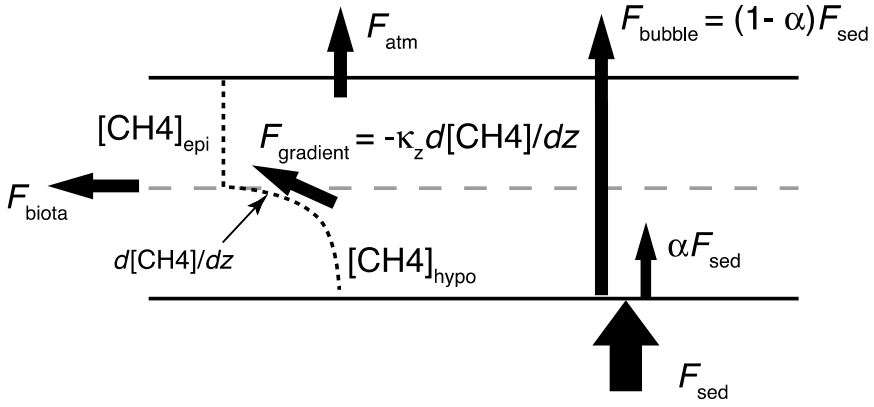

Figure 2: Conceptual diagram of methane flux pathways in a water column.

2.4.1 Diffusive

Transport of dissolved methane within the water column is governed by turbulent diffusion of dissolved gases from the bottom of the reservoir to the surface layer along the concentration gradient, dCH_4/dz, that develops as the water column stratifies. The flux (mg m^{-2} s^{-1}) is simply:

$$F_{gradient} = -\kappa_z \frac{d[\mathrm{CH4}]}{dz} \qquad (1)$$

where [CH4] is the concentration of the dissolved gas (mg m^{-3}), z is the vertical distance (m), and κ_z is the turbulent diffusivity (m^2 s^{-1}).

The flux of dissolved gases between the surface layer and the atmosphere, F_{atm}, depends on whether the surface layer is over-saturated (flux to the atmosphere) or under-saturated (flux into the water) with respect to the concentration in the atmosphere. In practice, F_{atm}, is typically calculated using the 'thin boundary layer' method (Figure 3) as:

$$F_{atm} = k\left(\left[C_{bulk\ water}\right] - \left[C_{bulk\ air}\right]\right) \quad (2)$$

where $C_{bulk\ air}$, and $C_{bulk\ water}$ are the concentrations of the gas measured in the atmosphere and in the bulk fluid just below the water surface, respectively, and k is a wind speed-dependent gas transfer velocity[2], k (m s^{-1}).

There are many field and laboratory studies of gas transfer that consistently show a slow increase in the gas transfer velocity with wind speeds below 3-4 m s^{-1} and a much faster increase in gas transfer velocity for winds > ~ 4 m s^{-1}, a speed associated with the formation of gravity-capillary waves. Estimates of GHG fluxes based on [CO2] and [CH4] measured in water must all include an assumption regarding the value of the gas transfer velocity, k.

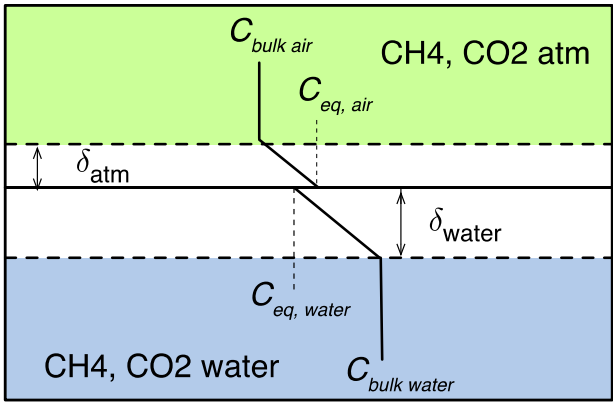

Figure 3: Diffusive flux of dissolved gases across the air-water interface. C_{eq} is the equilibrium concentration of the gas on the air and water sides of the interface, i.e. $C_{eq,\ water} = K_h C_{eq,\ air}$, where K_h is Henry's constant. The flux rate is limited by diffusion across diffusive boundary layers of thicknesses ∂_{atm} and ∂_{water} on the air and water sides of the interface, respectively. The boundary layer thicknesses are reduced as turbulence in the environment increases. In most cases, the rate limiting step is diffusion through the boundary layer on the water side of the interface. (Figure based on Liss and Slater 1974.)

The wind speed-dependence of the gas transfer velocity, k, reflects the relationship between turbulence in the water column and its generation by the wind. Vauchon *et al*. (2010) argue persuasively that the traditional approach of regressing fluxes as a function of wind speed is more accurately treated using a regression against water turbulence in the surface layer (which they quantify in terms of dissipation). The turbulence approach may do a better job of explaining variability in data sets because it is more hydrodynamic ally realistic. Danckwerts (1951) discusses gas transfer into liquids and argues that the rate governing step is likely to be the frequency with which the stagnant diffusive layer (∂_{water}, Figure 3) is renewed as turbulent eddies sweep it away into the body of the fluid away from the interface. The frequency of renewal increases with the intensity of the turbulence.

Measuring water column turbulence is time-consuming and costly. It is desirable, therefore, to establish site-specific relationships between wind speed, wind direction and water column turbulence. This allows better estimates of seasonal emissions using just wind speed and [CH4] (the surface layer concentration of CH_4 expressed as a partial pressure) data. The site specificity of these relationships reflects aspects of a particular system such as size and shape of the reservoir, sheltering by local topography and vegetation, and, possibly, larger-scale laminar water motions driven by heat and momentum transfer due to local meteorological and hydrologic conditions.

2 The gas transfer velocity is also referred to in the literature as a mass transfer coefficient and as a piston velocity.

2.4.2. Ebullition (Bubbles)

The ebullitive flux is the flux of a gas that occurs as bubbles pass through the water column and enter the atmosphere directly. The rate at which a bubble grows in size within the sediment depends on the rate of methane generation, which depends on temperature and the quantity and reactivity of organic matter, and the hydrostatic pressure which reflects both the depth and temperature of the overlying water and the atmospheric pressure. Eventually, the buoyant force of the bubble exceeds the forces arising from surface tension and the weight, porosity, and particle size of the overlying sediment acting to keep the bubble within the sediment and the bubble rises to the sediment-water interface, breaks free and rises to the water surface. Changes in pressure of the order of tens of cm of water have been observed to influence the rate of ebullition, i.e. passage of meteorological fronts can impact the flux as well as changes in water depth due to inflows and releases of water from the dam (Fechner-Levy and Hemond 1996).

2.4.3. Storage and Discharge Fluxes

The storage flux refers to the fate of accumulated dissolved gases following complete mixing of the water column (which typically occurs as a result of autumnal cooling in most reservoirs). During seasonal stratification, which occurs typically from late August to early June in southeast Queensland, the hypolimnion loses oxygen in early spring after which time the dissolved methane concentration builds up. Autumnal cooling causes the surface mixing layer to deepen progressively until it eventually reaches the bottom of the reservoir, at which point the water column has 'turned over'. As the surface layer deepens, it entrains methane-enriched water from the hypolimnion into the surface layer where it subsequently out-gases to the atmosphere as a diffusive flux. The increase in surface CH_4 concentration due to entrainment is expected to increase the diffusive flux to levels beyond those observed during spring - autumn prior to the onset of surface layer deepening.

We hypothesize also that deepening of the surface layer may impact the rate of biological consumption (F_{biota} in Figure 2) of dissolved methane through the redistribution of methanotrophic bacteria from dense layers at the top of the oxycline to homogeneously distributed throughout the surface layer and by changing the CH_4 concentration gradients adjacent to cell walls that may limit the rate of CH_4 uptake.

In reservoirs that discharge water from outlets located below the thermocline, the discharged water will contain elevated dissolved gas concentrations. The gases dissolved in the discharge water are released rapidly to the atmosphere within a short distance downstream of a dam and, for some dams, this can be the dominant methane flux pathway (Galy-Lacaux *et al*. 1999). This flux is sometimes referred to as the 'turbine flux' (Tremblay *et al*. 2005). Many Australian dams have been constructed with only deep water outlets (Sherman 2001).

2.4.4. Vegetation-Mediated Flux

Finally, some forms of littoral vegetation are know to directly mediate methane emissions through the plant itself. These emissions are likely to become quantitatively more significant as the surface area of a lake decreases because the area containing vegetation occupies a greater percentage of the total water surface area. Bastviken *et al*. (2004) cite literature values of plant emissions in the range 8 - 262 mg C m^{-2} d^{-1}. In reservoirs such emissions are generally not important because of the small amount of littoral vegetation (due to erosion of top soil resulting from changing water levels) and the relatively large areas of open water.

3. EXPERIMENTAL DESIGN

Reservoir methane emissions were identified as potentially the largest source of greenhouse gas emissions for the water supply system in South East Queensland. The data collected for this project was designed to reduce the uncertainty in current estimates (Hall *et al*, 2009) and to outline the potential for the mitigation of methane emission. Special focus was given to identifying spatial and temporal variability in emissions to better estimate the statistical uncertainty implicit in emission estimates based on sparse data and to facilitate the design of future experiments. Another important goal was to better estimate the fraction of methane dissolved and stored in the water column during spring and summer that is ultimately outgassed to the atmosphere following winter mixing of the water column. In addition, the research has provided baseline data for understanding the affect of dam inundation upon greenhouse gas emissions at Hinze Dam.

Seven field trips were undertaken during the project to resolve the temporal variability of emissions: 2-3 Dec 2009, 19-20 Jan 2010, 24 Feb - 1 Mar 2010, 1 - 8 Jun 2010, 30 Jun – 1 Jul 2010, 16 Jul 2010, and 13 Aug 2010. The original plan to conduct all measurements in Little Nerang Dam prior to 30 June 2010 had to be changed when the water level in the dam was drawn down during June to supplement domestic water supply following an operating problem at the Gold Coast desalination plant combined with the inability to sufficiently supplement water supply from Hinze Dam due to construction work on the intake tower at the time. Also, a large rainfall event caused significant spilling of Little Nerang Dam in February 2010 which, combined with the subsequent drawdown of the storage in June, further diminished our ability to accurately determine the fate of the stored methane in Little Nerang Dam. As of June 2010 the water column at Little Nerang Dam had not mixed and the remaining measurements were shifted to Hinze Dam which offered an opportunity to more accurately quantify the storage flux during seasonal overturn.

The location of all measurement sites visited as part of this project is shown in Figure 4 for Little Nerang Dam and in Figure 5 for Hinze Dam. At Little Nerang Dam, flux measurements were initially undertaken at sites LND05, LND Met, LND06, LND08, LND09 and LND10. As areas of high emissions were identified, additional measurement sites were added to provide better resolution of the spatial variability of emissions, e.g. PB transect line and bubble trap line in Figure 4.

Hinze Dam was initially sampled at sites Hinze01- Hinze12. Supplemental sites were added in the vicinity of Hinze06 and Hinze07 when this area was identified as having high spatial variability in emissions.

Water column profiles of dissolved methane were undertaken at a subset of the flux measurement sites at each dam.

The experimental design addressed in a preliminary fashion (due to resource constraints) temporal variability at sub-daily and seasonal time scales. Sub-daily variability was assessed by making continuous repeated measurements for several hours on a single day each at sites LND06 and LND10. Seasonal variability has been assessed by comparing measurements at a given site made during each of the field trips which were designed to include spring, summer, autumn and winter following complete mixing of the water column.

In addition, strings of bubble traps (inverted funnels that collect gas bubbles) were deployed during June to provide additional data on the magnitude and fine-scale (10s of metres) spatial variability of methane fluxes.

To provide the essential climatological and hydrodynamic context for assessing the flux measurements, a met station (air temperature, wind speed, wind direction, relative humidity, downwelling shortwave radiation, upwelling shortwave radiation, downwelling longwave radiation, upwelling longwave radiation) and high-precision thermistor chain (± 0.015 °C) were deployed near the centre of Little Nerang Dam at site LND Met.

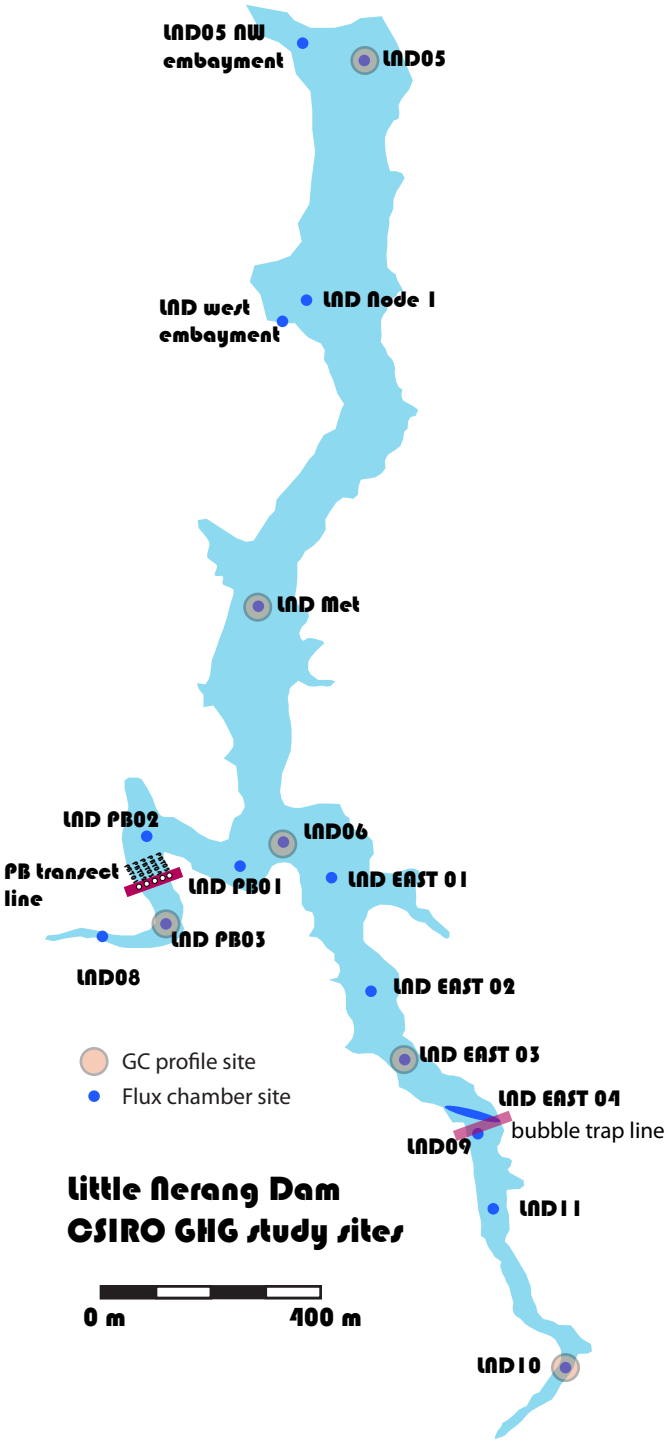

Figure 4: **Little Nerang Dam methane flux measurement sites. Blue ellipse denotes site LND EAST04 where the boat was allowed to drift across the channel during measurements.**

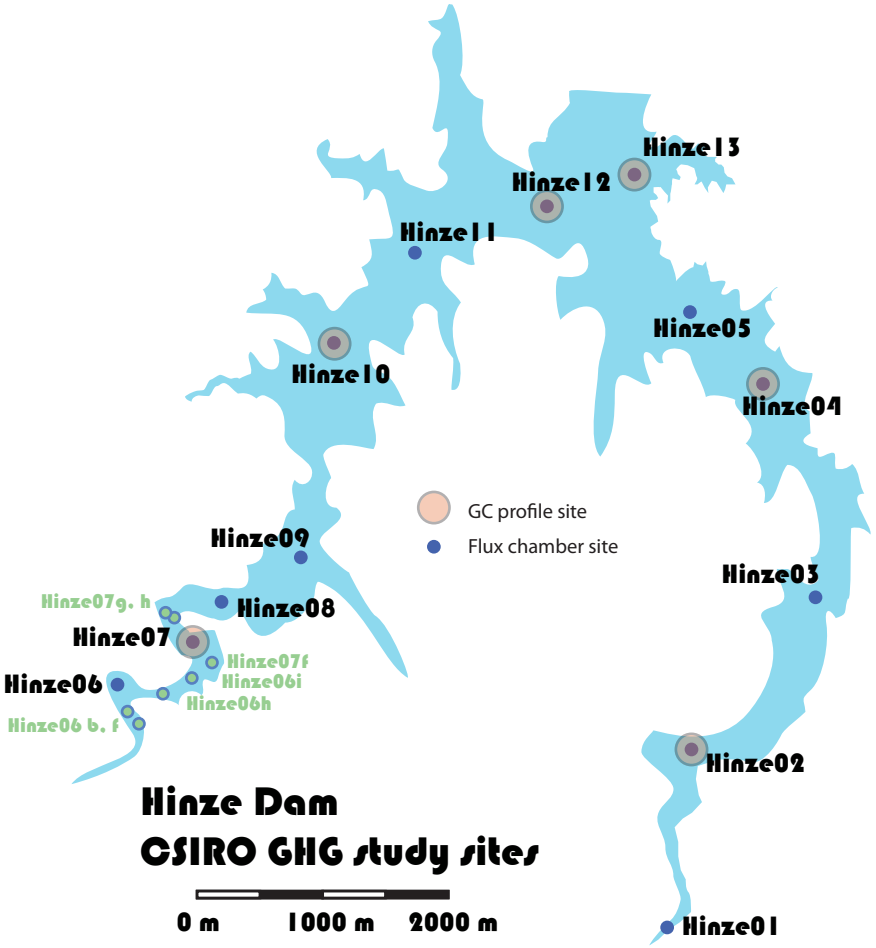

Figure 5: **Hinze Dam methane flux measurement sites. Large red circles denote sites where dissolved methane concentration profiles were measured.**

4. METHODS

4.1. Air-Water Interface Fluxes using Floating Chambers

The methane (and CO_2) fluxes between the water to the atmosphere was measured by recirculating air continuously through the headspace of a floating chamber and measuring this air continuously using a Picarro G1301 $CO_2/CH_4/H_2O$ gas analyser. The chambers were constructed to allow the head space to be adjusted easily by moving the floats up or down. Typically, the floating chamber head space had a volume of roughly 40 L (Table 1).

The head space air was recirculated through analytical grade tubing (Bev-a-line XX and Tygon Inert Tubing SE-200) using KNF N86 KTDBC brushless DC motor diaphragm pumps. Flow through the diaphragm pump could be adjusted continuously using Cole-Parmer PTFE flow meters (model 32044-82/TMRI-010315). In practice the flow rate was typically 5.5 ± 0.5 L/min, giving a chamber residence time of 7-8 minutes.

The gas passed through a manifold which allowed the Picarro G1301's built-in pump to draw off approximately 200 mL/min of gas for analysis before returning it to the recirculating line.

Table 1: Dates of floating chamber measurements and floating chamber configuration for each of the seven field trips.

Field Trip	Date	Site	Chamber	Chamber Head Space (mm)	Chamber Volume (L)
1	02-Dec-09	Little Nerang Dam	1	180	35.8
1	02-Dec-09	Little Nerang Dam	2	178	35.4
1	03-Dec-09	Little Nerang Dam	2	178	35.4
2	19-Jan-10	Little Nerang Dam	1	191	38.0
2	20-Jan-10	Little Nerang Dam	1	191	38.0
3	24-Feb-10	Little Nerang Dam	1	198	39.3
3	26-Feb-10	Little Nerang Dam	1	198	39.3
3	27-Feb-10	Hinze Dam	1	198	39.3
3	28-Feb-10	Hinze Dam	2	190	37.8
3	01-Mar-10	Little Nerang Dam	1	198	39.3
4	01-Jun-10	Little Nerang Dam	2	213	42.3
4	07-Jun-10	Little Nerang Dam	2	213	42.3
4	08-Jun-10	Little Nerang Dam	2	213	42.3
5	30-Jun-10	Hinze Dam	2	213	42.3
5	01-Jul-10	Hinze Dam	2	213	42.3
6	16-Jul-10	Hinze Dam	2	213	42.3
7	13-Aug-10	Hinze Dam	2	213	42.3

The typical deployment had a duration of 15 minutes and two deployments were performed sequentially at each site. The apparatus has an intrinsic response time of one minute, based on observations of controlled changes in intake gas concentrations. All analyses consider only the period of record commencing two minutes after the start of the deployment (when a rubber bung was inserted into the chamber vent) and finishing on or just before the time the chamber was recovered (when the bung was removed). Details regarding the response time of the floating chamber system are presented in Appendix 2.

4.2. Dissolved Methane Concentration

The diffusive flux is known to vary as a function of dissolved gas concentration in the surface layer and water turbulence and wind speed. Samples of water were collected for gas chromatography (GC) analysis of dissolved CH_4 during each floating chamber measurement (one sample per pair of chamber measurements at each site). GC analysis was performed by the Water Studies Centre at Monash University. Additional details regarding sample collection, storage and analysis are provided in Appendix 1.

GC measurements performed by UQ on samples collected before 23 February 10 were insufficiently accurate to be included in the analysis. Commencing with samples from 23 Feb 2010, all GC measurements were performed by the Water Studies Centre at Monash University and these measurements all showed a very high level of accuracy and repeatability.

4.3. Local Meteorology

Local meteorological conditions at each site were measured using a Kestrel 4500 Pocket Weather Tracker (barometric pressure, air temperature, relative humidity, wind speed and direction) deployed on a tripod with the axis of the wind sensor approximately 0.9 - 0.98 m above the water surface and logged every 20 seconds.

4.4. Water Turbulence

Water turbulence was measured at 64 Hz (x, y, z components) 15-20 cm below the water surface using a Nortek Vector Acoustic Doppler Velocimeter (ADV). Quantitative analysis of these data is outside the scope of this project and only qualitative presentation of results is attempted.

4.5. Floating Chamber Diffusive Flux Calculation

Diffusive fluxes measured with the floating chambers were calculated using linear regression to determine $d[CH4]/dt$ by fitting a line to the observed CH_4 concentration in the floating chamber head space. A typical example is shown in Figure 6. The correlation coefficient, r^2, was seldom < 0.95 and usually > 0.98. Knowing the head space of the chamber we can then compute the flux of methane across the air water interface, $F_{CH4\ diffusive}$ [mol m^{-2} s^{-1}] as,

$$F_{CH4\ diffusive} = 0.0121866 \frac{V_c p_{atm}}{(A_c T_c)} \frac{d}{dt} p'_{CH4} \qquad (3)$$

where V_c is the volume of the chamber (m^3), A_c is the water surface area enclosed by the chamber (m^2), p'_{CH4} is the concentration of methane [ppmv], p_{atm} is the local atmospheric pressure (atm), T_c is the air temperature (°K).

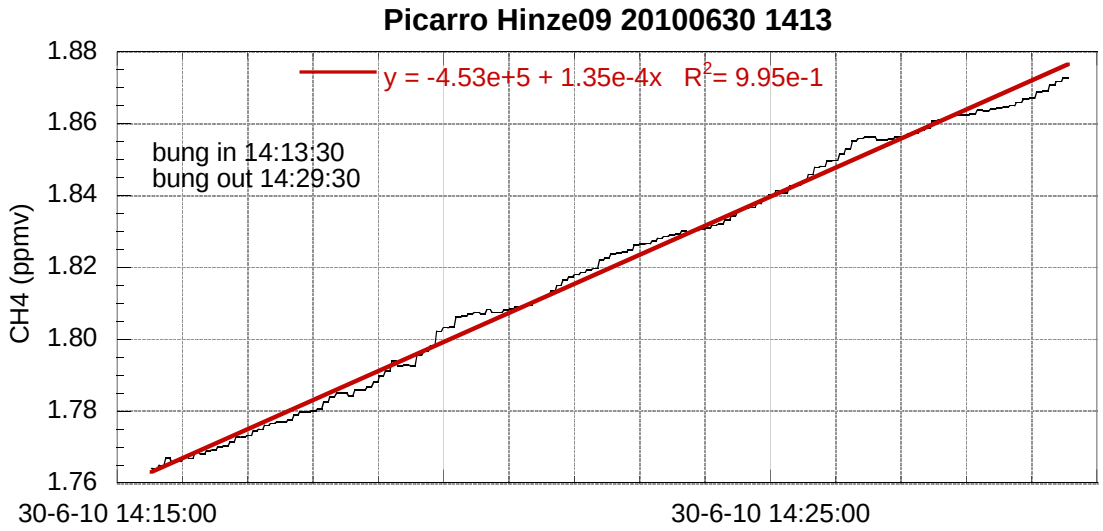

Figure 6: Example of linear regression used to compute diffusive methane flux. Data from Hinze Dam site Hinze09 on 30 June 2010.

A total of 202 floating chamber deployments were made in Little Nerang and Hinze Dams. 127 chamber measurements were analysed for a diffusive flux only. This included several measurements that showed contributions from bubbles but had sufficient periods of diffusive flux during the 15 minute deployment to allow the computation of the diffusive flux outside the periods impacted by bubble activity.

Of the 202 chamber measurements, 83 were dominated by bubble fluxes. Five of these 83 measurements were able to be analysed for the diffusive contribution to the overall flux in between bubble events. Bubble-dominated fluxes were computed using the end point concentrations and the time interval between them.

4.6. Floating Chamber Bubble Flux Calculation

In many cases, bubble activity caused large ‘steps’ in the concentration recorded by the Picarro gas analyser. An example of a FC measurement with both diffusive and bubble fluxes is shown in Figure 7. Diffusive fluxes are indicated by the yellow bands and are characterised by an effectively linear change in concentration with time. Bubble fluxes are shown in the blue ovals and are characterised by rapid increases in concentration that produce a 'step' in the concentration time series. Bubble fluxes were calculated by dividing the observed concentration change by the time interval between measurements (e.g. as indicated by the red circles in Figure 7) and using this value as $d[CH4] / dt$ in Equation 3.

At sites with a lot of bubble activity, the methane concentration in the chamber could exceed the gas analyser's maximum limit of detection (nominally 40 ppmv). In such circumstances, the gas analyser output updated irregularly once its limit of detection was exceeded, requiring us to terminate the deployment with the last normal output data point. This process meant that some of the deployments were shorter than the intended 15 minute duration and we had to make some assumptions regarding the likely flux of methane that occurred during the interval between the end of the measurement (when the instrument went out of range) and the nominal 15 minute deployment. Bubble flux data presented in this report are denoted as 'scaled' or 'instantaneous'. A 'scaled' flux assumes no methane was emitted after the instrument went out of range and is the most conservative estimate of the flux consistent with the data. An 'instantaneous' flux assumes that the flux computed from the shortened deployment continued at the same rate for the duration of the nominal 15 minute deployment. The true 15-minute flux cannot be lower than the 'scaled' flux but, in theory, it could be even higher than the 'instantaneous' flux.

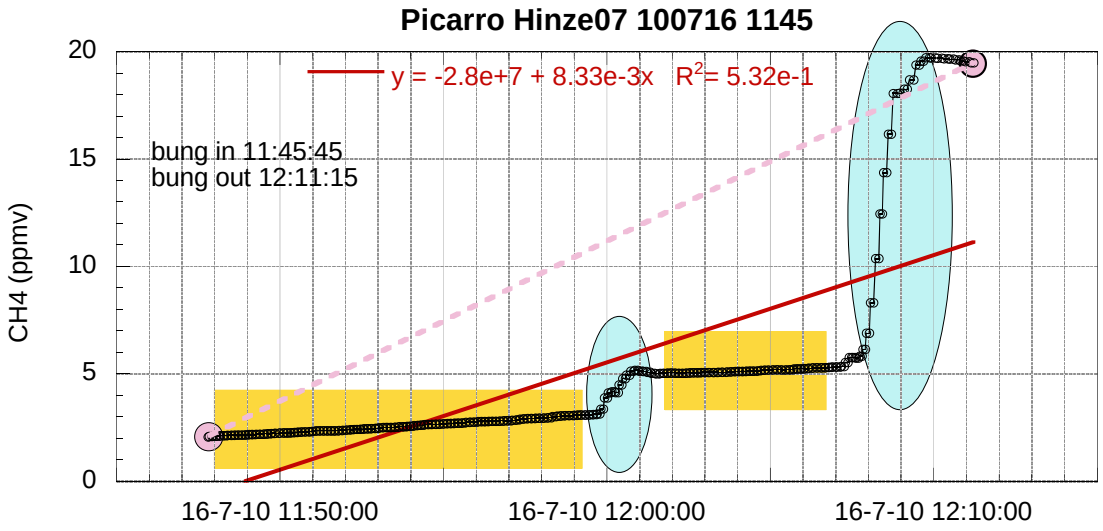

Figure 7: Example of bubbles in a flux chamber measurement. Gold shaded rectangles denote periods of diffusive flux only; blue shaded ellipses show entry of methane containing bubbles into flux chamber. Dashed line links end points used to compute net flux of methane. The solid red line denotes the best fit linear regression to the data.

4.7. Mean Reservoir Flux

The areal mean methane flux from Little Nerang and Hinze Dams, F_T was calculated as

$$F_T = \frac{\sum_{i=1}^{n} F_i A_i}{\sum_{i=1}^{n} A_i} \qquad (4)$$

where the surface area of each reservoir was divided into n component sub-areas, A_i, corresponding to local chamber flux measurement F_i. The sub-areas were selected based on sample site locations and reservoir geometry using best judgement as to how representative measurements made at the corresponding sample site were likely to be of the sub-area. Areas of the reservoir with high fluxes had more sample sites and smaller sub-areas in order to better resolve the spatial variability of the flux measurements.

4.8. Flux of Dissolved Methane

Measurement of the flux of dissolved methane required measurement of vertical profiles of water column dissolved methane. Water samples were pumped from depth through a garden hose attached to a YSI 6600v2 water quality sonde. The sonde data was used to control the depth of sampling and to measure relevant water column parameters such as dissolved oxygen, turbidity, temperature, and depth. On occasion, a bbe Fluoroprobe 3 was also deployed to measure profiles of CDOM, transmissivity, and chlorophyll fluorescence associated with various functional groups of phytoplankton.

4.8.1. Flux of Methane via Dam Releases

Depending on the level of the outlet valve in use, water released from Little Nerang Dam to the water treatment plant may contain varying concentrations of methane. An automated CH_4 monitoring system was borrowed from Environment Illimite (Montreal, Canada) and deployed in the building at the base of the dam formerly used for chlorination of discharged water. Water in the pipeline was collected

continuously from a valve located just downstream of the building. The water sample was transferred to the instrument inside the building using a garden hose. Unfortunately, a technical problem with the instrument has compromised the accuracy of the reported CH_4 and CO_2 concentrations and we have not undertaken any further analysis of these data.

4.8.2. Flux of Stored Methane during Seasonal Overturn

The storage flux was computed using a mass balance approach. The change in mass of stored methane during a time interval was computed as the difference in total mass of dissolved methane observed in the reservoir at the beginning and the end of the interval. Assuming negligible inflow and discharge from the dam during the interval, then the observed change in mass will equal the supply of methane produced in the sediments and dissolved into the water column hypolimnion, αF_{sed}, minus emission to the atmosphere, F_{atm}, and consumption by methanotrophic organisms, F_{biota}, (Figure 2).

Adopting a two-layer model of the dissolved methane concentration distribution with flux between layers, $F_{gradient}$, the governing equations are,

$$\frac{d[CH4]_{hypo}}{dt} = \alpha F_{sed} - F_{gradient} \tag{5}$$

$$\frac{d[CH4]_{epi}}{dt} = F_{gradient} - F_{biota} - F_{atm} \tag{6}$$

The total mass of CH_4 dissolved in the reservoir at time, t, $M_{CH4,\,t}$, (g) is computed as,

$$M_{CH4,\,t} = \int_0^H CH4(z,\,t)\,A(z)dz \tag{7}$$

where $A(z)$ is the area of the reservoir (m^2) at elevation z (m) above the bottom and $CH4(z, t)$ is the concentration of dissolved methane (g m^{-3}, equivalent to mg L^{-1}). We employ a frame of reference in which $z = 0$ corresponds to a reservoir volume of 0 (m^3).

Measured profiles of dissolved CH_4 were interpolated spatially to provide estimates of the total mass of methane dissolved in the water column at the time of a field trip. Taking the difference of these values between trips spanning seasonal overturn of the water column provides an indication of the amount of methane that has outgassed as a result of deepening of the surface mixed layer (and ultimately complete mixing of the water column) plus an amount removed by *in situ* oxidation (F_{biota} in Figure 2).

We did not have the resources to directly measure the biological consumption term, F_{biota}, however, it is possible to deduce this term by rearranging Eq (6) if one can specify the change in epilimnetic [CH4] over a time interval when the gradient and atmospheric fluxes can be estimated.

5. RESULTS

5.1. Dissolved Methane

5.1.1. Surface Layer CH_4 Concentration Distribution

Here we present the results of surface sampling of dissolved methane concentration for Little Nerang and Hinze Dams. According to Equation 2, the diffusive methane flux varies linearly with the concentration of dissolved methane in the surface layer. In the absence of direct chamber (or other) measurements, knowledge of the surface layer CH_4 concentration [CH4] offers the potential for improved estimation of the methane flux over long time scales given wind speed data alone through the application of Equation 2. Knowledge of the temporal and spatial variability of [CH4] provides a more accurate indication of the variability associated with such indirect methods of estimating fluxes across the air-water interface.

The minimum, maximum and mean surface [CH4] concentrations and the dates of sampling for Little Nerang Dam are presented in Table 2 and Table 3, and for Hinze Dam in Table 4 and Table 5. In Little Nerang Dam, surface layer dissolved methane concentrations ranged from 0.0082-0.184 mg-CH_4 L^{-1}. In Hinze Dam the range was smaller, varying from 0.0078 to 0.0458 mg-CH_4 L^{-1}. Averaging the mean site results over all sites in each dam gives a mean surface layer [CH4] of 0.030 mg-CH_4 L^{-1} (s.d. 0.028, n = 10) at Little Nerang Dam and 0.012 mg-CH_4 L^{-1} (s.d. 0.0040, n = 22) at Hinze Dam. Surface layer [CH4] was considerably more variable in Little Nerang Dam, where the median standard deviation was 46% of the mean flux compared to 17% in Hinze Dam.

Table 2: Average, minimum, maximum and standard deviation of surface layer [CH4] measured during 1-9 June 2010 in Little Nerang Dam.

		[CH4] (mg CH_4 L^{-1})				
Site	**n**	**mean**	**min**	**max**	**std dev**	**std dev/mean**
LND EAST03	3	0.0771	0.0134	0.1840	0.0761	0.99
LND EAST04	1	0.0172	0.0172	0.0172		
LND Met	5	0.0171	0.0090	0.0326	0.0084	0.49
LND Node 1	2	0.0129	0.0121	0.0137	0.0008	0.06
LND PB02	1	0.0158	0.0158	0.0158		
LND PB03	3	0.0293	0.0156	0.0477	0.0135	0.46
LND05	4	0.0111	0.0089	0.0135	0.0017	0.15
LND06	4	0.0197	0.0082	0.0401	0.0122	0.62
LND08	1	0.0165	0.0165	0.0165		
LND10	3	0.0852	0.0697	0.1090	0.0171	0.20
Average						**0.42**
Median						**0.46**

Table 3: Time of collection of Little Nerang Dam surface [CH4] samples.

Site	Date	Site	Date	Site	Date
LND05	2010-06-01	LND Met	2010-06-08	LND PB03	2010-06-09
LND05	2010-06-07	LND Met	2010-06-09	LND08	2010-06-08
LND05	2010-06-08	LND06	2010-06-01	LND EAST03	2010-06-02
LND05	2010-06-08	LND06	2010-06-02	LND EAST03	2010-06-08
LND Node 1	2010-06-08	LND06	2010-06-08	LND EAST03	2010-06-09
LND Node 1	2010-06-09	LND06	2010-06-09	LND EAST04	2010-06-01
LND Met	2010-06-01	LND PB02	2010-06-02	LND10	2010-06-02
LND Met	2010-06-02	LND PB03	2010-06-01	LND10	2010-06-08
LND Met	2010-06-07	LND PB03	2010-06-02	LND10	2010-06-09

Table 4: Average, minimum, maximum and standard deviation of surface layer [CH4] measured during 30 June and 13 August 2010 in Hinze Dam.

		[CH4] (mg CH_4 L^{-1})				
Site	**n**	**mean**	**min**	**max**	**std dev**	**std dev/mean**
Hinze01	1	0.0136	0.0136	0.0136		
Hinze02	3	0.0248	0.0126	0.0458	0.0149	0.60
Hinze03	2	0.0091	0.0085	0.0097	0.0006	0.07
Hinze04	4	0.0154	0.0085	0.0329	0.0102	0.66
Hinze05	2	0.0079	0.0078	0.0079	0.0001	0.01
Hinze06	4	0.0132	0.0122	0.0156	0.0014	0.11
Hinze06a	1	0.0176	0.0176	0.0176		
Hinze06b	1	0.0090	0.0090	0.0090		
Hinze06f	1	0.0091	0.0091	0.0091		
Hinze06h	1	0.0099	0.0099	0.0099		
Hinze06i	1	0.0138	0.0138	0.0138		
Hinze07	5	0.0145	0.0098	0.0238	0.0050	0.34
Hinze07f	3	0.0150	0.0126	0.0185	0.0025	0.17
Hinze07g	1	0.0103	0.0103	0.0103		
Hinze07h	2	0.0098	0.0096	0.0100	0.0002	0.02
Hinze07i	1	0.0089	0.0089	0.0089		
Hinze08	3	0.0115	0.0092	0.0128	0.0016	0.14
Hinze09	5	0.0114	0.0084	0.0162	0.0028	0.24
Hinze10	11	0.0130	0.0084	0.0375	0.0079	0.61
Hinze11	4	0.0147	0.0081	0.0251	0.0063	0.43
Hinze12	1	0.0084	0.0084	0.0084		
Hinze13	3	0.0081	0.0080	0.0082	0.0001	0.01
Average						**0.26**
Median						**0.17**

Table 5: Time of collection of Hinze Dam surface [CH4] samples.

Site	Date	Site	Date	Site	Date
Hinze01	2010-08-12	Hinze10	2010-06-29	Hinze07g	2010-07-01
Hinze02	2010-06-29	Hinze10	2010-06-29	Hinze07h	2010-07-01
Hinze02	2010-07-15	Hinze10	2010-06-30	Hinze07h	2010-08-13
Hinze02	2010-08-12	Hinze10	2010-06-30	Hinze07	2010-06-29
Hinze03	2010-07-15	Hinze10	2010-06-30	Hinze07	2010-06-30
Hinze03	2010-08-12	Hinze10	2010-06-30	Hinze07	2010-07-01
Hinze04	2010-06-29	Hinze10	2010-07-01	Hinze07	2010-07-15
Hinze04	2010-07-15	Hinze10	2010-07-15	Hinze07	2010-08-12
Hinze04	2010-07-16	Hinze10	2010-07-16	Hinze07f	2010-07-01
Hinze04	2010-08-12	Hinze10	2010-08-12	Hinze07f	2010-07-16
Hinze05	2010-07-15	Hinze10	2010-08-13	Hinze07f	2010-08-13
Hinze05	2010-08-12	Hinze09	2010-06-30	Hinze06i	2010-06-30
Hinze13	2010-07-15	Hinze09	2010-07-01	Hinze06h	2010-07-01
Hinze13	2010-07-16	Hinze09	2010-07-15	Hinze06	2010-07-01
Hinze13	2010-08-12	Hinze09	2010-08-12	Hinze06	2010-07-15
Hinze12	2010-06-29	Hinze09	2010-08-13	Hinze06	2010-08-12
Hinze11	2010-06-30	Hinze08	2010-06-30	Hinze06	2010-08-13
Hinze11	2010-06-30	Hinze08	2010-07-15	Hinze06f	2010-07-01
Hinze11	2010-07-01	Hinze08	2010-08-12	Hinze06a	2010-06-30
Hinze11	2010-08-12	Hinze07i	2010-07-01	Hinze06b	2010-06-30

5.1.2. Spatial and Temporal Variability of Surface [CH4] in Little Nerang Dam

The spatial distribution of surface layer dissolved CH_4 in Little Nerang Dam was measured twice during June 2010, with a 1 week interval between surveys. Short-term (1-7 day) changes in the spatial variability of [CH4] are shown in Figure 8 and all of the individual measurements are shown in Figure 9. Both surveys showed an increase in concentration towards the upstream ends of the reservoir and both showed generally higher concentrations on the last day of each survey. The second survey (7-9 June) measured higher average [CH4] at most sites (Figure 8c) with particularly large increases (> 100%) in concentration between consecutive days at sites LND Met, LND06, and LND EAST03 on 8 June and 9 June.

5.1.3. Spatial and Temporal Variability of Surface [CH4] in Hinze Dam

Short-term changes in surface [CH4] at individual sites in Hinze Dam are shown in Figure 10 for the period from 29 June 2010 - 13 August 2010. The average values for each site during the three field trips are shown in Figure 11. Similar to Little Nerang Dam, a trend towards higher [CH4] at the upstream ends of the reservoir was observed on each trip. Apart from the prominent increases in [CH4] during 12-13 Aug 2010 at sites Hinze02, Hinze04 and Hinze10, the observed concentrations at any site only varied by about ± 20% between trips.

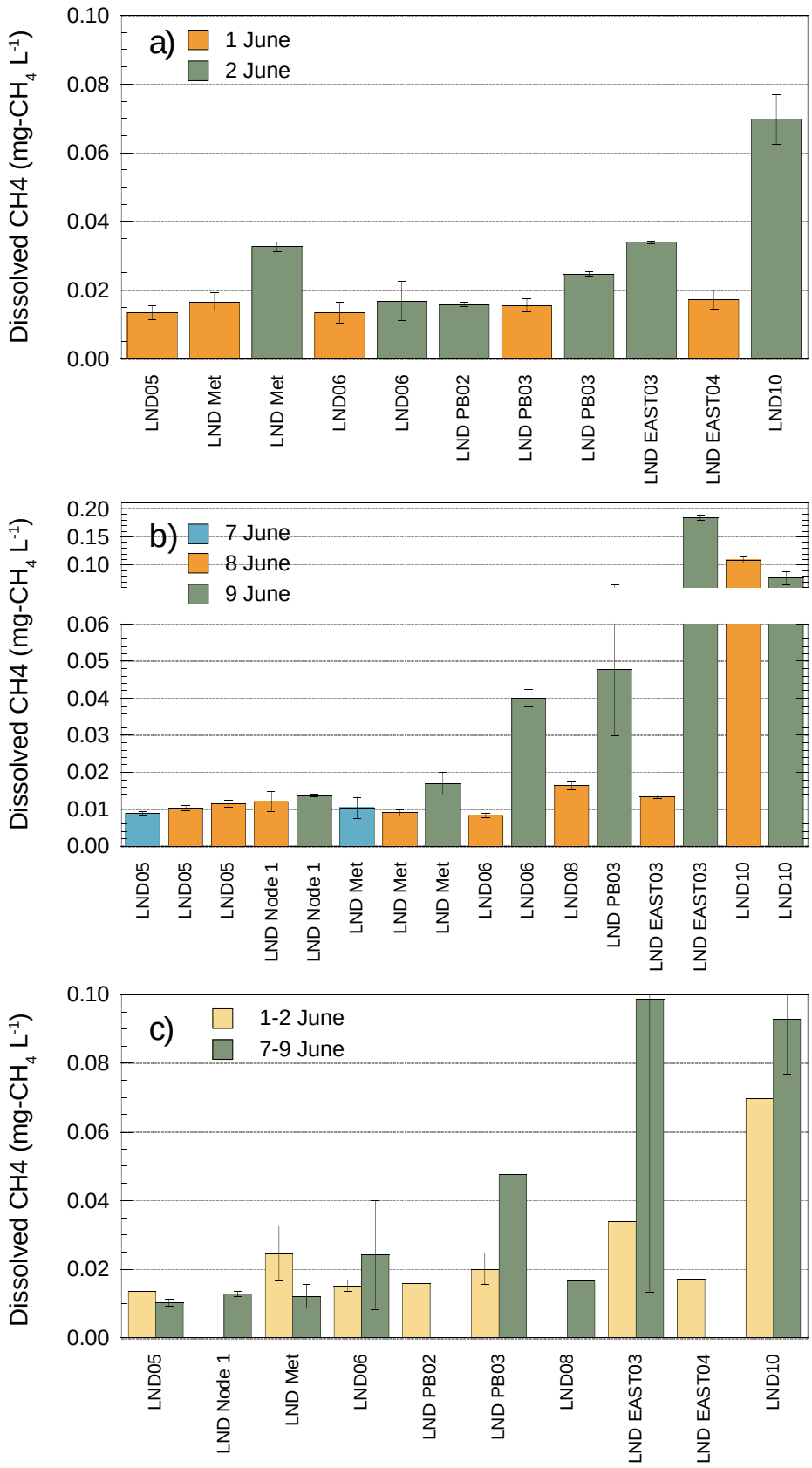

Figure 8: Surface methane concentrations at Little Nerang Dam on: (a) 1-2 June 2010 (a); (b) 7-9 June 2010 (b). (c) Average of all surface methane concentrations made at each site for each trip. Error bars in (a) and (b) are the standard deviation of replicate measurements. Error bars in (c) show the standard deviation of all measurements at a site. All samples were collected at a depth of 0.25 m except for site LND10 on 2 June 2010 which was collected at 1.25 m depth.

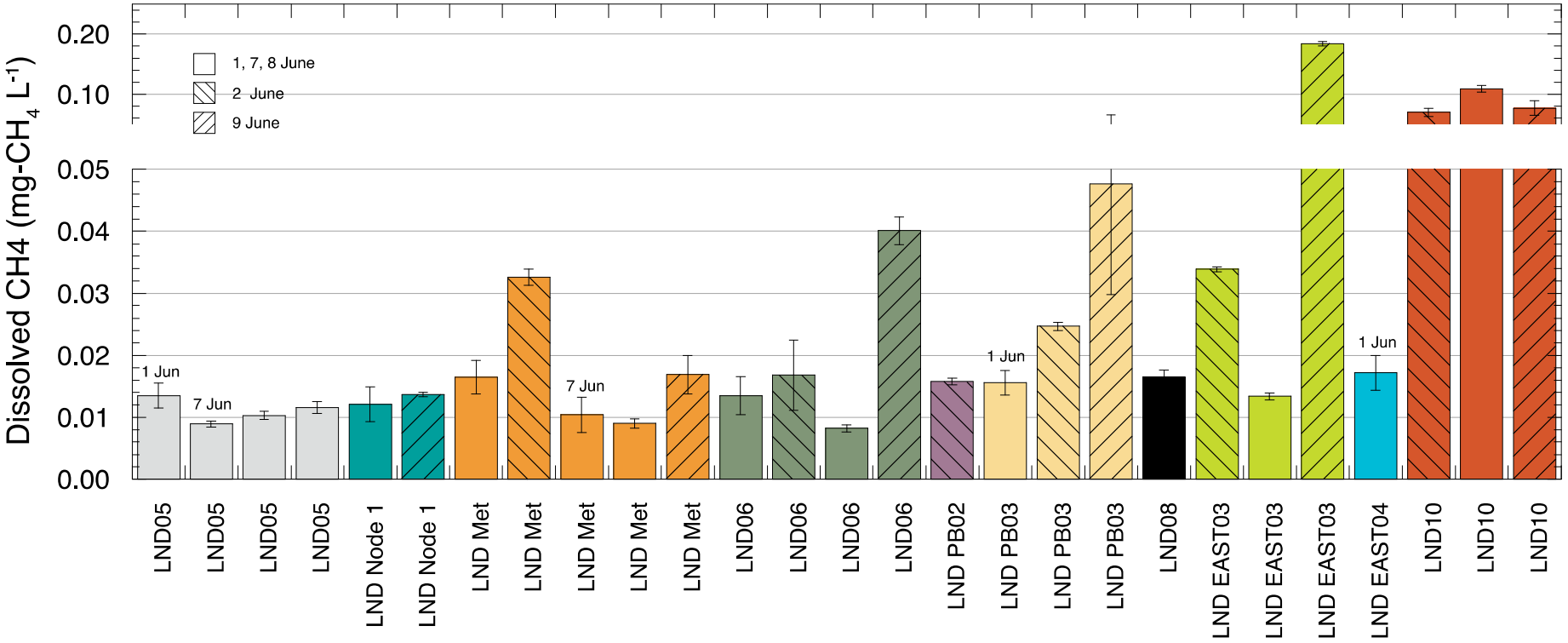

Figure 9: Spatial and temporal variability in surface layer dissolved methane concentration in Little Nerang Dam. Data collected during 1-9 June 2010. Dates for each sample (left to right) are given in Table 3. The concentration in the surface layer increases from the dam wall (LND05) to the distal ends of both reservoir arms (LND PB03/LND08 and LND10). Variability at a site is greatest at sites with higher ebullition. Error bars denote the standard deviation of replicate measurements. Note scale break at 0.05 to 0.10.

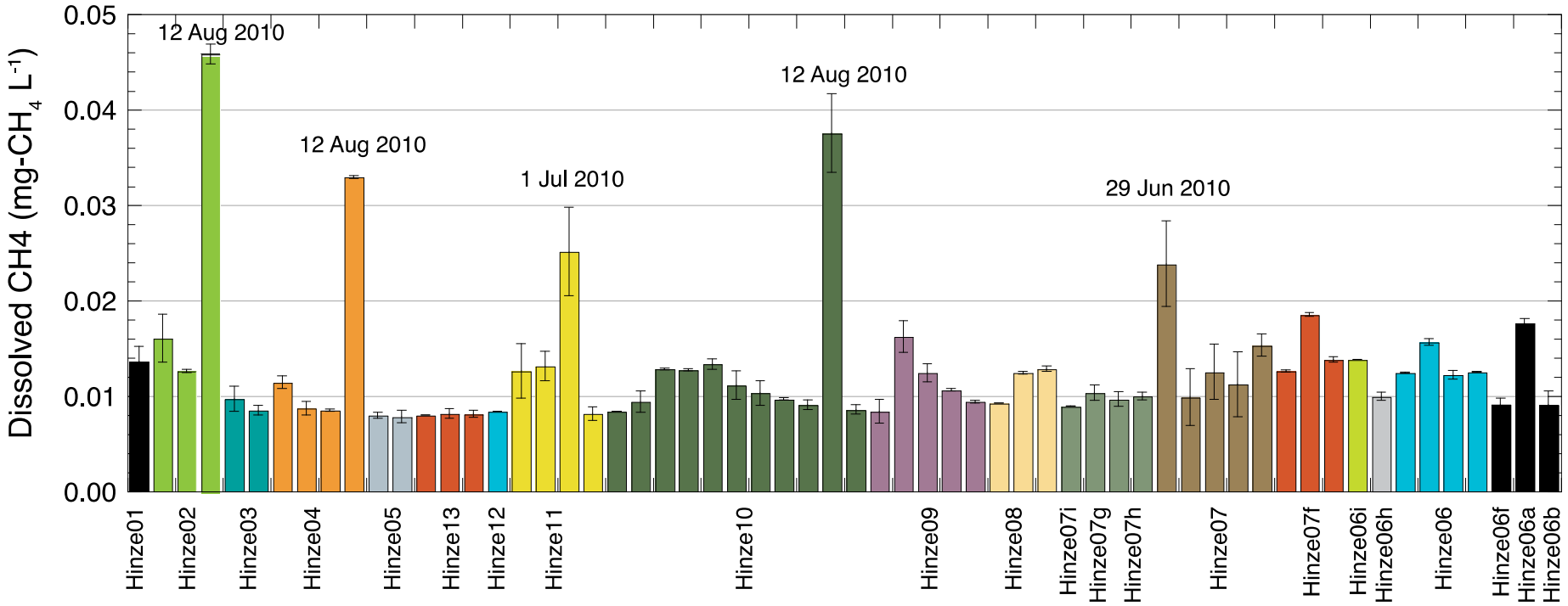

Figure 10: Spatial and temporal variability in surface layer dissolved methane concentration in Hinze Dam. Data collected during 3 field trips between 29 June 2010 and 13 August 2010. Prominent increases on 12 Aug 2010 probably reflect entrainment of hypolimnetic water due to seasonal overturn. Wind direction on 12 Aug was from the NE (blowing from site Hinze13 towards site Hinze02). The methane concentration generally increases towards the upstream ends of both arms (Hinze02, Hinze06). Sites are presented in spatial order. Hinze 13 is closest to the dam wall. Colours denote specific sites with bars drawn in chronological order (29 Jun - 12 Aug 2010) from left to right. Dates for each sample (from left to right) are given in Table 5. Error bars denote the standard deviation of replicate measurements during a single site visit.

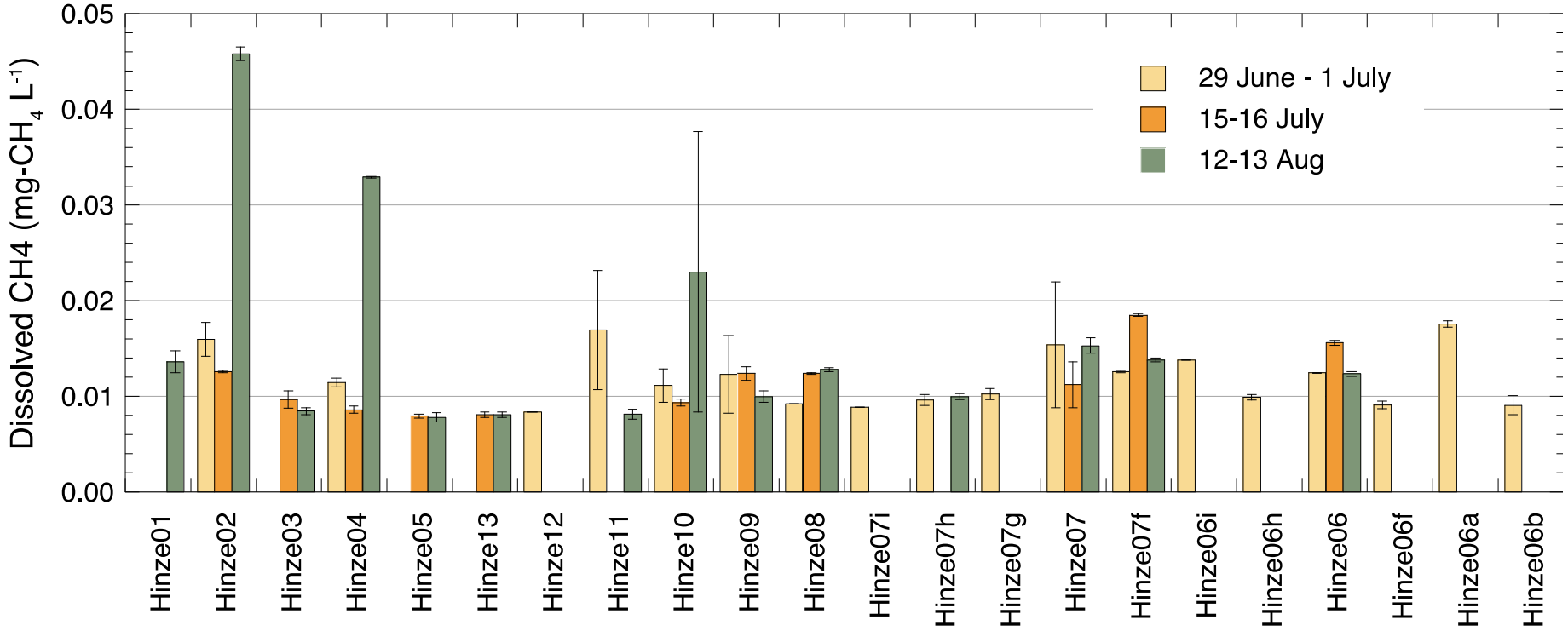

Figure 11: Average of all surface methane concentrations made at each site for each winter field trip at Hinze: 29 June - 1 July, 15-16 July, and 12-13 August 2010. Error bars show the standard deviation for multiple visits to a particular site during one trip.

5.1.4. Spatial Distribution of Dissolved CH_4

A total of 36 vertical profiles were measured successfully at the two reservoirs (Table 6). On 29 June 2010 two profiles (morning and afternoon) were measured at Hinze 10.

Table 6: Dissolved methane profile site list.

Date	Sites Profiled	Number of Depths Sampled	Date	Sites Profiled	Number of Depths Sampled
23 Feb 2010	LND Met	6	29 June 2010	Hinze02	5
	LND05	11		Hinze04	9
				Hinze07	6
				Hinze10	22
				Hinze12	10
2 June 2010	LND EAST03	2	30 June 2010	Hinze10	11
	LND Met	14		Hinze11	11
	LND PB03	3			
	LND05	15			
	LND06	12			
	LND10	2			
8 June 2010	LND05	16	1 July 2010	Hinze07	6
				Hinze09	9
				Hinze10	11
				Hinze11	11
9 June 2010	LND EAST03	9	15 July 2010	Hinze02	10
	LND Met	13		Hinze04	10
	LND Node 1	16		Hinze07	11
	LND PB03	3		Hinze10	31
	LND06	12		Hinze13	21
	LND10	3			
			12 Aug 2010	Hinze02	3
				Hinze04	3
				Hinze07	8
				Hinze10	3

The vertical profiles of CH_4 in Little Nerang Dam (Figure 12) show an accumulation of dissolved methane over time below a depth of approximately 10 m. The concentration at depth typically increased with distance upstream from the dam wall (LND05), although on 2 June 2010 the concentration between 11 and 18 m depth was less at LND06 than at LND Met. The following week the concentrations increased steadily in the upstream direction. On 9 June 2010 there is evidence of an intrusion of relatively methane-rich water at a depth range of 10-12 m in the vicinity of the dam wall (sites LND05 and LND Node 1). The persistent strong chemocline below 10 m shows that autumnal cooling had not yet caused the water column to mix below this depth.

The Hinze Dam profiles (Figure 13) show very little horizontal variability above the chemocline. The surface layer deepened from 18 m on 29 June to 28 m by 15 July. Complete mixing of the water column appears to have occurred by 12 August 2010 as suggested by the lack of vertical concentration gradients and the general increase in dissolved [CH4] throughout the top 20 m compared to the profiles on the previous two surveys. The surface [CH4] on 12 August was about four times higher than measured during the previous field trips.

Co-location of the CH_4 concentration gradient with the thermocline and oxycline in both reservoirs was confirmed through comparison with water quality sonde profiles (data not shown) collected by the research team and confirmed at Hinze Dam by comparison with data collected by Seqwater using an automated profiler system located at site Hinze13. The concentration gradient was strongest at the top of the chemocline and varied from 0.36 to 0.95 g-CH_4 m^{-4} in Hinze Dam. In Little Nerang Dam during June, the maximum concentration gradient ranged from 0.95 to 1.2 g-CH_4 m^{-4}. Based on these observations we assume a representative concentration gradient of 1 g-CH_4 m^{-4} for the estimation of the flux from hypolimnion to epilimnion, $F_{gradient}$ in the section 5.4.

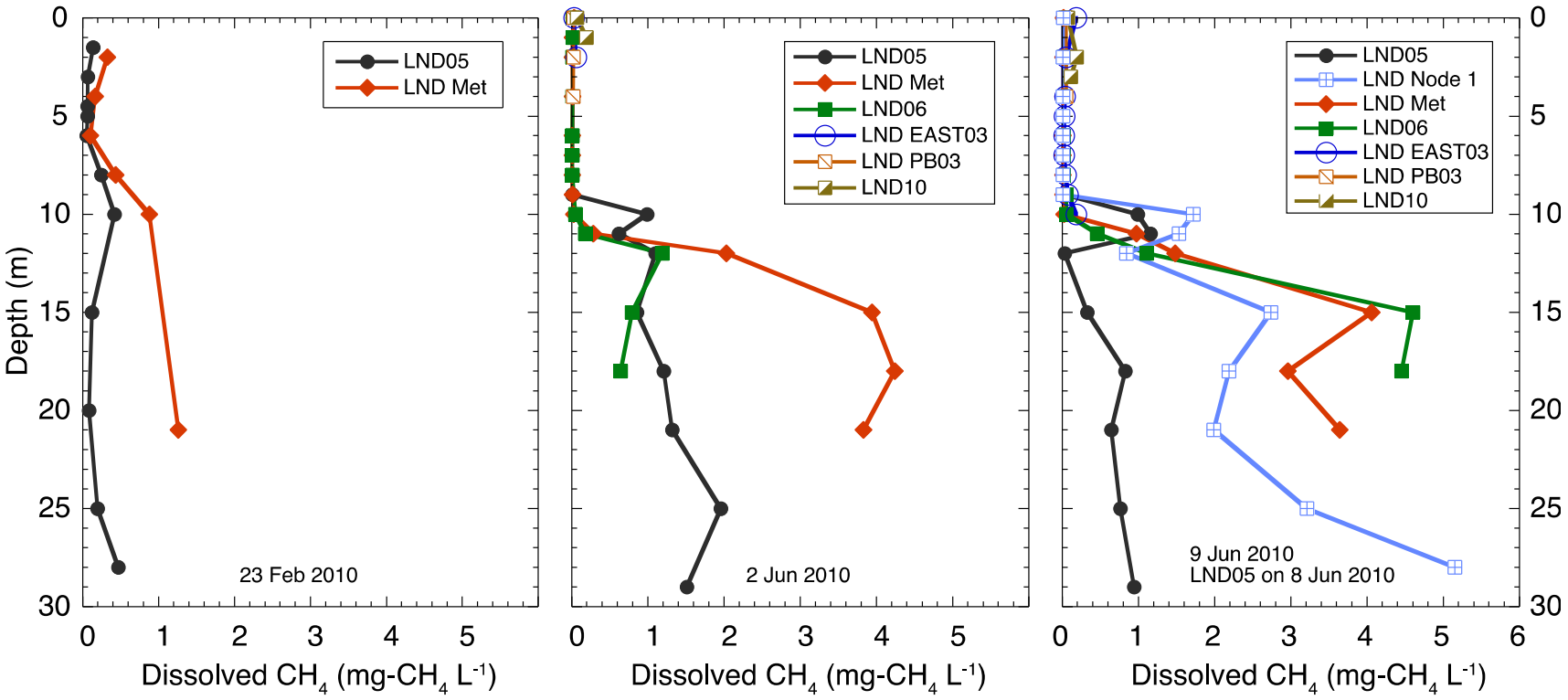

Figure 12: Dissolved CH_4 profiles at Little Nerang Dam on 23 Feb, 2 June, and 8-9 June 2010.

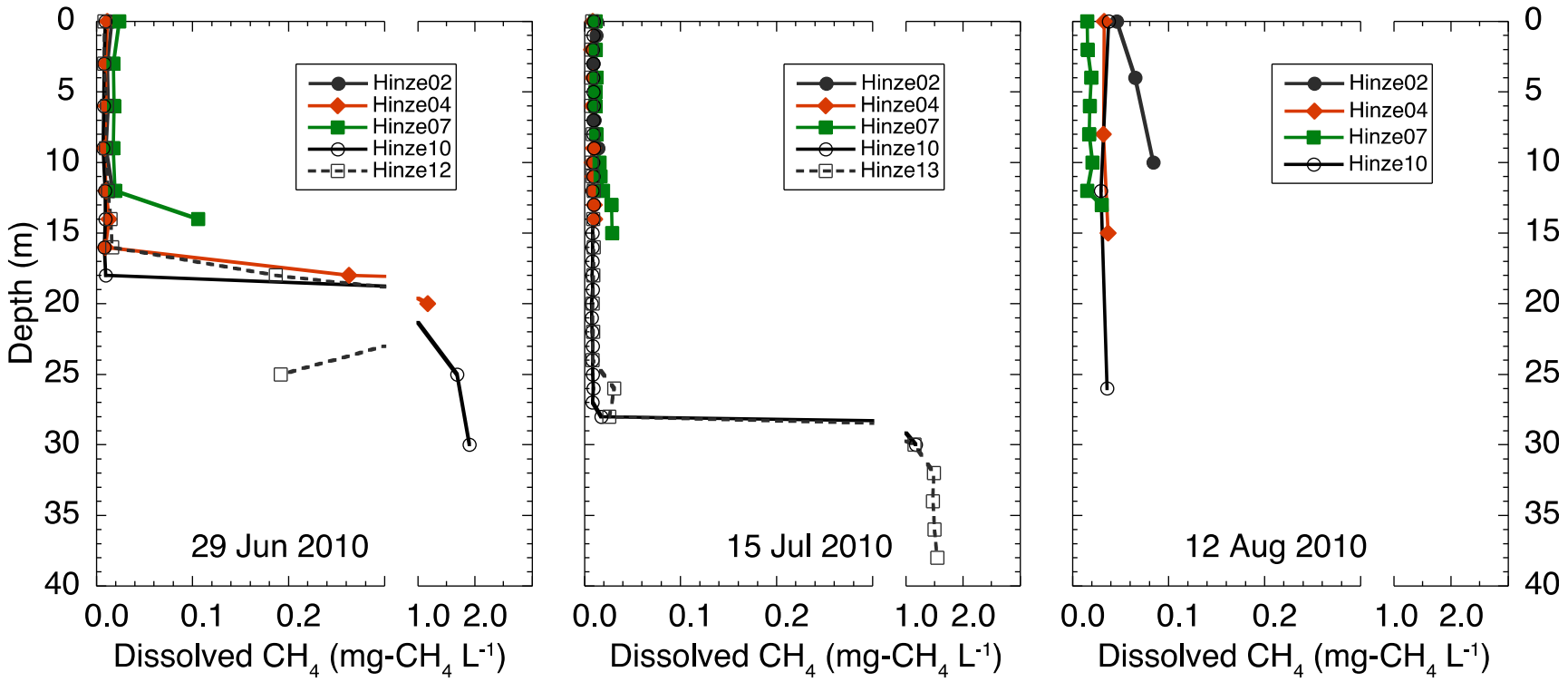

Figure 13: Dissolved CH_4 profiles at Hinze Dam on 29 June, 15 July, and 12 Aug 2010. Surface mixed layer deepened from 17 m to 28 m between 29 June and 15 July 2010. Complete mixing of the water column is evident on 12 August 2010; there is little vertical concentration gradient and concentrations in the top 20 m have increased substantially compared to the earlier profiles. Note break in x-axis.

5.2. Flux Chamber Measurements

5.2.1 Little Nerang Dam

5.2.1.1. Spatial Variability of CH_4 Flux

The spatial variability of the methane flux was investigated during four field trips (2-3 Dec 2009, 19-20 Jan 2010, 24 Feb - 1 Mar 2010, 1-8 Jun 2010). Reservoir-scale variability is shown in Figure 14 and small-scale variability in Figure 15. During each trip a pronounced longitudinal gradient in CH_4 flux was observed with the lowest flux close to the dam wall and the highest fluxes at the upstream ends of both arms of the reservoir. Fluxes varied between sites by a factor of 10 - 100 times along the length of the dam. The observed spatial gradient persisted across the seasons.

Based on these observations, the reservoir could be broken into three regions characterised by: consistent low fluxes with no bubbles between the dam wall (LND05) and the meteorological station (LND Met); moderate fluxes with occasional bubble events between LND Met and the confluence of the tributary arms (LND06); and persistent high fluxes with frequent bubble events between LND06 and the distal ends of both reservoir arms.

During the 24 Feb - 1 Mar field trip, measurements were made at a finer spatial resolution along a transect across the western arm (PBT01 - PBT05) and along the arm between LND06 and LND10 to better resolve the spatial gradients in fluxes (Figure 15). On 26 Feb 2010, medium-scale (100s of metres) variability was examined and fluxes increased 100-fold between the confluence (LND06) and both upstream arms. The small-scale (10s of metres) transect measured on 1 Mar 2010 showed a 6-fold variation in flux between sites with larger fluxes observed from the channel centre to the outside edge of the bend (PBT03 - PBT05); this is a region where deposition of catchment organic matter might be expected to be greater compared to the inside of the bend.

Measurements made during the Feb 2010 and Jun 2010 field trips at LND East02, LND East03 and LND East04 all fell in the range of 4.7 - 34 mmol-CH_4 m^{-2} d^{-1} (75 - 540 mg-CH_4 m^{-2} d^{-1}). Variability between measurements within a site was similar for all three sites. For the measurements at LND East04, the boat was allowed to drift across the width of the channel in order to capture a flux 'representative' of the full channel width, whereas the boat was anchored (but allowed to swing on the anchor) at the other two sites. This suggests that the small-scale spatial variability in this section of the reservoir is similar to the temporal variability observed at a 'fixed' site where the position of the boat may vary within a radius of up to 10 m depending on the wind.

5.2.1.2. Spatial Variability of CO_2 Flux

During the first three field trips (Dec 2009, Jan 2010, Feb-Mar 2010) the CO_2 flux was from the atmosphere into the water at all but the most upstream sites (Figure 14). Because the flux chamber measurements were performed during the daytime, this result shows that the reservoir experiences significant local photosynthesis by the phytoplankton community. At the most upstream sites, the flux was always to the atmosphere and demonstrates net heterotrophy (community respiration exceeds photosynthetic production) at these locations. Notably, during the last field trip in early winter, the entire reservoir was heterotrophic which may reflect lower availability of light due to a deeper surface mixing layer and shorter days.

Medium scale variability of CO_2 fluxes on 26 Feb 2010 was large, varying by a factor of almost 3 from -8 to -24 mmol m^{-2} d^{-1}, whereas variability at small scale was much less, with fluxes ranging from -7.3 to -12 mmol m^{-2} d^{-1} (Figure 15).

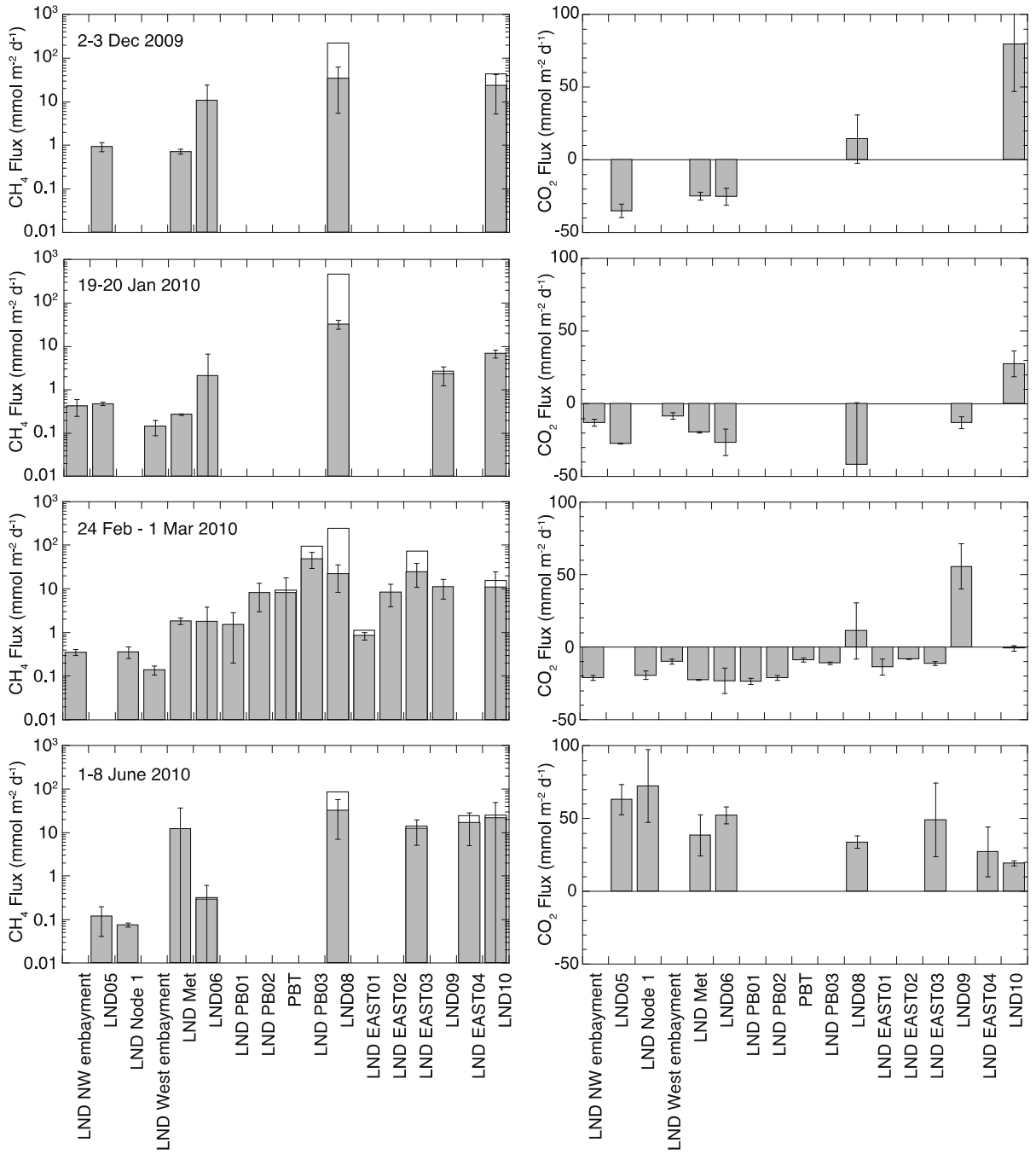

Figure 14: Reservoir-scale spatial variability in CH_4 and CO_2 fluxes in Little Nerang Dam during each field trip: 2-3 Dec 2009, 19-20 Jan 2010, 24 Feb - 1 Mar 2010, 1-8 Jun 2010. Shaded bars denote 'scaled' flux; hollow bars denote 'instantaneous' flux. Note logarithmic scale for CH_4 flux. Error bars denote standard deviation of flux measurements.

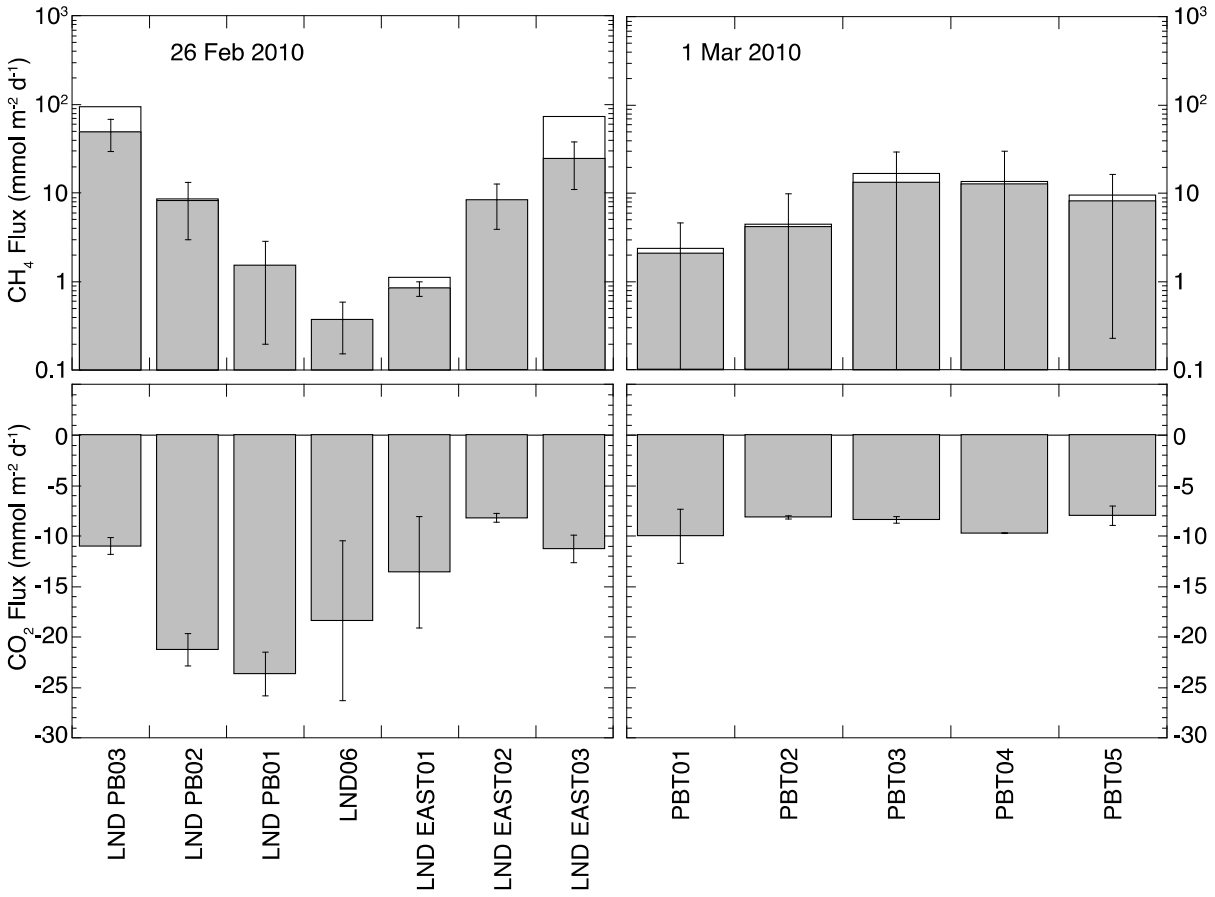

Figure 15: Small - medium scale spatial variability of floating chamber CH_4 flux measurements at Little Nerang Dam along the two tributary arms (26 Feb 2010) and across the western tributary (1 Mar 2010). See Figure 4 for exact locations. Shaded bars denote 'scaled' flux; hollow bars denote 'instantaneous' flux. Note logarithmic scale for CH_4 flux. Error bars denote standard deviation of flux measurements.

5.2.1.4. Short-Term Temporal Variability of CH_4 and CO_2 Fluxes

The temporal variability of flux chamber measurements at individual sites in Little Nerang Dam is shown in Figure 16 to Figure 19. Short term variability was explicitly studied at sites LND10 (2-3 Dec 2009, Figure 16) and LND06 (20 Jan 2010, Figure 17) by performing sequential floating chamber measurements as frequently as practically possible over periods of 9 and 12 hours.

At site LND10, continuous deployments were undertaken from 2156 h on 2 Dec through 0028 h on 3 Dec following three measurements close to midday. During this period individual fluxes varied by up to a factor of 50 (Figure 16) when considering 'instantaneous' fluxes or a factor of 10 considering 'scaled' fluxes. During this experiment, CO_2 fluxes varied by roughly a factor of 4 and were always from the water to the atmosphere demonstrating net heterotrophy on a local scale. For both gases, fluxes increased from midday to 2320 h and then remained relatively unchanged through 0028 h.

Similar temporal variability was observed at site LND06 on 20 Jan 2010 where measurements were made between 0700 – 1600 h (Figure 17). CH_4 fluxes varied by up to a factor of 80 due to the occasional presence of bubbles between 0841 h and 0924 h. There was also a trend towards increasing fluxes of both gases throughout the experiment with the highest fluxes observed during mid-afternoon. In contrast to LND10, the CO_2 flux at LND06 was always into the water demonstrating net autotrophy at this location.

An interesting feature of the observations at LND06 (Figure 18) is the very large difference in emissions between days on 2 - 3 Dec 2009 and on 24, 26 Feb 2010. In both cases, the average daily emission varied by a factor of 10 between days on the same field trip.

5.2.1.5. Seasonal Variability of CH_4 Fluxes

No significant seasonal trend in measured methane fluxes was observed at Little Nerang Dam. At sites LND06, LND10 (Figure 18) and LND08 (Figure 19) variability during a day was as large as variability between field trips. At LND Met (Figure 19) a sudden peak in emissions in Feb 2010 interrupted what may otherwise have been a steady decrease in methane flux during the project. The impact of a very large inflow in February and anomalously large drawdown of the reservoir later in the year confounds the interpretation of the data on a seasonal basis.

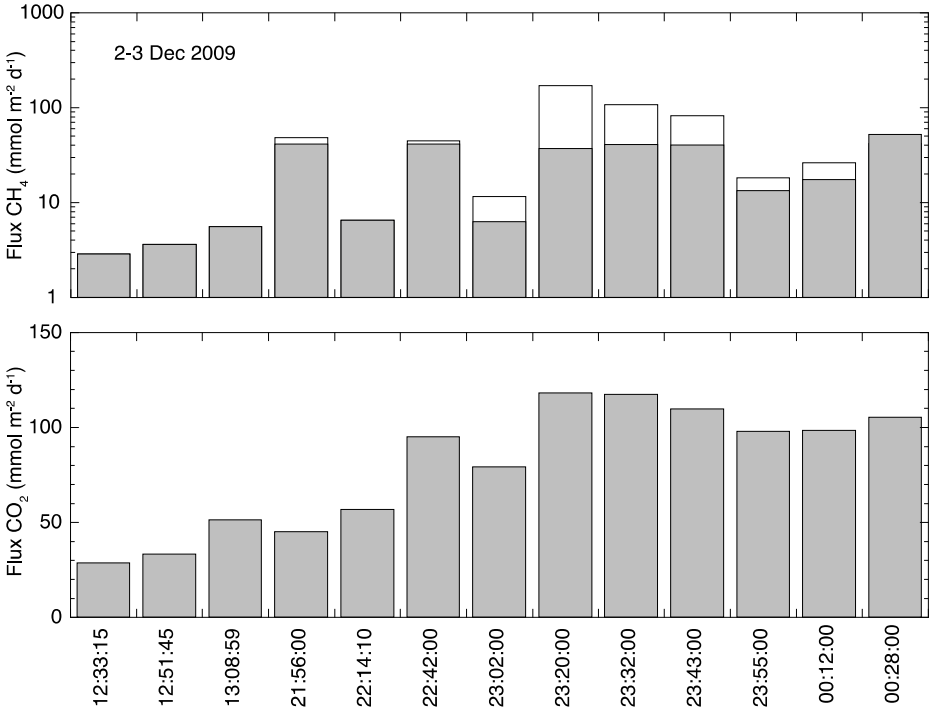

Figure 16: Short term variability of CH_4 and CO_2 flux measured at site LND10 on 2-3 Dec 2009. Solid bars denote 'scaled' flux; hollow bars denote 'instantaneous' flux.

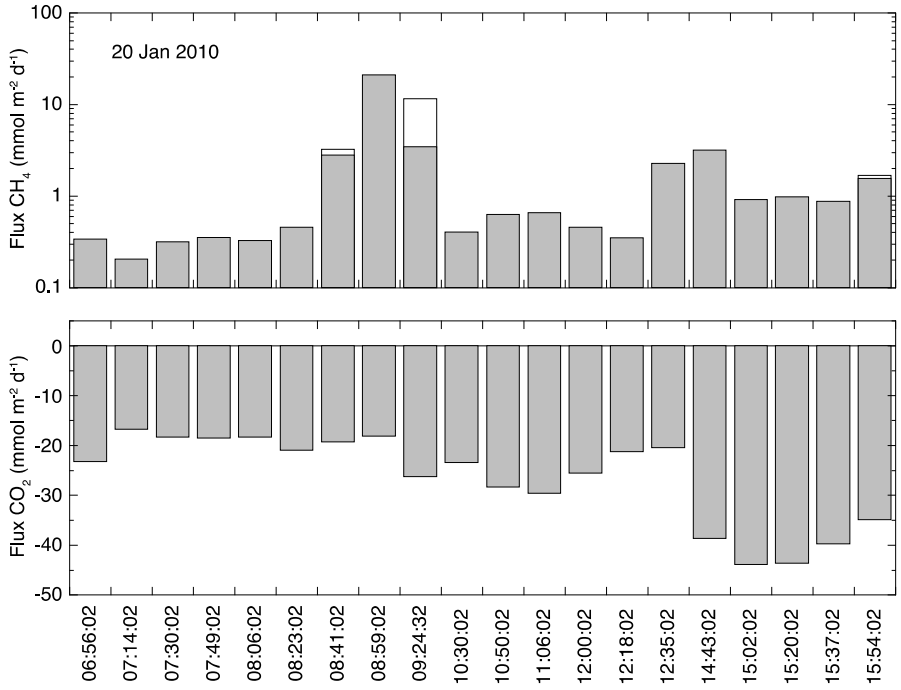

Figure 17: Short-term variability of CH_4 and CO_2 fluxes measured at site LND06 on 20 Jan 2010. Solid bars denote 'scaled' flux; hollow bars denote 'instantaneous' flux.

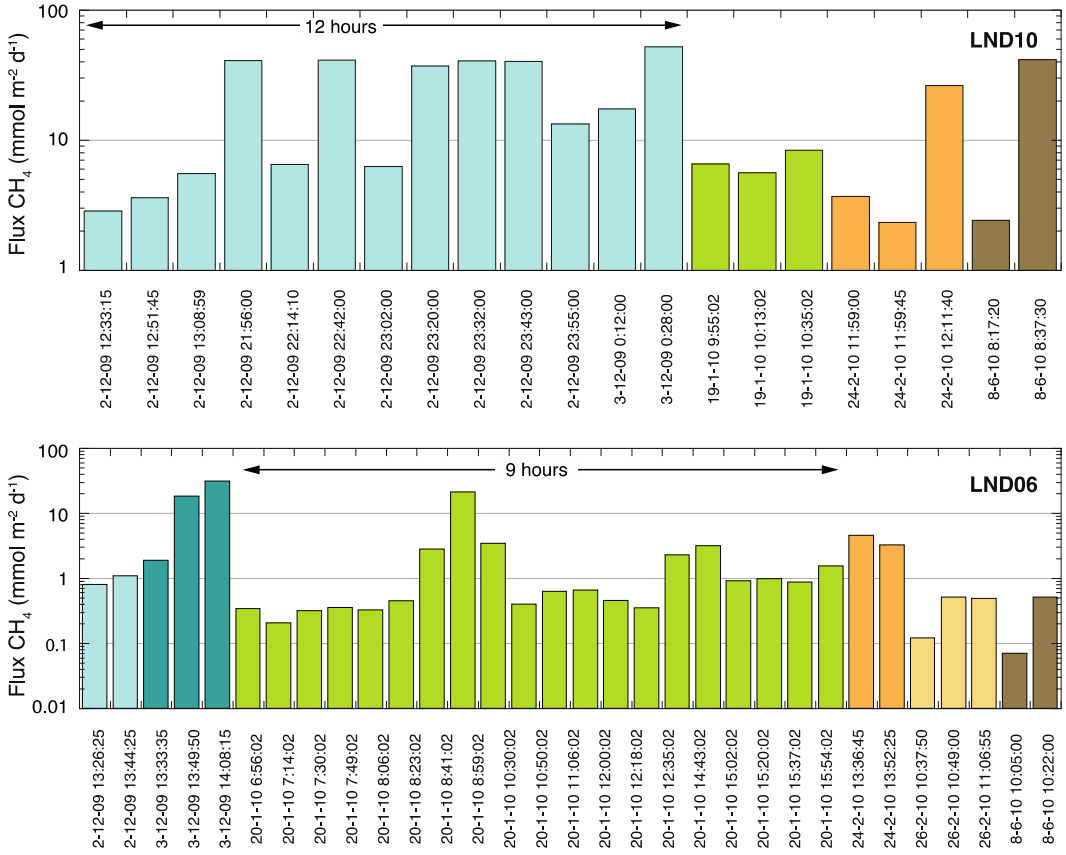

Figure 18: Short-term and seasonal variability of floating chamber CH_4 flux at Little Nerang Dam sites LND10 (top) and LND06 (bottom). Colours denote a single day's survey.

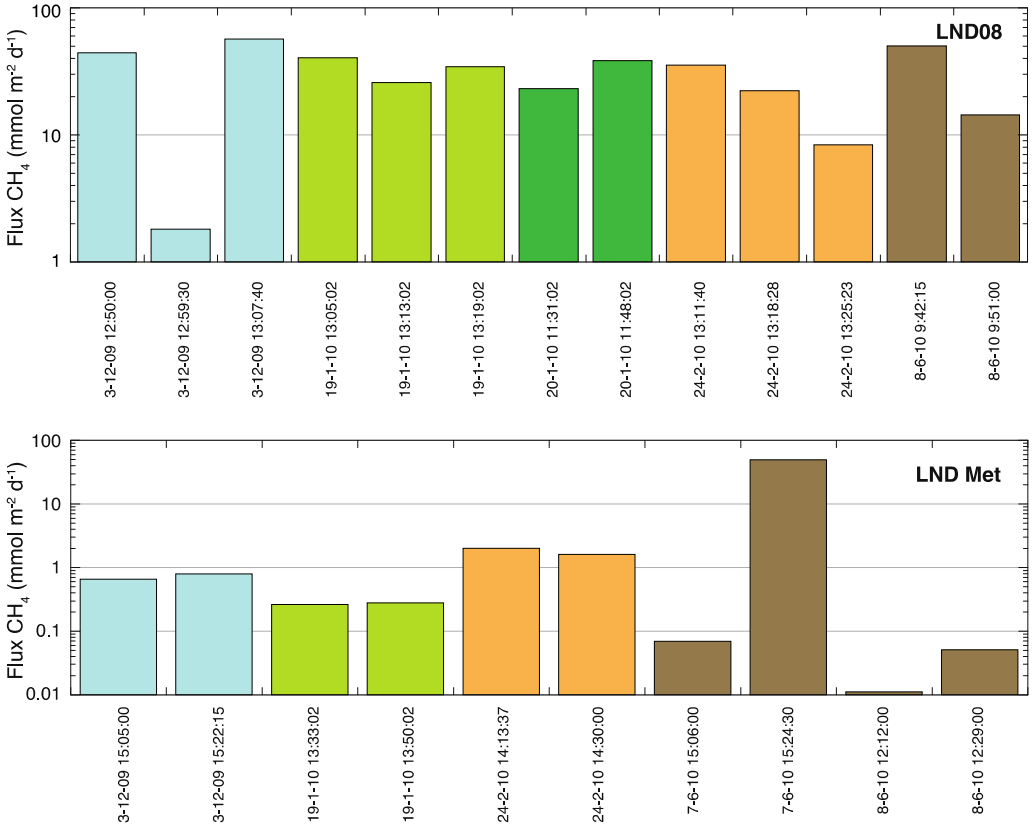

Figure 19: Seasonal variability of floating chamber CH_4 flux at Little Nerang Dam sites LND08 (top) and LND Met (bottom). Colours denote a single day's survey.

5.2.2. Hinze Dam

Flux chamber measurements were made in Hinze Dam in late summer and three times during winter (27-28 Feb 2010, 30 Jun -1 Jul 2010, 16 Jul 2010, 13 Aug 2010) in an attempt to capture the impact of seasonal overturn of thermal stratification on the flux of methane from the reservoir. Limited resources and the much larger extent of Hinze Dam meant that less extensive spatial coverage of the reservoir was possible compared to Little Nerang Dam. Based on the experience at Little Nerang Dam measurement sites were chosen to try to best resolve the most significant spatial gradients in fluxes in Hinze Dam.

5.2.2.1. Spatial Variability of CH_4 flux

All flux measurements made at Hinze Dam are presented, organised by field trip, in Figure 20. The first survey was performed during Feb 2010 and revealed relatively uniform fluxes in the arm receiving water from Little Nerang Dam (~ 1 mmol m^{-2} d^{-1} from Hinze01 to Hinze05). Fluxes were lowest in the deep main basin of the reservoir closest to the dam wall (Hinze10 - Hinze13) and there was a strong gradient of fluxes increasing towards the upstream end at Hinze06 where the flux was 25-100 times greater (~ 25-130 mmol-CH_4 m^{-2} d^{-1}; range reflects scaled and instantaneous flux values) than the fluxes in the main basin near the dam. This pattern of fluxes increasing towards the deposition zone at the upstream end of the reservoir was very similar to that observed in Little Nerang Dam.

The second field trip to Hinze Dam (30 Jun - 1 Jul 2010) focused on resolving the spatial gradients in the high flux region around Hinze06 and Hinze07. The measurements revealed very large (50-fold) differences in fluxes over distances of 50 – 100 m (e.g. fluxes at sites Hinze07i, Hinze07h and Hinze07g, Figure 20).

Time constraints only allowed for measurements at four sites across both arms during the third field trip (16 July 2010, Figure 20). Fluxes were the lowest recorded at sites Hinze04, Hinze13 and Hinze10. This was despite the fact that, during the preceding fortnight (1 - 15 July 2010), the surface mixed layer of the reservoir deepened from 18 to 28 m and, by inference, entrained dissolved CH_4 into the surface layer (Figure 13).

The final field trip was timed to coincide with water column turnover. Turnover was accompanied by an increase surface layer [CH4] (Figure 9) and higher fluxes at sites Hinze10, Hinze09 and Hinze06 compared with preceding visits to these sites. Hinze07f continued to emit at ~ 38 mmol m^{-2} d^{-1}.

The third (16 Jul 2010) and fourth (13 Aug 2010) field trips confirmed the persistence of high fluxes (~ 3-65 mmol m^{-2} d^{-1}, mean 27) at sites Hinze07f and Hinze07h – there was little change in temperature (< ~ 0.5 °C) at the bottom of the water column and there was always 5 – 7 mg L^{-1} of dissolved oxygen at the bottom of the water column (Figure 39).

The reservoir-scale longitudinal gradient characterised by CH_4 fluxes being highest at the upstream ends of the reservoir was observed during each of the four field trips.

5.2.2.2. Spatial Variability of CO_2 Flux

Hinze Dam exhibited net heterotrophy during all four field trips; the CO_2 flux was always from the water to the atmosphere. This contrasts strongly with Little Nerang Dam's observed autotrophy.

In contrast to the gradient in CH_4 flux with the highest fluxes at the upstream end, the CO_2 flux was consistently lowest at the upstream end of the reservoir near sites Hinze06 and Hinze07 (Figure 20). The CO_2 flux was substantially higher (~ 250 mmol m^{-2} d^{-1}) in the Little Nerang River arm (Hinze01 - Hinze05) than elsewhere in the reservoir where the flux ranged from 0.6-240 (mean 98) mmol m^{-2} d^{-1}. Note that the Little Nerang arm was only measured thoroughly during the Feb 2010 field trip. However, site Hinze04 emitted CO_2 at a similar rate when measured again on 16 Jul 2010.

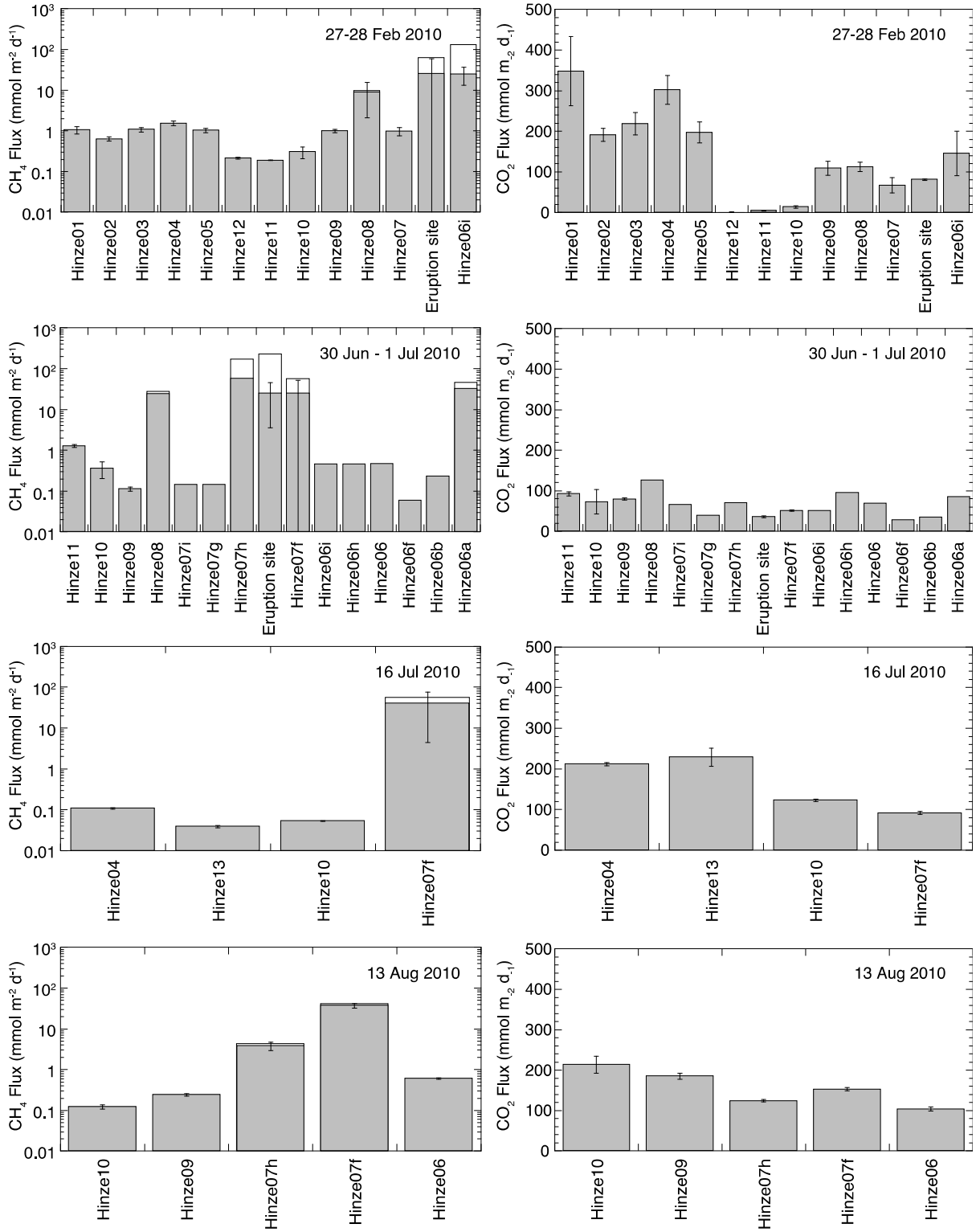

Figure 20: Reservoir-scale spatial variability in CH_4 and CO_2 fluxes in Hinze Dam during each field trip: 27-28 Feb 2010, 30 Jun - 1 Jul 2010, 16 Jul 2010, 13 Aug 2010. Shaded bars denote 'scaled' flux; hollow bars denote 'instantaneous' flux. Note logarithmic scale for CH_4 flux. Error bars denote standard deviation of flux measurements where more than one deployment was made on the day.

While performing a measurement at Hinze07 on 28 Feb 2010, a large eruption of bubbles was observed a short distance away (Figure 21). Bubbling was so intense that the surface was effervescent. Figure 22 shows typical conditions at nearby site Hinze07f which typically emitted ~ 34-51 mmol-CH_4 m^{-2} d^{-1} (scaled - instantaneous). Intense, but relatively infrequent, bubble events are often observed by the local rangers (Fairall, pers. comm.). Although short-lived, the emission from this eruption could well be in the range 10^4 - 10^5 mmol-CH_4 m^{-2} d^{-1} based on our observations of surface disturbance during high measured chamber fluxes approaching 100 mmol-CH_4 m^{-2} d^{-1}.

Figure 21: Massive bubble event at Hinze Dam near site Hinze07 on 28 Feb 2010. The diameter of the disturbed area is approximately 5 m.

Figure 22: Disturbance of water surface near Hinze07f. The continuous stippling of the surface is characteristic of this part of the dam where fluxes often approach 1000 mg m^{-2} d^{-1}.

5.2.2.3. Temporal Variability

No attempt was made to examine short-term (diurnal) variability in fluxes at any of the Hinze Dam sites. Average fluxes at each site during each field trip are shown in Figure 20. Although fluxes measured on 16 July were the lowest observed at three of the four sites visited, there was no obvious trend in fluxes between February and August.

The low fluxes in mid-July were surprising given that [CH4] was not substantially different compared to 1 July (Figure 11) and the average wind speed recorded on the boat during mid-July was almost double that during the previous field trip (data not shown). Inspection of temperature profiles collected at the same time as [CH4] samples revealed a shallower surface mixed layer depth in mid-July compared to the other trips. This suggests less vigorous mixing within the upper water column and presumably less frequent renewal of the surface film at the air-water interface which is believed to govern the air-water flux of dissolved gases. Water turbulence was measured using an ADV and this data could confirm or refute this hypothesis. However, the ADV data have not been analysed due to lack of resources.

5.2.3. Bubble Flux Variability

When bubbles enter the floating chamber, they are the dominant contribution to the large flux measurements. Nearly forty percent of the chamber measurements (82 of 202) indicated the presence of bubbles. We now consider the probability distribution of the measured bubble fluxes exceeding a specific magnitude.

Figure 23 shows the probability distribution of both 'scaled' and 'instantaneous' fluxes for the 82 measurements impacted by bubbles. Fifty percent of the instantaneous measurements exceeded 26 mmol-CH_4 m^{-2} d^{-1}. Considering the conservative 15-minute scaled fluxes we find that 50% exceed 17.5 mmol-CH_4 m^{-2} d^{-1} (Figure 23, Table 7).

Table 7: Methane bubble flux statistics. the instantaneous flux is the measured flux during the chamber deployment. The scaled flux is a conservative estimate that assumes no additional CH_4 is emitted during the interval between the end of the measurement and 15 minutes from the beginning of the measurement.

	Instantaneous Flux mmol-CH_4 m^{-2} d^{-1}	Scaled Flux mmol-CH_4 m^{-2} d^{-1}
Minimum	0.6	0.5
Maximum	1,773.3	69.2
Points	82.0	82.0
Mean	83.4	22.2
Median	25.6	17.5
Std Deviation	210.6	18.0

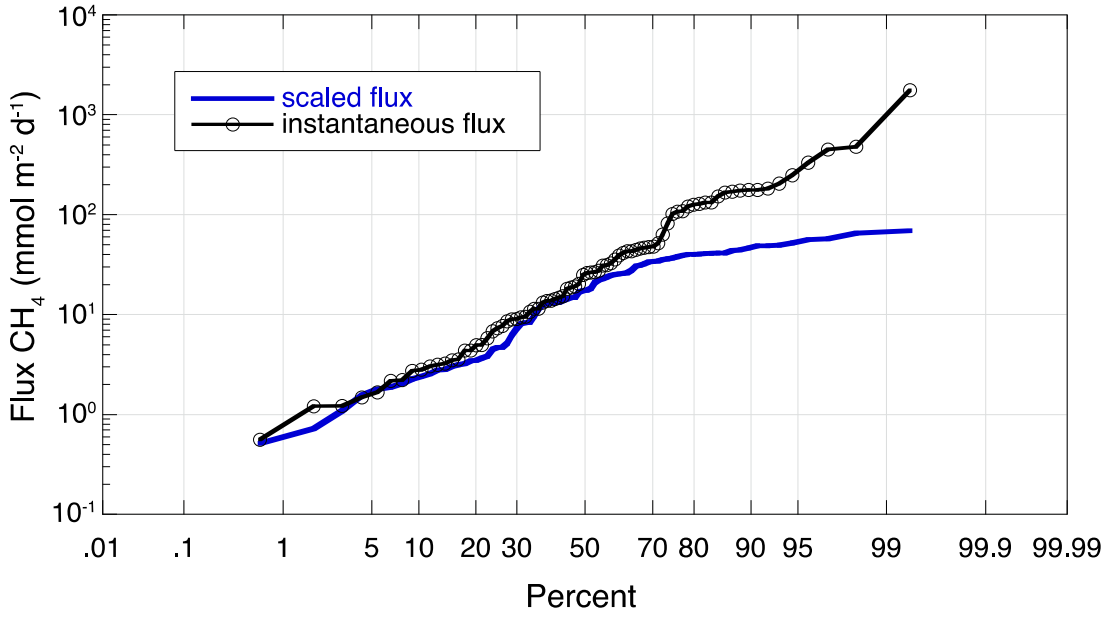

Figure 23: Probability distribution of the 'instantaneous' measured and 15-minute 'scaled' bubble fluxes of methane.

The observed frequency of bubble events provides a test of whether or not the bubble event fluxes are biased towards a high value. Should a chamber deployment's duration be less than the average interval between bubble events then it is likely that the flux may be overestimated compared to a hypothetical 'true' value.

The exceedence probability for the period between conspicuous bubble events measured at the high flux sites (LND10, Hinze06i, Hinze07f) are shown in Figure 24. These sites demonstrate qualitatively similar behaviour. The mean period between bubble events at Hinze06i and Hinze07f was 320 ± 230 (s.d.) seconds. At LND10 the mean period was 345 ± 195 (s.d.) seconds. The median intervals were 267 and 379 s, respectively.

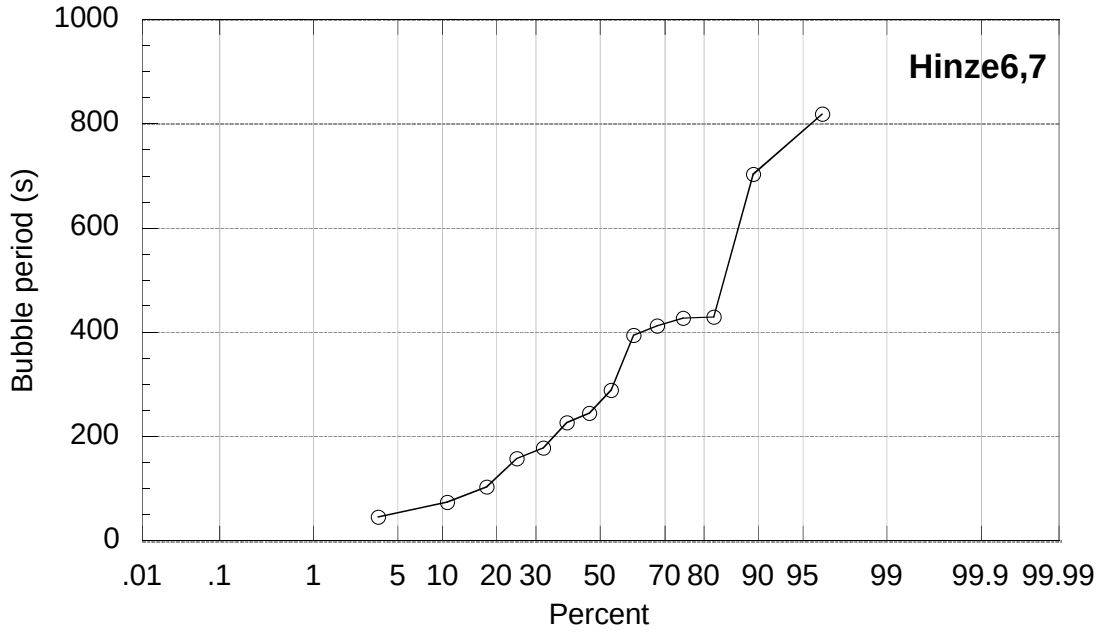

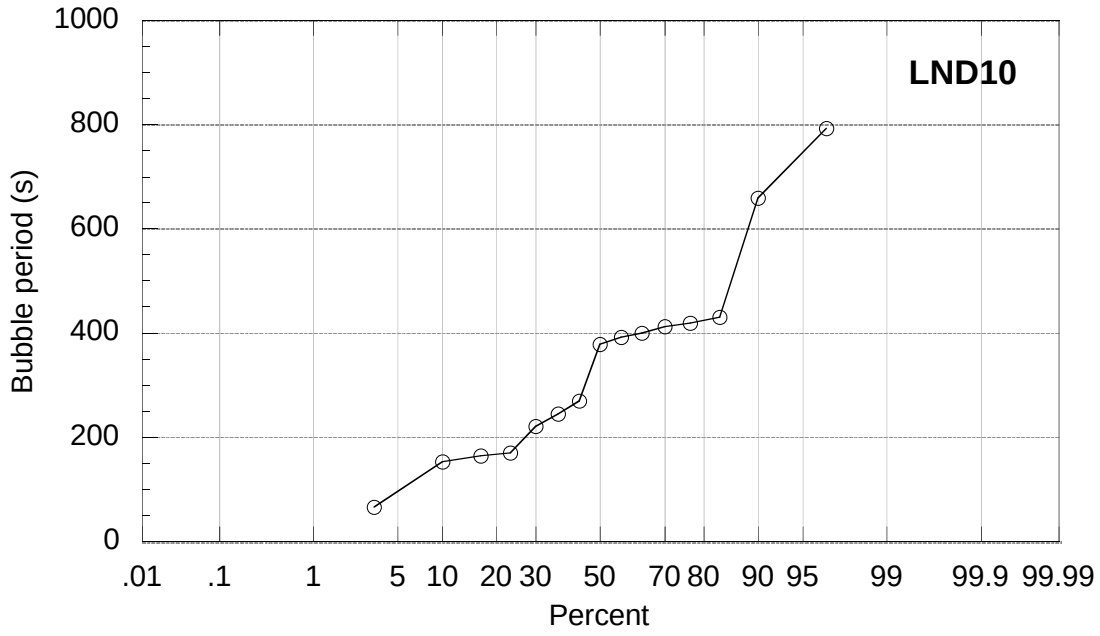

Figure 24: Probability of bubble event period at sites Hinze06i, Hinze07f and LND10. Only chamber measurements including bubble events are considered.

5.3. Whole of Reservoir Flux Estimates

The areal mean methane fluxes were calculated for Little Nerang and Hinze Dams using Equation (4). Two approaches were taken to the averaging and interpolation of flux chamber measurements to allow whole-reservoir estimates:

1. Average all measurements performed at a site during the entire project to give a single estimate of the average flux for that site. The mean values for each site were then used to produce a single estimate for each reservoir's average emission.

2. Average all data for each site visited during a single trip and compute the mean reservoir flux on a trip by trip basis. For sites that were not visited during a trip, the lowest value of the adjacent measured sites during that trip was assumed to apply. For example, if the flux was measured at sites Hinze07 and Hinze09 but not at Hinze08, the lower of these measured fluxes was assumed to apply to the fractional area of the reservoir represented by site Hinze08.

Both approaches were applied to 'instantaneous' and 'scaled' flux values. The results are shown in Figure 25. Whole reservoir estimates of the methane flux computed using the scaled fluxes (light-grey bars) provide the most conservative estimate consistent with the data. Considering all the data, the areal mean methane fluxes from Little Nerang Dam were 135 and 61 mg-CH_4 m^{-2} d^{-1} (8.4 and 3.8 mmol m^{-2} d^{-1}) using 'instantaneous' and 'scaled' data, respectively. For Hinze Dam the corresponding values were 44 and 28 mg-CH_4 m^{-2} d^{-1} (2.8 and 1.8 mmol m^{-2} d^{-1}), respectively.

Note that Little Nerang Dam was sampled across summer, autumn and winter and an annual mean flux can be computed. Hinze Dam was sampled once in early autumn and more intensively throughout the winter until seasonal overturn occurred. Furthermore, funding constraints reduced the number of flux measurement sites that could be visited at Hinze Dam during winter so there is much more uncertainty associated with the spatial extrapolation of measured values in Hinze Dam. Based on the observation during the Feb 2010 sampling at Hinze that the dominant emitting area was the western arm, a decision was made to place more emphasis on measuring fluxes in this arm.

The main basin plus the eastern arm of Hinze Dam (sites Hinze01-Hinze05 plus Hinze11 - Hinze13) represents about 70% of the total surface area of the reservoir and accounted for 10-25% of the total flux for three of the four field trips and 2-3% for the 15-16 July trip. The low contribution during the mid-July trip may incorporate an overestimate of the flux arising from the lack of any measurement upstream of site Hinze07f so that the consistently large fluxes observed at Hinze07f during each trip was extrapolated upstream following the calculation protocol.

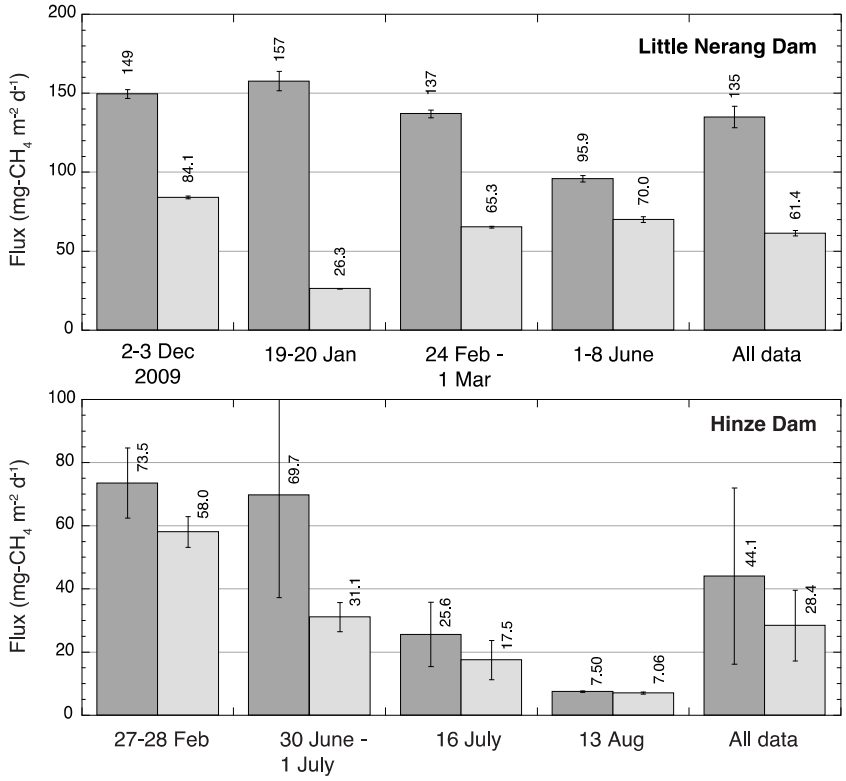

Figure 25: Areal mean CH_4 fluxes measured at Little Nerang Dam (top) and Hinze Dam (bottom). Estimated whole reservoir fluxes are shown for each field trip and for all data. Dark bars represent 'instantaneous' flux measurements whereas light bars represent the most conservative 'scaled' flux values.

5.4. Dissolved Methane Storage Flux

The relative lack of horizontal variability in the Hinze Dam dissolved [CH4] profiles (Figure 13) allowed mass balance calculations to be performed for each date by averaging all observed concentrations at a given depth to provide a mean concentration profile representative of the entire reservoir.

The total mass of dissolved methane in Hinze Dam (computed using Equation 7) decreased from 37.4 tonnes to 4.4 tonnes between 1 July 2010 and 12 August 2010 (Table 8) as the surface layer of the reservoir progressively deepened during winter cooling. The corresponding areal loss rates were 166 mg-CH_4 m^{-2} d^{-1} (10 mmol m^{-2} d^{-1}) during 1-15 July 2010 and 45 mg-CH_4 m^{-2} d^{-1} (2.8 mmol m^{-2} d^{-1}) during 15 July - 12 August 2010.

Table 8: Hinze Dam water stored methane, water level and surface area. Capacity was taken from seqwater.com.au/public/dam-levels. Volume is calculated assuming a volume of 161070 ML when full corresponding to a reference level of 82.20 m AHD.

Date	Hinze Capacity	Hinze Water Level (derived)	Mass of Dissolved CH_4 in Reservoir (tonnes CH_4)	Reservoir Surface Area (ha)	Observed Loss of Dissolved CH_4 Expressed as Surface Flux (mg-CH_4 m^{-2} d^{-1})
1 July 2010	96.9%	81.67	37.4	926	
15 July 2010	96%	81.51	15.9	917	166
12 August 2010	94.5%	81.25	4.4	912	45

6. DISCUSSION

6.1. Spatial Distribution of Dissolved CH_4 and CH_4 Flux

Both surface layer dissolved methane concentration, [CH4] (Section 5.1), and the measured CH_4 fluxes (Section 1.1) were highest at the upstream ends of both reservoirs. As well, ebullition was always visible and occurred at the highest rates at these locations in both dams. These areas are believed to be the deposition zones for fresh organic matter arriving from the catchment – a hypothesis consistent with observations of the exposed bottom during draw down of Little Nerang Dam (A. Grinham, personal communication; Figure 26). These deposition zones are shallower and as a result experience generally greater temperatures at the sediment-water interface. The combination of higher organic matter loading and warmer temperatures would support higher methane production rates than elsewhere in the reservoir. In addition, the shallower water depth facilitates bubble fluxes relative to the diffusive flux because: 1) the lower hydrostatic pressure will allow more rapid bubble growth and more frequent bubble detachment and emission; and 2) there is less time for methane in bubbles to dissolve into the water during the passage of the bubble through the water column to the atmosphere.

When aggregated over the entire reservoir to compute the areal mean methane flux, the spatial variability of the measured fluxes reveals how important it is to resolve areas of high fluxes. In Little Nerang Dam, 80% of total reservoir CH_4 emissions emanated from 10% of the surface area. In Hinze Dam, 60% of the total CH_4 flux came from 6% of the surface area.

Little Nerang Dam exhibited higher dissolved CH_4 concentrations in the surface layer compared to Hinze Dam. Both reservoirs had qualitatively similar spatial gradients with dissolved CH_4 increasing towards the upstream ends of the reservoirs dam (Figure 9 and Figure 10, Table 4). The spatial gradient was more pronounced in Little Nerang Dam due to the very high concentrations at LND10. In Hinze Dam the concentration typically ranged from 0.008 mg-CH_4 L^{-1} (0.5 mM) near the dam to 0.014 mg-CH_4 L^{-1} (0.9 mM) at the upstream sites of both arms. In Little Nerang Dam the corresponding range was from 0.01 to 0.09 mg-CH_4 L^{-1} (0.6 - 5.6 mM). Concentrations and temporal variability were lowest at the deepest sites in both reservoirs (Hinze12, Hinze13, Hinze5, LND05, LND Node1).

The higher dissolved [CH4] in Little Nerang Dam during 7-9 June (Figure 12) may reflect the influence of runoff from a rainfall event on 3 June followed by the passage of a cold front with higher than usual winds and cold, clear night skies that increased the intensity of convective mixing during the evenings and cooled the epilimnion by 0.5 °C. The cold inflows could facilitate exchange of water between the accumulated debris and the overlying water column at the upstream ends of the reservoir. In addition, penetrative convection will entrain dissolved CH_4 from the top of the chemocline into the surface mixed layer as the surface layer deepens. Note also that the turbulence produced by penetrative convection is also known to facilitate gas transfer across the air-water interface (Macintyre 1998; Schladow *et al*. 2002).

We believe the large increase in dissolved methane in the surface layer of Hinze Dam on 12-13 Aug 2010 reflects the impact of complete mixing (seasonal overturn) of the water column. Methane accumulated at depth in the basin near the dam wall would have been mixed into the water column as a result of penetrative convection that mixed the water column completely on 26 July 2010. Only water > 27-30 m deep could have contributed to the observed increase. Strong winds blowing from the dam towards Hinze02 during the site visit would have carried the higher-CH_4 water towards sites Hinze04 and Hinze02. The lack of a spike in concentration at either site Hinze03 or Hinze01, however, is not consistent with this hypothesis.

Although the analysis for Hinze Dam is limited to winter conditions, the spatial gradients are expected to be a persistent feature of both storages throughout the year.

Figure 26: Accumulation of coarse woody debris at upstream end of Little Nerang Dam. Photos courtesy A. Grinham.

6.2. Are Large, Infrequent Bubble Events Important?

Large, short-duration bubble events are frequently observed by staff at the reservoirs but were not captured by any of our measurements. One very large example of such an event was observed in Hinze Dam and photographed and we estimate emissions from this event to be in the range of 10^5 to 10^6 mg-CH_4 m^{-2} d^{-1} with a duration of 5 minutes and occurring over a region of roughly 10 metres diameter. If such an event occurred on a daily basis at a single site it would add less than 0.03 mg-CH_4 m^{-2} d^{-1} to the total flux for Hinze Dam.

6.3. Diffusive Fluxes

The diffusive flux of gases across the air-water interface is generally assumed to scale with both wind speed and their concentration just below the water surface. When the floating chamber method is used to measure gas fluxes, it is generally assumed that a linear change in concentration with time indicates that diffusive fluxes dominate. Data collected in this project departs from this assumption. Figure 27 plots the measured diffusive fluxes of CO_2 and CH_4 against the product ([CH4]*wind) of surface layer dissolved CH_4, [CH4], and the mean local wind speed measured on the boat during the deployment. We did not measure pCO_2 and make the assumption that pCO_2 is linearly related to [CH4] for illustrative purposes.

It is apparent from the data that CO_2 fluxes measured in this project conform much more closely with the assumed diffusive flux scaling than do the CH_4 fluxes despite the fact that the CH_4 fluxes appeared, from visual inspection of the floating chamber data, to also be diffusive. This implies that another process may be contributing to the 'diffusive' flux of methane from these reservoirs. Yves Prairie (University Quebec at Montreal, pers. comm.) has speculated about the possibility of micro-bubble fluxes of methane. In this case, one can think of a very fine mist of bubbles continuously rising through the water column and escaping to the atmosphere. Such a process would produce a linear change with time of headspace CH_4 concentration in the floating chamber headspace, qualitatively similar to the conventional 'diffusive' flux, but driven by methane production in the water column and sediments rather than by diffusion of dissolved methane. We can only speculate about this, but our data are consistent with the micro-bubble hypothesis.

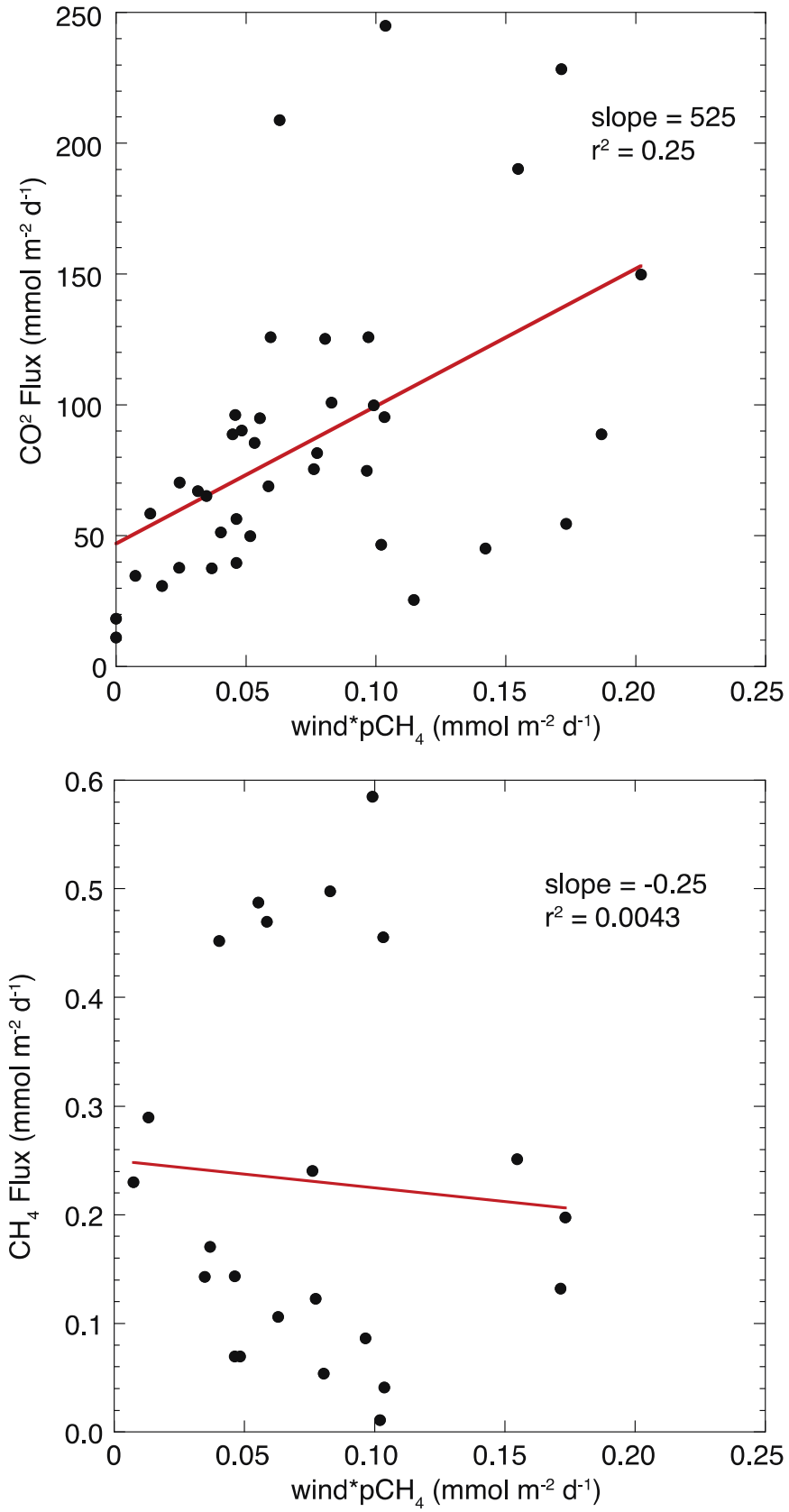

Figure 27: Diffusive fluxes of CO_2 (top) and CH_4 (bottom) versus the product of [CH4] and mean local wind speed at the time of measurement.

6.4. Fate of Stored Methane during Overturn

The data collected do not allow us to conclusively identify the fate of stored methane that disappeared during seasonal overturn of the thermal stratification. We know that the reduction in stored methane can only occur through a combination of atmospheric exchange and biological consumption. In this project, the relative proportions lost through each pathway could not be explicitly determined as no data on the microbial population in the reservoir were collected. However, it is possible to interpret our data in the context of estimates of the flux pathways in Figure 2 and compare these estimates with those reported for other lakes and reservoirs.

For example, if we assume that the microbial population has not changed over time, i.e. that it remains in balance with the diffusive flux along the chemocline (i.e., its food supply), and the epilimnion [CH4] concentration does not change, then $F_{biota} = F_{gradient} - F_{atm}$ and the loss of stored methane must have been lost to the atmosphere. How well does this estimate of F_{biota} compare with observations elsewhere in the world?

6.4.1. Gradient Flux Estimate

Although vertical turbulent diffusivity, κ_z, was not directly measured, it can be estimated for Hinze Dam from detailed (2 m spacing, 10 minute temporal resolution) thermistor chain data collected during 1998-1999 (Jones and Sherman 1999). During spring 1998, the average daily temperature at 14, 25 and 29 m depth increased linearly with time from 9 Sep 1998 to 24 Dec 1998 ($r^2 > 0.92$). The second derivative of the temperature gradient, d^2T/dz^2 was computed using finite differences from the available data and the thermal diffusivity was calculated as:

$$\kappa_z = \frac{\frac{dT}{dt}}{\frac{d^2T}{dz^2}} \tag{8}$$

Using this method, the vertical diffusivity was computed as 2.6×10^{-6} m^2 s^{-1}. This is approximately 30 times the level of molecular diffusivity of heat and consistent with observations across a large number of reservoirs, including similar calculations performed for Chaffey Dam, NSW (Sherman *et al*., 2000). Because mass is not transported more quickly than heat we can use this value of diffusivity to compute the maximum expected methane flux through the chemocline, $F_{gradient}$, as 2.6×10^{-6} g-CH_4 m^{-2} s^{-1} or 228 mg-CH_4 m^{-2} d^{-1}.

6.4.2. Biotic Consumption Estimate

Methanotrophs are obligate aerobes and are typically found within or near the top of the oxycline where their position allows them to consume the methane that diffuses vertically upward along the concentration gradient while accessing oxygen supplied from above. If we assume the methanotroph population does not change appreciably during the interval between field trips and that their ability to assimilate methane is not impacted by being redistributed throughout the water column as a result of autumnal deepening, then the observed loss in mass of dissolved methane can be assumed to have been lost to the atmosphere.

According to Equation (6), the gradient flux must be distributed between the change in epilimnetic CH_4, exchange with the atmosphere and consumption by biota. Over the top 16 m of the water column, the loss of dissolved CH_4 between 1 and 16 July was equivalent to a flux of 4 mg-CH_4 m^{-2} d^{-1}. Assuming an average diffusive flux to the atmosphere of 9.1 mg-CH_4 m^{-2} d^{-1} (the average of all purely diffusive flux measurements at Hinze Dam was 9.1 ± 8.1 mg-CH_4 m^{-2} d^{-1}) leads to a biotic consumption of roughly 220 mg-CH_4 m^{-2} d^{-1}. Bastviken *et al*. (2002) studied bacterial methane oxidation in three lakes and reported a range of average oxidation rates of 0.25 – 81 mg-C m^{-2} d^{-1} (equivalent to 0.33 – 108 mg-CH_4 m^{-2} d^{-1}). Our estimate of the oxidation rate in Hinze Dam is a factor of two higher than the high value of Bastviken *et al*. (2002) measured under colder conditions in

Sweden, but within the 10-700 mg-C m^{-2} d^{-1} range of area-specific methane oxidation rates reported by other researchers as cited by Bastviken *et al*. (2003).

6.4.3. Sediment Methane Production Estimate

The rate of production of methane in the sediments and dissolved into the hypolimnetic water can be estimated from the observed change in [CH4] in the hypolimnion and the gradient flux. The mass of CH_4 in the hypolimnion (below 25 m depth = elevation 56.67 m AHD) on 1 July 2011 was 2.68 x 10^{10} mg CH_4 and the sediment area at this elevation is 1.73 x 10^6 m^2. Assuming CH_4 began accumulating with the nominal onset of seasonal stratification on 1 September requires a net supply of 51 mg-CH_4 m^{-2} d^{-1}. Adding in the vertical diffusive transport increases α F_{sed} to approximately 276 mg-CH_4 m^{-2} d^{-1}, where α is the fraction of the sediment flux that dissolves into the hypolimnion. Next, we constrain α using the measured total reservoir flux, i.e.

$$F_{Total} = F_{atm} + F_{bubble} = F_{atm} + (1 - \alpha)F_{sed}$$

which simplifies after substituting α F_{sed} = 276 to

$$F_{sed} = F_{Total} - F_{atm} + 276$$

giving a range of 295 – 310 mg-CH_4 m^{-2} d^{-1} for F_{sed}, the sediment methane production rate. The corresponding values indicate that roughly 90% of the sediment methane production is dissolved into the hypolimnion.

In fact, the true supply may be greater than this because the surface mixed layer (SML) in July was already 18 m deep, and seasonal deepening of the SML would have reduced the volume of the hypolimnion while entraining dissolved CH_4 into the SML where it would be outgassed to the atmosphere. During normal spring and summer stratified conditions at Hinze Dam, the SML is typically < 5 m deep and rarely exceeds 7 m depth (Jones and Sherman, 1999).

6.4.4. Loss of Stored Dissolved Methane during Water Column Overturn

Between 1 and 16 July 2010 the loss of dissolved methane was equivalent to an average flux of 166 mg-CH_4 m^{-2} d^{-1} (Table 8), whereas the estimated emission from the flux chamber measurements was in the range 18 – 70 mg-CH_4 m^{-2} d^{-1} at this time (Figure 25). Even after allowing for a 30% error in the mass balance calculation, the resultant flux is substantially greater (by up to 40 mg-CH_4 m^{-2} d^{-1}) than the areal mean emission estimated for Hinze Dam at this time. To reconcile the difference requires a combination of increased biotic consumption of CH_4 and a systematic underestimate of the reservoir flux based on the floating chamber measurements.

Floating chambers are generally believed to overestimate diffusive fluxes because turbulence produced by the flow of water around the chamber edges increases turbulence (Vachon *et al*. 2010). It is possible, however, that our floating chamber measurements are biased towards underestimates of the diffusive flux because our measurements are made during the day and often under very calm conditions. Calm conditions reduce the relative contribution of turbulence generated by the chamber. Measurement during the daytime samples the water column at its least turbulent and it could be that turbulence and surface mixed layer deepening caused by penetrative convection produce higher emissions late at night (Macintyre 1998; Schladow *et al*. 2002) and consistent with the nighttime observations at Little Nerang Dam (Figure 16). Given that the loss of dissolved methane would be expected to appear as a diffusive flux and that apparent 'diffusive' CH_4 fluxes seldom exceeded 30 mg-CH_4 m^{-2} d^{-1}, a systematic bias in the floating chamber measurements of 130% is unlikely and therefore cannot explain the difference.

It is also possible that the spatial resolution of the floating chamber (FC) measurements did not sufficiently resolve the true variability in the reservoir's flux and that low measured fluxes were incorrectly extrapolated when computing the areal mean flux for the reservoir. This error would be greatest for the 14-15 July and 12-13 August measurements due to the reduced sampling effort. However, it is unlikely that higher spatial resolution would have increased the mean diffusive flux sufficiently to account for the offset.

It is difficult to assess the magnitude of any error associated with changes in the biotic consumption of CH_4. At 215 mg-CH_4 m^{-2} d^{-1}, a 20-30% increase in the population would be required to explain the difference between the mass budget and surface flux measurement approaches (i.e. a ± 30% change would correspond to ± 65 mg-CH_4 m^{-2} d^{-1}). But the differences in mid-July and August 2010 would require a population (and/or consumption rate) increase and this may be unlikely given that the decreasing temperature would be expected to decrease reproduction and consumption, and the (presumed) homogeneous redistribution of the biota within the deepening surface mixed layer would deny them (or at least reduce) their ability to aggregate at the top of the chemocline to exploit the large diffusive flux. It is not known how important CH_4 concentration gradients close to the cell walls are for the uptake of methane by methanotrophs and what effect disrupting these gradients would have.

We conclude that the loss of dissolved methane was predominantly through outgassing to the atmosphere. The epilimnion concentration of methane was less than half of the threshold concentration required for bacterial uptake in Lake Constance measured by Schmidt and Conrad (1993), which suggests that enhanced biotic consumption during seasonal overturn is unlikely. Furthermore, Schmidt and Conrad (1993) measured a residence time of 4-6 days for methane in the epilimnion and it is possible that the majority of outgassing occurred during the intervals between field trips if the most recent significant deepening of the surface mixed layer occurred more that a few days before the field trips. This hypothesis is supported by automated water quality profiler data collected by Seqwater (data not shown) which show the major mixing events occurring on 9 July 2010 and 26 July 2010.

6.5. Monitoring Strategies for Environments with High Spatial and Temporal Variability in Fluxes

Designing a monitoring strategy for a reservoir with strong spatial gradients in gas fluxes and with a significant proportion of the total methane flux due to bubbles is very challenging. Recall that 80% of the methane flux was emitted from just 10% of the surface area in Little Nerang Dam and that 100-fold changes in methane flux were observed over distances of 50-100 metres. Fluxes in the high flux regions are dominated by periodic bubble emission events and exhibit high temporal variability. Ideally, a monitoring strategy should provide a representative sample of the spectrum of bubble events (Section 0) and allow for multiple concurrent deployments of bubble chambers, flux chambers, etc. to resolve the important spatial gradients in fluxes. The monitoring strategy spectrum ranges from synoptic surveys of ambient methane concentrations in the air above the water surface (Grinham *et al*. 2011) to long-duration unattended measurements, e.g. bubble traps, that effectively integrate the flux over time at a single location to short-term hands-on flux chamber measurements that provide more insight into the temporal variability of fluxes and better insight into the relative contributions of diffusive and bubble flux processes and the environmental processes that control these fluxes. In practice, financial and logistic constraints will require some compromise between the objectives of providing the most representative estimate of fluxes from an entire reservoirs and understanding about the mechanisms that control these fluxes.

Long term deployments of bubble traps, for example, can capture emissions over periods of days to weeks. This may prove an effective strategy to deal with the high temporal variability of emissions dominated by bubbles provided the deployment is long enough to effectively average over the full frequency spectrum of bubble events. The use of bubble traps may require more site visits than alternative approaches as distinct site visits are required for trap deployment, sampling of trap head-space gas, and trap collection. In addition, fluxes measured with bubble traps generally require measurement of gas concentrations using gas chromatography in the laboratory and are not amenable to real-time analysis using gas analysers in the field due to limited sample volumes collected by the

traps. In addition, bubble trap fluxes are not known until the end of the experiment and they are of limited value for the a priori selection of measurement sites. However, bubble traps can be deployed concurrently at a number of sites, limited only by the number of traps available, and if located well-enough to resolve the important spatial gradients in fluxes, can improve the accuracy of whole-reservoir flux estimates.

The bubble trap method may not provide sufficient accuracy for reservoirs dominated by diffusive fluxes. As the duration of a deployment increases, the build-up in head space gas concentration, by changing the air-water concentration difference, changes the flux from what the 'true' value is. This feedback between the headspace gas concentration and the air-water flux is one of the motivations for keeping chamber deployment times as short as possible, especially in systems dominated by diffusive fluxes. For systems dominated by bubble fluxes, the feedback between head space gas concentration and the diffusive flux probably introduces only a small error.

Short-term FC deployments, as we have used, provide detailed information regarding the nature and timing of water-air fluxes but can only be conducted at one site at a time. Using the CSIRO FC protocol, it is possible to sample up to eight sites in a day (the actual value depends on whether two or three replicates are required, travel time between sites, etc.). Because the FC method allows real-time quantification of site fluxes, it provides more flexibility to adapt the number and location of measurement sites in response to real-time observations of fluxes and is therefore very useful for resolving fluxes in regions with strong spatial gradients.

An unexpected issue encountered in this project was the occurrence of methane fluxes so high that they caused the gas analyser to exceed its maximum limit of detection (LOD). This raises an important issue regarding the use of the Picarro-flux chamber system for measuring CO_2 and CH_4 fluxes in systems with strong ebullition. When the concentration is within the instrument's LOD, the system provides excellent insight into the nature of bubble emissions as the concurrent CO_2 and CH_4 concentration data can show the arrival of individual bubble events and allow the calculation of the bubble's gas composition (in terms of CO_2 and CH_4). However, when the concentration exceeds the LOD, an assumption has to be made regarding what the emission would have been during the remainder of the chamber deployment. We adopted a conservative strategy that underestimates the 'true' 15-minute flux by assuming no further emission of gas occurred after the instrument's LOD was exceeded. Picarro has since added a feature that allows the user to reduce the sensitivity of the gas analyser in order to extend the maximum LOD, but this is a very recent development and we have not tested it with this project's equipment.

Ultimately, we believe the best approach involves a combination of FC and bubble trap methods. The FC method allows a rapid assessment of the important processes and the location of emission 'hot spots'. This information can be used to design a bubble trap deployment strategy so that the spatial gradients identified using the FC method are resolved by the subsequent bubble trap deployments. The bubble trap deployments can then be used to perform the temporal averaging needed to reduce the uncertainty associated with short-term temporal variability of bubble fluxes that impacts FC measurements.

7. CONCLUSIONS

Methane emissions to the atmosphere from both Little Nerang Dam and Hinze Dam are at the upper end of the range of emissions reported for reservoirs and lakes in boreal and tropical climates (1 – 113 mg-CH_4 m^{-2} d^{-1}) (Tremblay *et al*. 2005). Averaging over all measurements and across the entire surface of the reservoirs, Little Nerang Dam emitted at least 61 mg-CH_4 m^{-2} d^{-1} and potentially 135 mg-CH_4 m^{-2} d^{-1} or more. Hinze Dam emitted in the range 28 – 44 mg-CH_4 m^{-2} d^{-1}.

Emissions from both reservoirs showed a marked spatial variation along their lengths. The highest emissions are at the distal ends remote from the dam wall, and the highest emissions are dominated by bubble events occurring in relatively small regions of the reservoirs. In Little Nerang Dam, about 80% of the total reservoir emissions came from 10% of the total reservoir area. In Hinze dam, 60% of the emissions came from 6 % of the total surface area. These observations are markedly different from the consensus approach which tends to view reservoir methane emissions as relatively uniform spatially. A very recent work (Del Sontro *et al*. 2011) has demonstrated, in a major African hydropower reservoir, a similar localisation of high emissions. We attribute these elevated emissions to regions in the upstream arms of the reservoirs which are deposition zones for fresh organic matter from the catchment. Only the Little Nerang River arm of Hinze Dam did not have a region with high bubble emissions. We assume that the Little Nerang Dam, a short distance upstream, intercepted most of the particulate organic material.

Considered against the marked spatial variations of methane emissions, there was no consistent temporal variation in methane emissions on either a short diurnal time scale, or on a seasonal time scale. We note that both storages are in a semi-tropical zone with a somewhat limited water temperature variation.

Examination of the release of the "stored" methane in Hinze Dam during the winter overturn suggested that the majority of the storage methane flux, which ranged from 45 – 166 mg-CH_4 m^{-2} d^{-1}, was outgassed to the atmosphere (Section 6.4.4). This flux was only determined for a 6-week period of cooling from late June to mid-August and our data do not allow generalisation to longer periods.

The storage flux could not be determined for Little Nerang Dam because of an atypical inflow event followed by excessive drawdown of the storage which prevented access to the storage during the crucial winter overturn cooling period. A flood in February 2010 replaced much, if not all, of the water from the top 12-14 m in Little Nerang Dam and displaced the seasonal thermocline from a typical depth of about 4 m down to 10 m. In addition to flushing out any methane stored in the water column above 12-14 m depth (which would have outgassed to the atmosphere a short distance from the dam), the inflow, by displacing the thermocline downwards, reduced the volume of water available to store methane and may have sharpened the vertical gradient of [CH4] thereby increasing the gradient flux in Little Nerang Dam above typical levels. Thermistor chain data collected by CSIRO in Little Nerang Dam during 1998-1999 (not shown) showed that the surface mixed layer remained between 2 – 4 m deep until at least late April.

A specific objective of this work was to evaluate the suitability of the floating chamber/CRDS (Cavity Ring-down spectrometer) system for measuring reservoir methane and carbon dioxide fluxes. Based on the results, we consider that this technique is capable of measuring diffusive fluxes with high precision over relatively short deployment times (15 minutes) and provides a relatively quick method for quantifying fluxes over large storages. This sensitivity and precision comes at a price – the propensity of the instrument to "hang up" when a large bubble or a stream of small bubbles enters the floating chamber. This precludes developing an unbroken time series and requires estimating fluxes by interpolation methods which are quite conservative and may lead to underestimates of high fluxes. These difficulties can be overcome by "detuning" the instrument. At the time of the field study, this capability was not available. More recently, the manufacturer has incorporated the ability for the user to trade off sensitivity against a maximum limit of detection.

In addition, the CRDS proved to be very robust and tolerant of field conditions in SEQ On one occasion, inadvertent immersion of a gas line drew water into the gas analyser. It was possible to service the unit in the field and resume measurements within two days. Alternative gas analyser technologies that have been employed in the past (Tremblay 2005) require desiccation of the gas stream to the analyser and introduction of liquid water generally requires major time-consuming repairs that cannot be carried out in the field.

Should the marked spatial variation in methane emissions be characteristic of all storages, it is clear that accurate measurement of total fluxes requires spatially selective sampling of the reservoir with greater density of measurements in the high emitting zones. These areas cannot be determined *ab initio*. Identification of deposition zones and anecdotal information of frequent bubbles will provide some guidance, but a more rigorous approach requires an initial spatially uniform survey followed by more concentrated measurements to quantify the emissions from the most productive areas. Deployment of conventional bubble traps is a means to getting integrated bubble flux measurements over a longer time.

Our current hypothesis is that the large methane fluxes in Little Nerang and Hinze Dams are a natural consequence of a high organic matter load supplied from the rainforest vegetation, steep slopes and high rainfall of the catchment. The organic load is deposited at the upstream ends of the reservoirs and subsequently converted to CO_2 and CH_4 by microbial activity.

The potential to mitigate CH_4 emissions from these reservoirs is limited to the elimination of the storage flux component of the total emission budget. The data do not allow us to accurately determine the contribution of the storage flux to the total annul flux because the measurements in Hinze Dam were limited to winter conditions after the onset of surface layer deepening. To eliminate the storage flux would require maintaining dissolved oxygen concentrations above approximately 2 mg L^{-1} in the hypolimnion. This could be accomplished by artificial destratification or hypolimnetic oxygenation and would ensure that methane does not accumulate in the hypolimnion. Preventing elevated [CH4] concentrations in the hypolimnion may also reduce the [CH4] concentration in the surface layer to some extent and therefore produce potentially a small reduction in the diffusive flux of methane to the atmosphere.

The data collected in both reservoirs confirmed large bubble fluxes from regions with consistently high dissolved oxygen (> 6 mg-O_2 L^{-1}) concentrations at the bottom of the water column. This implies that there is little, if any, scope to reduce methane production rates in the sediments and therefore little scope to reduce the bubble flux which contributed 60-80% of total emissions from the reservoirs. Furthermore, we recommend caution regarding the application of artificial destratification as this will likely raise the sediment temperature by 5-8°C and potentially double methane production rates. We note that increasing hypolimnetic dissolved oxygen concentrations has been shown (Rod Jung, EBMUD, pers. comm.) to provide additional water treatment benefits through the reduction of DOC (lower disinfection byproduct formation) and reduced forms of Fe and Mn (lower treatment chemical costs). Reduction of the methane storage flux may be considered as an ancillary benefit of this reservoir water quality management strategy.

8. RECOMMENDATIONS

1. Our work quantified methane emissions from two sub-tropical drinking water storages. Other Australian studies (commercial in confidence – results not available) have focussed on cold-water hydropower storages in Tasmania and in the Alpine regions of NSW (Snowy Hydro). International investigations have been almost exclusively on hydropower storages in the wet tropics, or in cold boreal storages. None of these regions is fully representative of the bulk drinking water storages serving the major Australian urban areas, nor of the many inland water storages primarily for irrigated agriculture. A study aimed at quantifying the emissions from a temperate urban water storage with a protected catchment, and from an inland storage where most of the sediment input is eroded soil (and associated carbon) would greatly facilitate generalising our results to all types of storages across Australia. A better knowledge of emissions from such storages would also improve decision making regarding the installation of water quality measures such as mixers and oxygenation, as carbon credits may be claimable (or sold) also for the reduced emissions due to these devices.

2. Anecdotal evidence and limited personal observation suggests that urban water retention ponds may be strong sources of greenhouse gases. While the surface area of each pond is small, they are numerous in most urban areas. If the emissions are substantial they may be a significant net source. Accordingly, a preliminary survey of methane emissions from several urban ponds (in summer – time of highest likely emission rates) is warranted to define if a problem really exists or not.

3. This project has generated an extensive data set of observations which shows the spatial and temporal variations of methane fluxes (especially bubble component) which are, in part, stochastic. This is an excellent departure point for a desk top study aimed at designing more efficient/optimised sampling/investigation strategies for a specified level of precision. The results would aid other measurements of this type.

4. The seasonal storage component was the least well quantified component in this study. This is partially due to having to relocate from Little Nerang Dam to Hinze Dam due to access problems, as well as insufficient data on in situ CH_4 oxidation rates to better define the microbial component of the total internal uptake at overturn. Literature values for a suite of (cold) Swedish lakes vary by a factor of 300. We recommend a small experimental study aimed at generating more realistic values for this parameter under Australian conditions (warmer waters and much higher concentrations of fine clay particles in general) which is critical to accurately quantifying the internal uptake term. The use of isotope chemistry that potentially allows the tracking of ^{13}C between CO_2 and CH_4 holds much promise in this regard.

5. While not strictly an urban water issue, we note that the waters disposed from shale and coal gas extraction may contain significant amounts of methane and CO_2 even if most of the methane has been extracted. A preliminary survey of the water disposal basins is warranted as a precautionary input into the regulatory process.

APPENDIX 1 - Calculation of Dissolved CH_4 Concentration using GC Data

A 12.4 mL Exetainer was filled with 7.5 mL of sample plus 0.5 mL of ZnCl2 preservative, leaving a headspace of 4.4 mL.

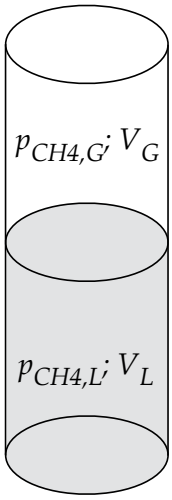

The concentration (g L^{-1}) of methane dissolved in a volume of water, V_L, in a container with headspace volume, V_G, can be calculated as,

$$[\mathrm{CH_4}] = \frac{M_{Tot}}{V_L} = P_{CH_4,g}\left(V_L K_H + \frac{V_G}{R\,T}\right)\frac{m_{\mathrm{CH_4}}}{V_L} \qquad (1)$$

where

M_{Tot} = total mass of methane in the vial [g]

Total vial volume = $V_G + V_L$ [L]

$[CH4]_{,g}$ = partial pressure of CH_4 in headspace gas [atm]

K_H = Henry's constant = 1.3-1.5 x 10-3 [atm^{-1} mol L^{-1}]

R = universal gas constant = 0.08205746 [L atm K^{-1} mol^{-1}}

T = sample temperature [K]

m_{CH4} = molar mass of methane = 16.042460 [g mol^{-1}]

This calculation assumes that the headspace gas has come to equilibrium with the dissolved gas. Bringing $[CH4]_{,g}$ inside the brackets in Eq1 the first term in the brackets is the number of moles of CH_4 in the water and the second term is the number of moles of CH_4 in the headspace gas.

The amount of CH_4 in the headspace is simply the partial pressure (in atm) of CH_4 as measured using gas chromatography. If the concentration is reported as ppm or ppmv one need simply divide by 10^6 to obtain the partial pressure in atm.

According to Henry's Law the concentration of CH_4 dissolved in the water is:

$$[CH_4]_L = K_H\,[CH4]_{,g} \quad [\text{mol L}^{-1}] \tag{2}$$

The mass of CH_4 in the water is

$$M_{CH4,L} = [CH_4]_L\, V_L\, m_{CH4} = K_H\,[CH4]_{,g}\; V_L\, m_{CH4} \tag{3}$$

The mass of CH_4 in the gas phase is

$$M_{CH_4,g} = \left(\frac{P_{CH_4,g} V_G}{R\,T}\right) m_{CH_4} \tag{4}$$

where the term in brackets is simply the number of moles of gas computed using the universal gas law.

The total mass of CH_4 in the container is simply $M_{Tot} = M_{CH4,L} + M_{CH4,g}$ which, divided by the volume of the liquid in the container yields, after some rearrangement of terms, the mass concentration (g L^{-1}) given by Equation 1.

Technically, a correction should be made to allow for the methane in the headspace air at the time the sample was collected. For all practical purposes this can be computed using Equation (4) with the atmospheric concentration (1.73 ± 0.02 ppmv) which, assuming a head space volume of 4.4 mL (as per the CSIRO sampling protocol used at Little Nerang and Hinze Dams) gives for 1 atm total pressure and 25 °C

$$M_{CH4,corr} = 4.8 \times 10^{-9}\ \text{g}$$

Application of this correction reduces the dissolved CH_4 concentration in the surface mixed layer by about 12% whereas the correction below the oxycline is < 1%. Note that at some of the very high air-water flux locations in both Little Nerang and Hinze Dams the ambient CH_4 concentration in the atmosphere was observed to change frequently within the range 2 - 5 ppmv and so the correction at these sites is higher in absolute terms.

APPENDIX 2 - Floating Chamber Design

The floating chambers used for this project were constructed from the design used by Environment Illimite and Hydro Quebec. The dimensions of the chamber as constructed are shown in Figure 28.

The volume of the floating chambers with a head space[3], *H*, is

$V = H\,(0.291 \times 0.440 + \pi\, 0.150^2) = 0.1987\, H$ (m^3)

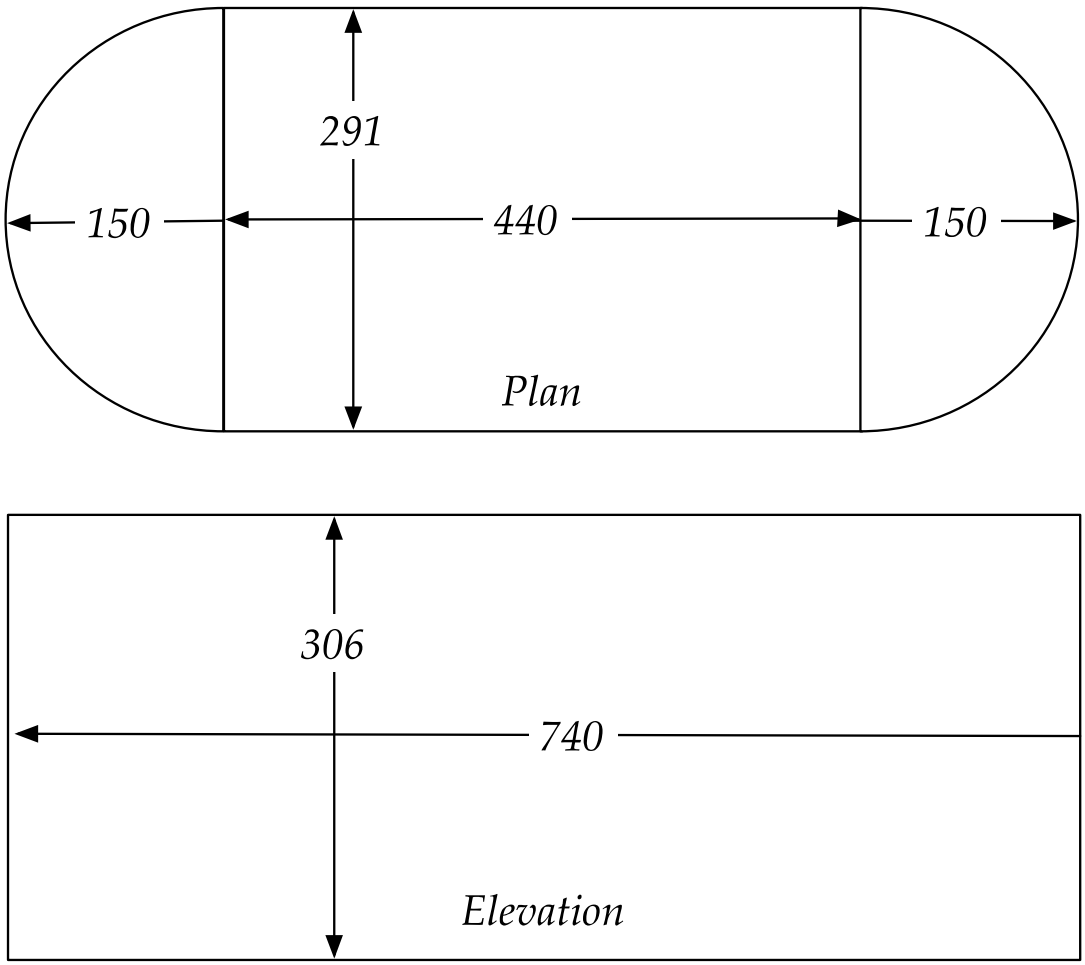

Figure 28: Floating chamber design.

The chamber was supported using PVC pipes filled with marine floatation foam connected to the chamber at user-selected levels. By allowing the head space to vary, the rate of change of CH_4 concentration can be manipulated, i.e. the 'sensitivity' of the system could be varied in response to changes in gas flux. In practice, the high fluxes measured required the selection of a large *H* so that the deployments could take place over longer periods before the gas analyser would go out of range.

Mounting brackets allowed the ADV to be attached below the chamber so that water turbulence could be measured a short distance below the air-water interface and directly underneath the chamber.

[3] Headspace is the volume of the chamber occupied by gas and is measured as the distance between the water surface and the bottom surface of the top of the floating chamber.

Figure 29: Photo of floating chamber with ADV attached using a temporary mounting bracket.

Figure 30: ADV mounting brack*et al*lows vertical and horizontal adjustment of measurement volume.

Figure 31: Floating chamber deployed in the field. Headspace gas is recirculated through the black and clear tubing. The ADV can be seen to the right of the chamber just below the surface.

System Response Time

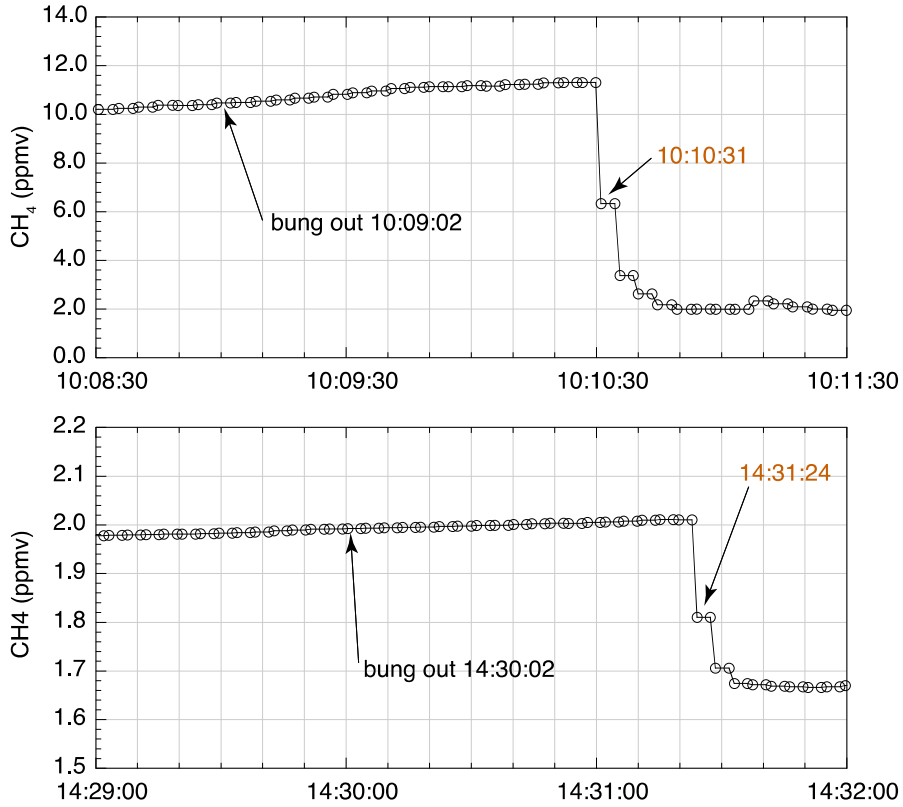

Figure 32: Response time of floating chamber - Picarro gas analyser system following removal of the bung from the chamber (i.e. step change in conditions).

The response time of the floating chamber system was tested by removing the bung and observing the time delay before a change in the reported gas concentration was observed. Values for the delay ranged from 47 - 90 seconds with 80-90 seconds being the most representative value (Figure 32). All analysis of chamber deployment data considers only data reported between 120 seconds after the bung was inserted into the chamber to the time the bung was removed. This ensures the reported values do not reflect transient effects at the beginning or end of each deployment.

APPENDIX 3 - Ancillary Data

Meteorology and Stratification

Meteorological and thermistor chain data were collected at site LND Met through out the project. The instrumentation was the same as described by Sherman *et al*. (1998). Project specific details are noted below. Numerous problems, reflected as periods of intermittent operation, were experienced with the power supply due to fouling of the solar panels by birds and limited solar availability during winter months and periods of heavy cloud cover. Mean daily values for downwelling shortwave radiation, net longwave radiation, air temperature, relative humidity and wind speed are plotted in Figure 33. Little Nerang Dam is a sheltered environment with a mean daily wind speed between 1 and 1.5 m s^{-1}. Cloudy conditions prevailed during much of the year with incident shortwave radiation considerably less than clear sky values from mid-December to mid-January, early February and late February - early March.

Adjustment for thermal losses due to the dome cooling effect experienced by the Kipp and Zonen radiometers was performed by computing the average reported radiation during periods of no sunshine and then subtracting that amount from the from all reported data. This led to a correction for the lower dome (upwelling shortwave radiation) of -4.59 W per square meter for the period of November through 18th of March and -4.84 W per square meter for the period from 18th of March through 24th of August.

The dome cooling correction for the upper dome (which measures downwelling shortwave radiation) was -1.39 W per square meter from November through 18th of March 2010 and -1.8 W per square meter from 18th of March through 24 August.

A high precision thermistor chain was deployed at the met station with thermistors at depths of 0.4, 0.65, 0.9, 1.15, 1.4, 1.65, 2.15, 3.15, 4.15, 6.15, 7.15, 12.15, 14.15, 16.15, 18.15, 20.15, 25.15, and 29.15 m below the water surface. On 4 May 2010 the location of the thermistors was adjusted by lifting up the deeper thermistors and bundling them further up the chain. This had the effect of raising the thermistors originally below 12.15 m by nearly 6 m so that the 14.15 m thermistor was lifted to 8.02 m and the 16.15 thermistor was raised to 10.19 m. In addition, a comparison of temperature data from the 6.15 and 2.15 m thermistors following the vertical showed that the 6.15 and 7.15 m thermistors had inadvertently been raised by about 4.5 m, i.e. the 7.15 m thermistor was raised to 2.65 m.

Thermistor chain data collected during the first 3 weeks in February 2010 are shown in Figure 34. The arrival of a large inflow event immediately prior to 7 February is clearly seen in the rapid decrease in temperature over the top 5 m of the water column and an increase in temperature at 6 and 7 m. Inflowing water, probably with a temperature close to 21 °C, entered the water column at a depth of approximately 6 m. The original surface layer water (warmer than the inflow) was lifted up by the inflow and spilled over the dam. Mixing caused by the energy of the inflow contributed to the thermal stratification over the top 2 m. As the dam spilled, the warm surface layer water was replaced by colder water from the inflow - this produced the decrease in temperature in the shallower thermistors.

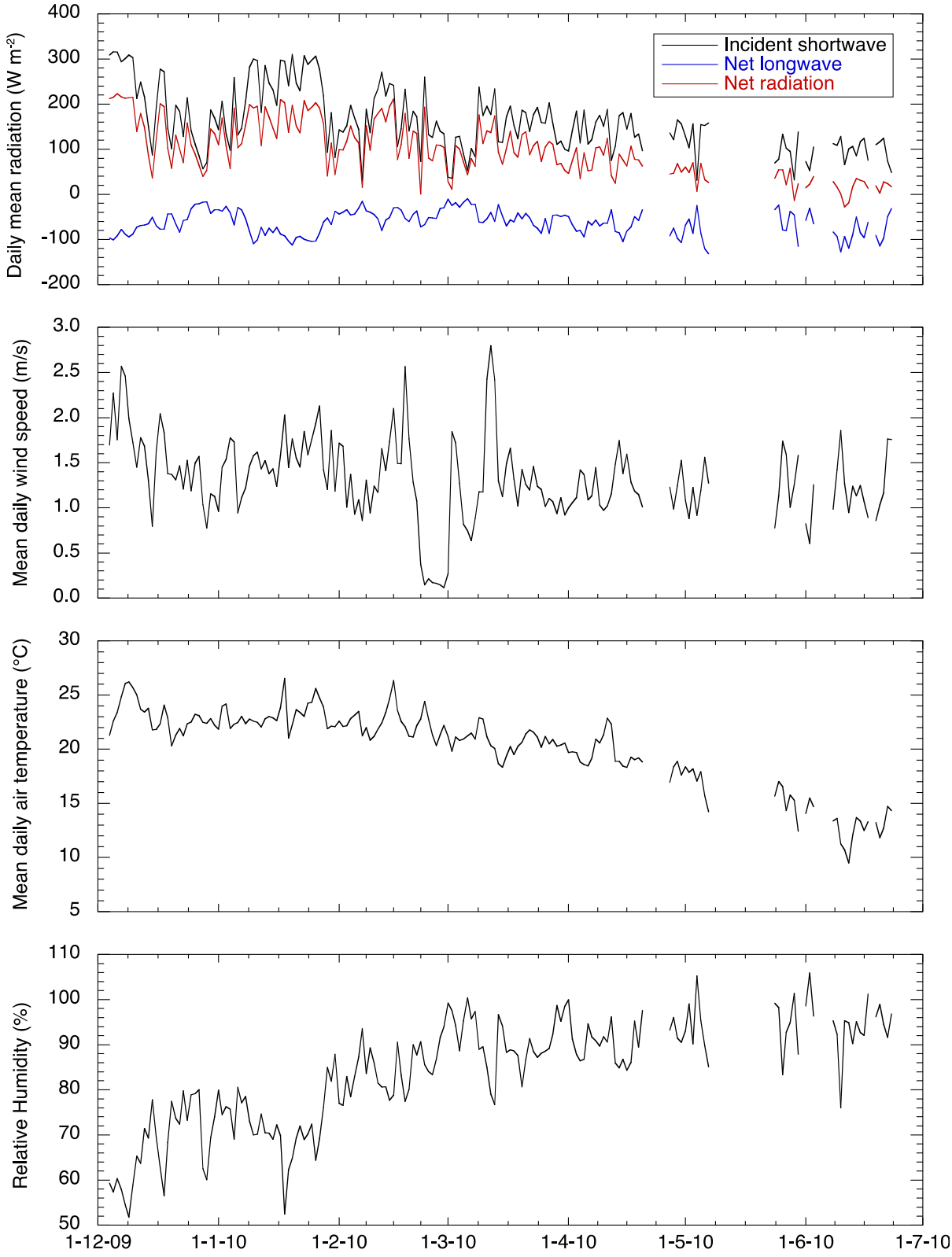

Figure 33: Mean daily meteorological data measured at site LND Met. Gaps in record indicate days with one hour or more missing data. An envelope drawn across the top of the incident shortwave radiation data (top) would indicate the 'clear sky' value.

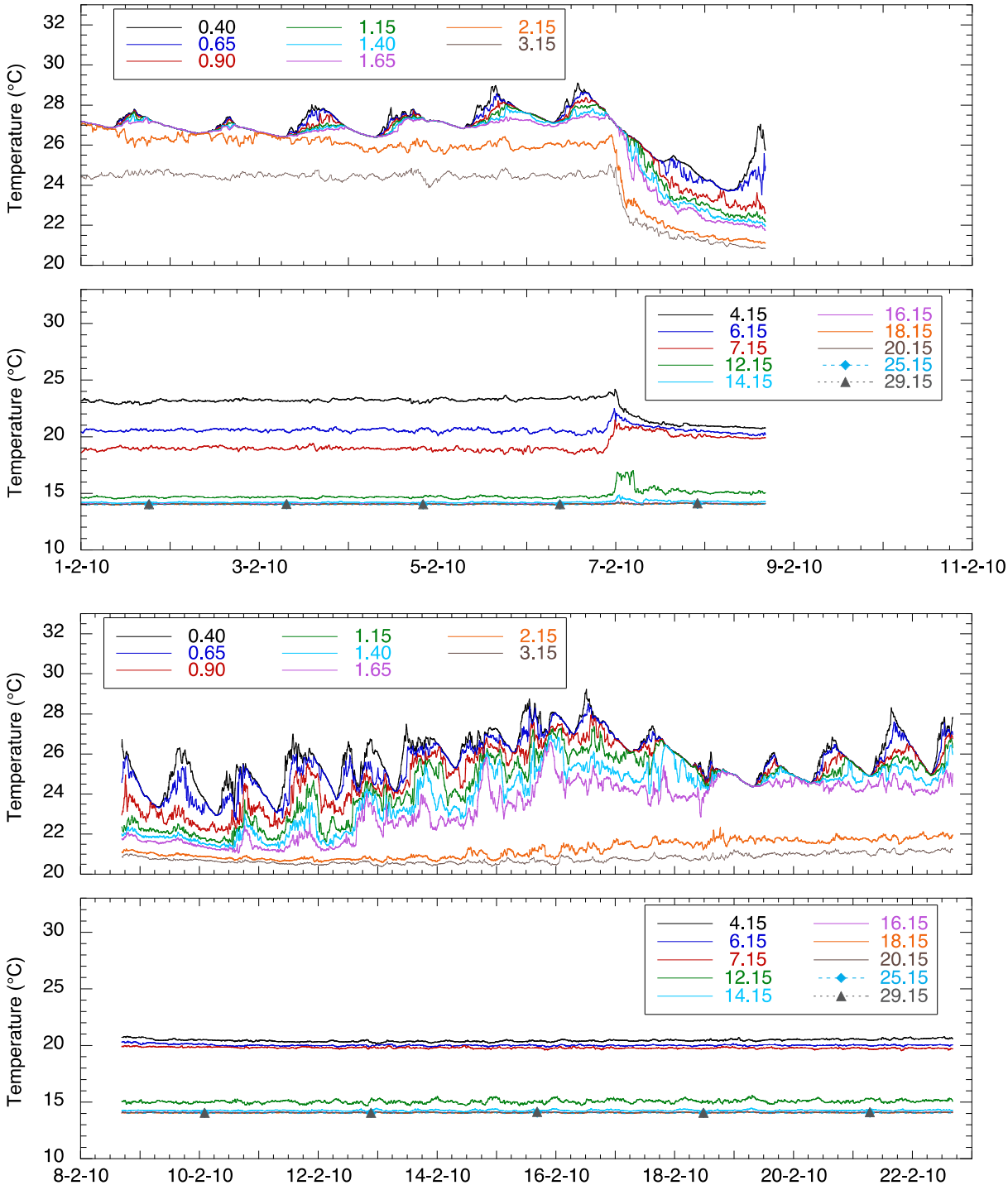

Figure 34: Little Nerang Dam thermistor chain traces during Feb 2010. Legend denotes depth of thermistors in metres below the water surface. The arrival of the storm inflow just before 7 Feb can be seen in the top two panels as the rapid decrease in temperature over the top 4 m and an increase in temperature at 6.15 and 7.15 m. The inflow extended to as deep as 12.15 m. Convergence of traces indicates surface layer deepening due to wind mixing and penetrative convection. For example, the top panel shows mixed layer deepening to 2.15 m until 3 Feb and only to 1.65 m from 4 - 7 Feb. From 9 - 18 Feb the surface mixed layer is mainly < 1 m deep and then deepens to 1.65 m on 18-19 Feb.

Water Quality Sonde Profiles

Vertical profiles of turbidity, temperature, depth, dissolved oxygen, pH and chlorophyll fluorescence were collected using a YSI 6600v2 water quality sonde and a bbe Fluoroprobe3 periodically during the project. YSI profiles were collected at the same time as depth sampling for dissolved methane.

Profile data collected on all dates at site LND05 in Little Nerang Dam are shown in Figure 35. The temperature profile data show a shallow diurnal surface mixed layer of 2-3 m depth during the January and February 2010 field trips. The surface layer has deepened to about 11 m during the June 2010 trip. The oxygen profile data show a strong oxycline from 3-5 m depth on 22 Jan 2010 which deepened to 9 m prior to the February 2010 survey. The water column was anoxic below 11 m depth at all times. A prominent local maxima in chlorophyll fluorescence was present at 8-10 m during Jan 2010 and slightly deeper at 11-12 m depth in February but had disappeared by June. The chlorophyll fluorescence peaks coincided with local maxima in conductivity and may indicate the presence of an intrusive flow. The temperature and dissolved oxygen profiles also suggest that inflows played a relatively more important role than meteorological forcing (wind mixing and night-time cooling) in the mixing dynamics of the top 10 m of the water column: had wind stirring and penetrative convection been responsible for the deepening of the oxycline between January and February, the temperature gradient between 2 and 10 m depth would more likely have been steeper (i.e. more similar to that observed in June).

Longitudinal profile surveys were conducted at Little Nerang Dam on 24 Feb, 2 Jun and 9 Jun 2010 and are show in Figure 36 - Figure 38. Apart from normal diurnal heating in the upper 5-7 m of the water column, the temperature profiles show little evidence of horizontal gradients with the exception of 2 June (Figure 37). On this date, longitudinal gradients in dissolved oxygen and local maxima/minima in turbidity, fluorescence and pH between 9 and 12 m depth indicate the presence of an intrusive flow.

Profile data for Hinze Dam is shown in Figure 39. On 1 Jul 2010, profiling was conducted only in the eastern arm (sites Hinze07 - Hinze11) and completed by 1100h. There was relatively little evidence of horizontal gradients. A prominent oxycline was observed coincident with the thermocline between 18 and 22 m depth. A prominent peak in turbidity occurred at 21-22 m which coincided with a local minima in pH. This most likely indicates the redox state in the water column, i.e. the conversion of dissolved Fe and Mn between reduced and oxidised states accompanied by the formation of fine particulate forms of these compounds. On 15 July 2010, profiling occurred throughout the day and the temperature profile data show more horizontal variability. This variability was most likely produced by diurnal heating (afternoon profiles warmer than morning profiles) combined with wind-driven movement of the surface layer that carried the warmer water to the downwind end of the reservoir – winds were from the northwest and would shift surface layer water towards the eastern arm of the reservoir (Sites Hinze02 - Hinze04).

On 15 July 2010 the seasonal thermocline has moved downwards to between 23 and 30 m. The turbidity and pH peaks have shifted downwards to 28-30 m depth and provide the most reliable evidence of the maximum depth of mixing of the surface layer between 1 July and 15 July. By 12 August 2010, the entire water column appears to have mixed – the turbidity and pH maxima were no longer present and the temperature stratification at site Hinze10 clearly shows evidence of complete overturn of the water column at this site.

Conversion of Dissolved Oxygen Concentration Units

During the first 3 field YSI profile surveys the instrument was configured to output dissolved oxygen concentration as a percentage of saturation whereas all subsequent surveys output the concentration in units of mg-O2 L^{-1}. To convert % saturation to mg-O2 L-1 the formula recommended by the USGS (http://water.usgs.gov/admin/memo/QW/qw81.11.html) is used:

ln DO = Al + A2 100/T + A3 ln T/100 + A4 T/100 + S [B1 + B2 T/100 + B3 (T/100)2]

where:

DO is the saturation concentration of dissolved oxygen (mL L-1) as temperature, T (°K), and salinity S (ppt).

The coefficients A1-B3 are:

Al = -173.4292
A2 = 249.6339
A3 = 143.3483
A4 = -21.8492
Bl = -0.033096
B2 = 0.014259
B3 = -0.001700

To convert to concentration units of mg-O2 L^{-1}, [O2] = 1.4276 * DO.

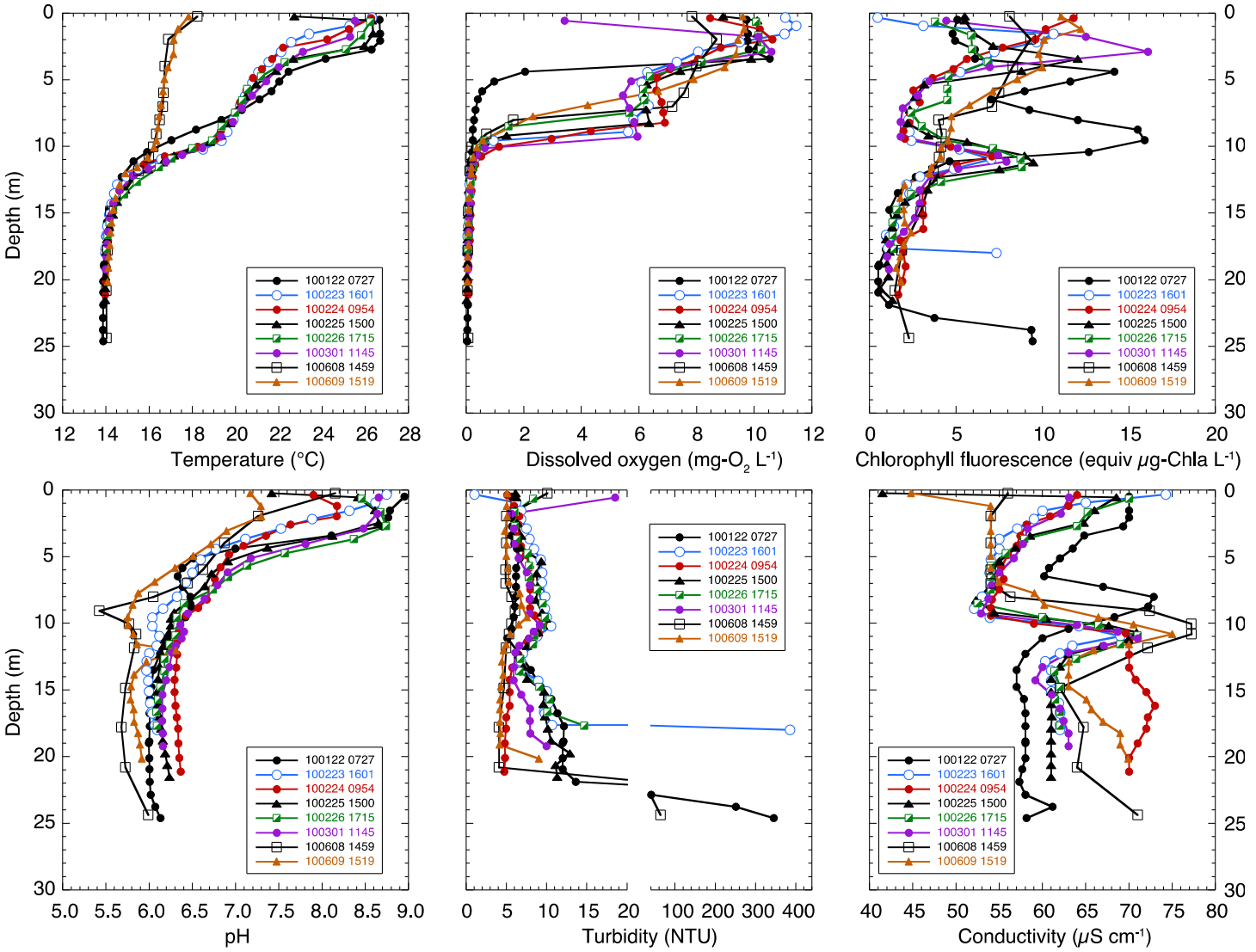

Figure 35: YSI sonde depth profile data collected near the dam wall (LND05) at Little Nerang Dam on 22 Jan 10, 23-26 Feb 10, 1 Mar 10, and 8-9 Jun 10.

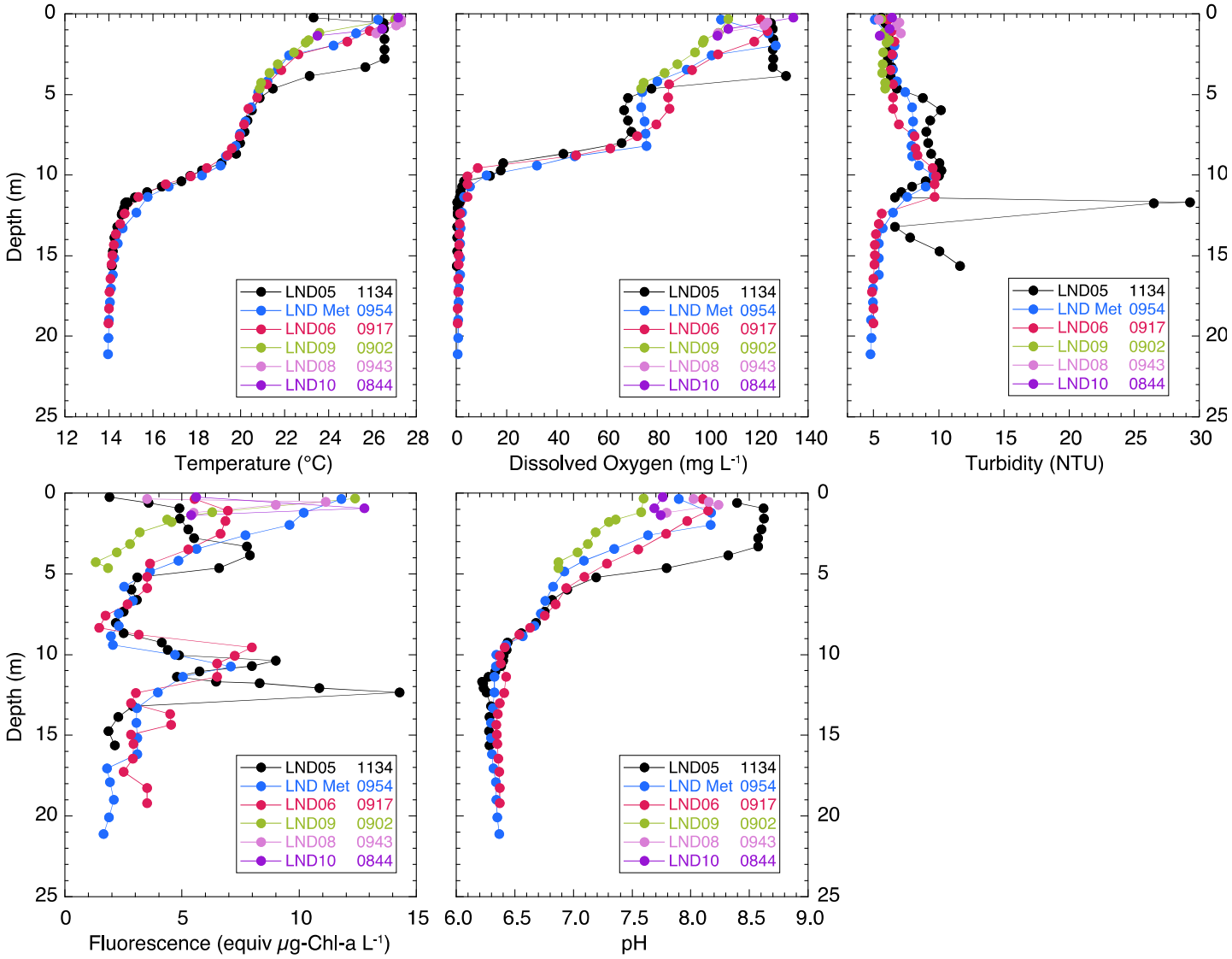

Figure 36: YSI sonde profiles on 24 Feb 2010 at Little Nerang Dam sites.

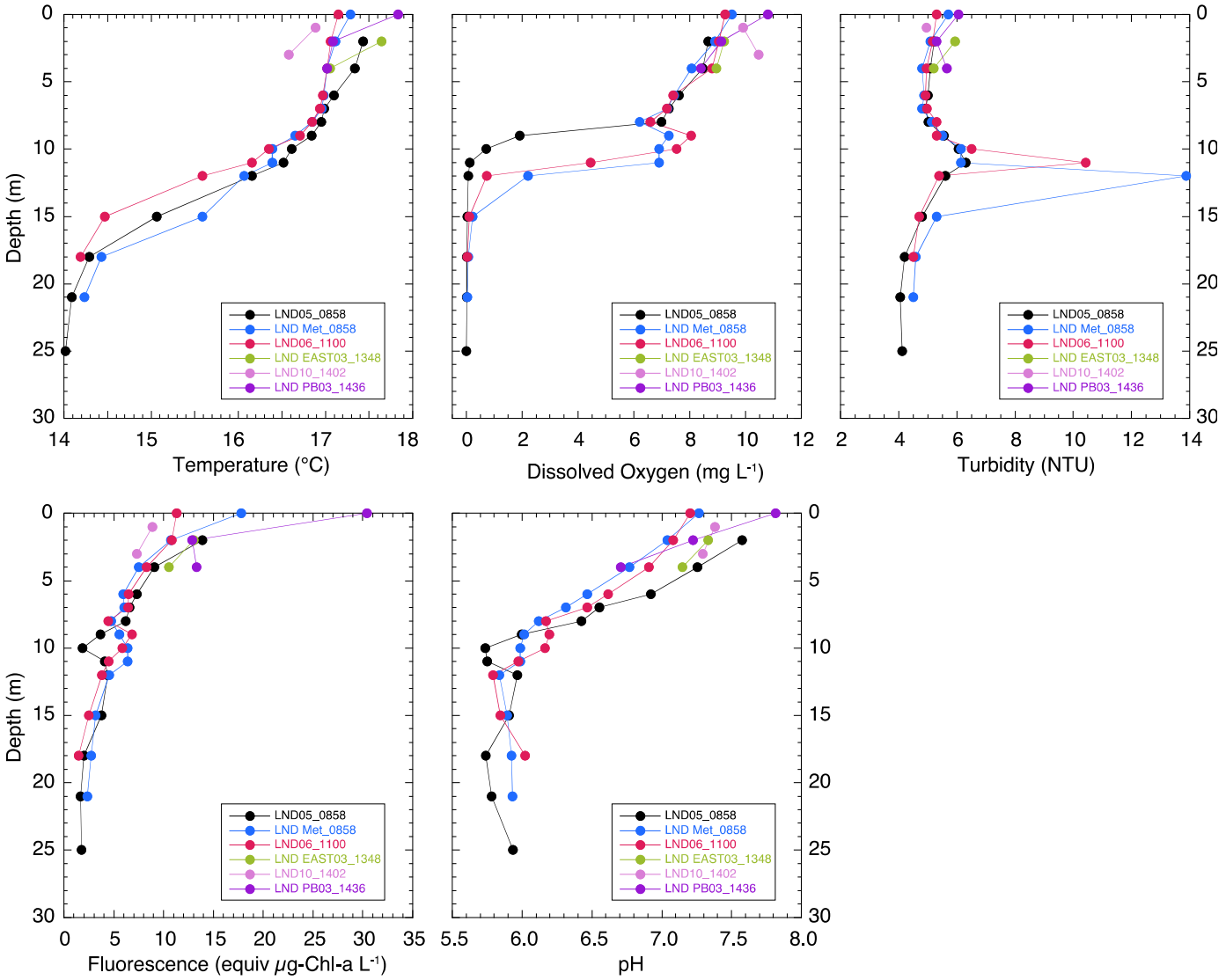

Figure 37: YSI sonde profiles on 2 Jun 2010 at Little Nerang Dam stations LND05, LND Met, LND06, LND East03, LND10, and LND PB03. Legend indicates site and time of sampling (hhmm).

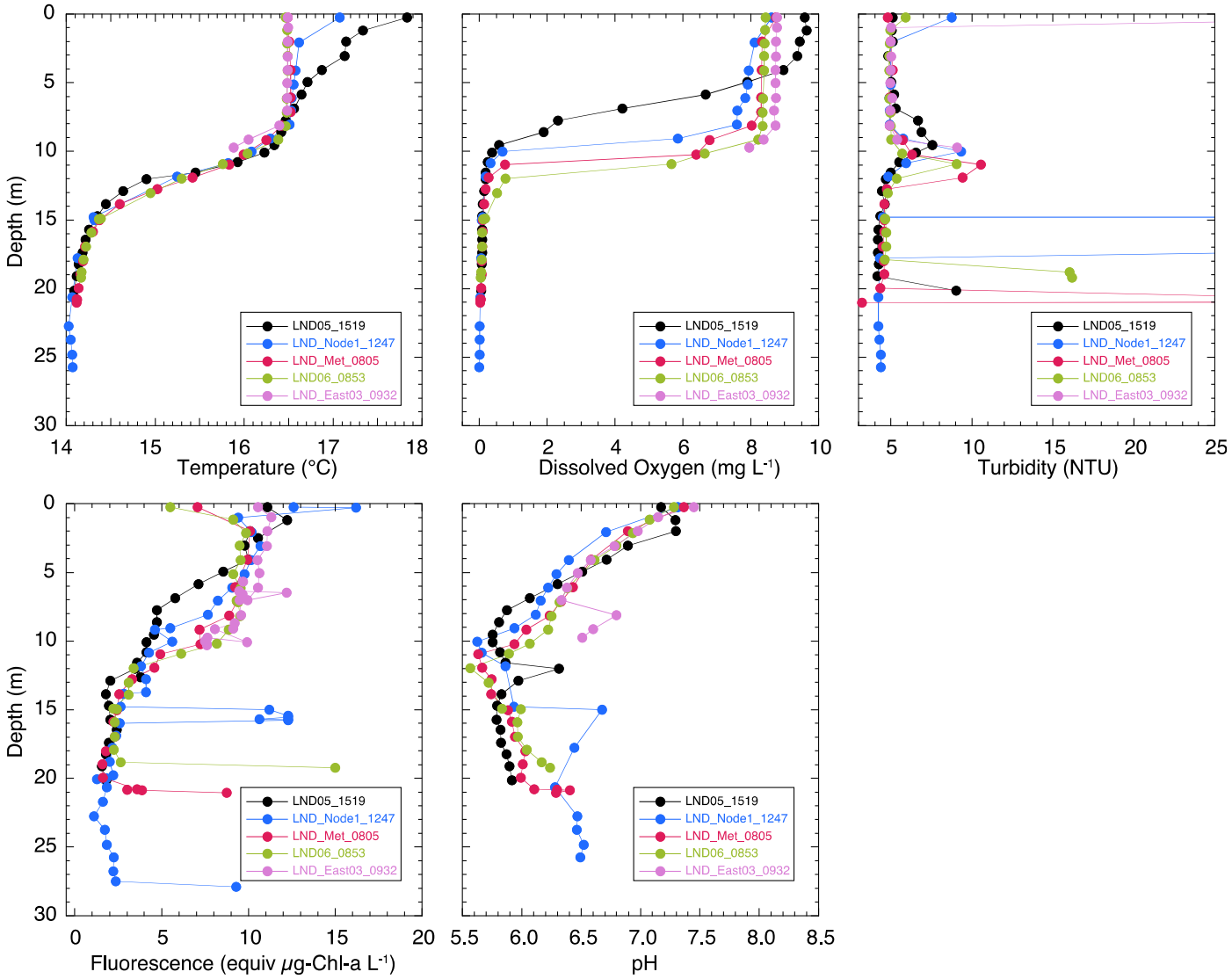

Figure 38: YSI sonde profiles on 9 Jun 2010 at Little Nerang Dam stations LND05, LND Node1, LND Met, LND06, LND East03. Legend indicates site and time of sampling (hhmm).

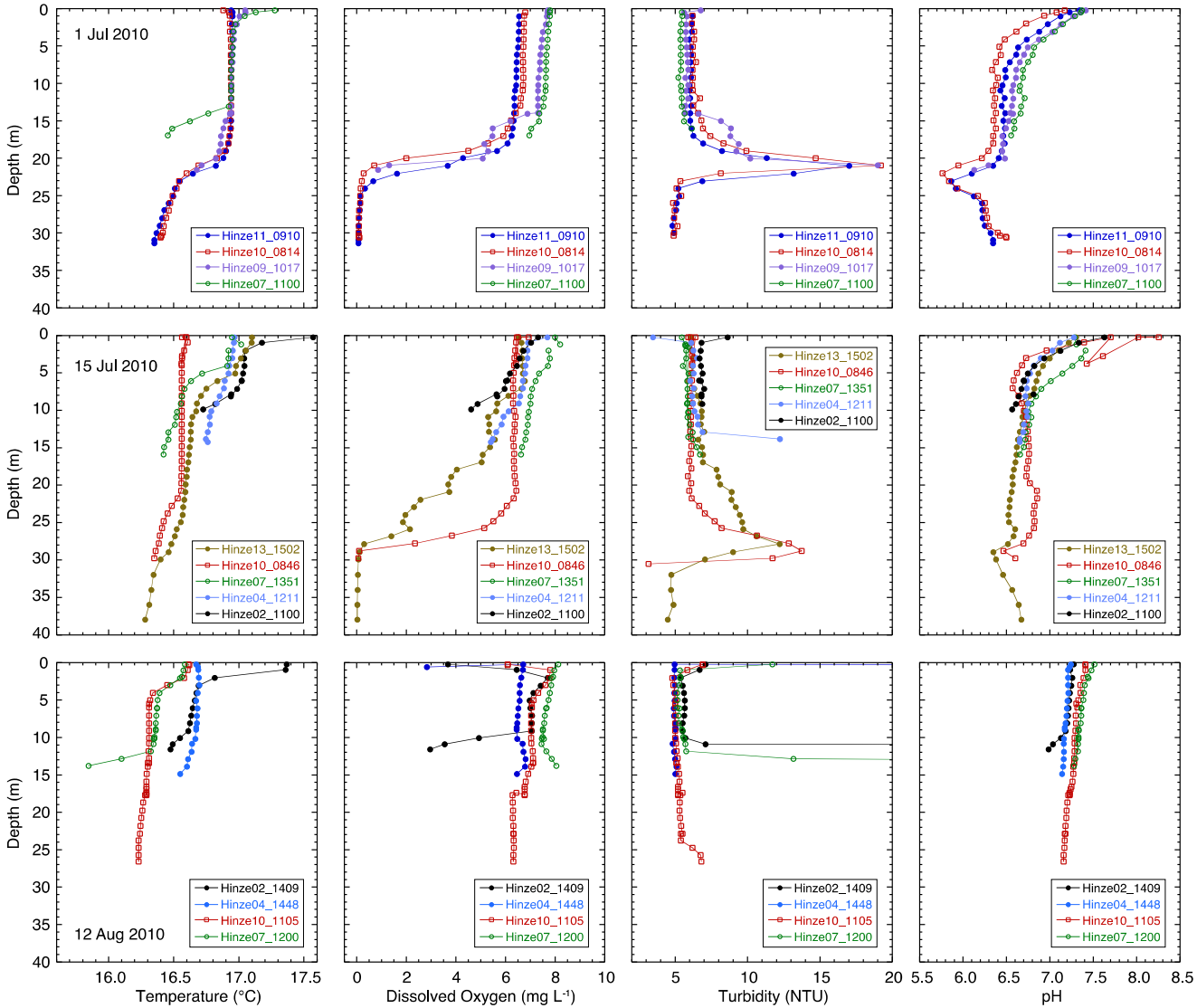

Figure 39: YSI sonde depth profile data (from left to right - temperature, dissolved oxygen, turbidity and pH); (top row is 1 July 2010, middle row is 15 July 2010, bottom row is 12 Aug 2010. Legend lists site and time of day of measurement (*hhmm*).

GLOSSARY

ADV	Acoustic Doppler Velocimeter - an instrument that uses sound to measures water velocity in 3 orthogonal coordinate directions by measuring the Doppler shift of very fine particles moving with the water.
[CH4]	The concentration of dissolved methane in the water expressed as a partial pressure that is experienced when the gas is allowed to equilibrate with air at atmospheric pressure.
GWP	Global warming potential.
pCO_2	The concentration of dissolved carbon dioxide in the water expressed as a partial pressure that is experienced when the gas is allowed to equilibrate with air at atmospheric pressure.
pCH_4	The concentration of dissolved methane in the water expressed as a partial pressure that is experienced when the gas is allowed to equilibrate with air at atmospheric pressure.

REFERENCES

Aril, G., S. Richard, and F. Guérin. 2006. *In situ measurements of dissolved gases (CO_2 and CH_4) in a wide range of concentrations in a tropical reservoir using an equilibrator.* Science of the Total Environment 354: 246–51.

Anonymous. 1996. Trouble bubbles for hydropower. New Scientist 29.

Bastien, J., A. Tremblay, and A. Scanlon. 2009. *CO_2 and CH_4 fluxes from Tasmanian aquatic systems, Australia*. Verh. Internat. Verein. Limnol. **30**: 854–57.

Bastien, J., Fréchette, J.-L., & Hesslein, R. H. 2008. *Continuous Greenhouse Gas Monitoring System – Operating Manual.* Manitoba Hydro, Department of Fisheries and Oceans Canada, Hydro-Québec.

Bastviken, D., Ejlertsson, J., & Tranvik, L. (2002). *Measurement of methane oxidation in lakes: A comparison of methods*. Environmental Science & Technology, 36(15), 3354-3361.

Bastviken, D., Ejlertsson, J., Sundh, I., & Tranvik, L. (2003). *Methane as a source of carbon and energy for lake pelagic food webs.* Ecology, 84(4), 969-981.

Bastviken, D., J. Cole, M. Pace, and L. Tranvik. 2004. *Methane emissions from lakes: Dependence of lake characteristics, two regional assessments, and a global estimate*. Global Biogeochemical Cycles 18: GB4009.

Cole, J. J., N. F. Caraco, G. W. Kling, and T. K. Kratz. 1994. *Carbon dioxide supersaturation in the surface waters of lakes*. Science 265: 1568–70.

Cole, J. J. and others. 2007. *Plumbing the global carbon cycle: Integrating inland waters into the terrestrial carbon budget*. Ecosystems 10: 171–84.

Danckwerts, P. V. 1951. *Significance of liquid-film coefficients in gas absorption*. Industrial & Engineering Chemistry **43**: 1460–67.

Downes, M.T. 1988. *Aquatic nitrogen transformations at low oxygen concentrations*. Applied and Environmental Microbiology, 54, 172-175.

Fearnside, P. M. 1995. *Hydroelectric Dams in the Brazilian Amazon as Sources of `Greenhouse' Gases*. Environmental Conservation **22**: 7–19.

Fearnside, P. M. 2005. *Do Hydroelectric Dams Mitigate Global Warming? The Case of Brazil's Curuá-una Dam*. Mitigation and Adaptation Strategies for Global Change **10**: 675 – 691.

Fechner-Levy, E. J., & Hemond, H. F. (1996). *Trapped methane volume and potential effects on methane ebullition in a northern peatland.* Limnol. Oceanogr., 41, 1375-1383.

Galy-Lacaux, C., R. Delmas, G. Kouadio, S. Richard, and P. Gosse. 1999. *Long-Term Greenhouse Gas Emissions From Hydroelectric Reservoirs in Tropical Forest Regions.* Global Biogeochem. Cycles 13:503-517.

Grinham, A., Dunbabin, M., Gale, D., & Udy, J. (2011). *Quantification of ebullitive and diffusive methane release to atmosphere from a water storage*. Atmospheric Environment **45**(39): 7166-7173.

Hall, M., J. West, J. Lane, D. De Hass, and B. Sherman. 2009. *Energy and Greenhouse Gas Emissions for the SEQ Water Strategy*. CSIRO.

Hall, M. R., J. West, B. Sherman, J. Lane, and D. De Haas. 2011. *Long-Term Trends and Opportunities for Managing Regional Water Supply and Wastewater Greenhouse Gas Emissions*. Environmental Science & Technology **45**: 5434–40.

Huttunen, J. T., J. Alm, E. Saarijärvi, K. Matti Lappalainen, J. Silvola, and P. J. Martikainen. 2003. *Contribution of winter to the annual CH_4 emission from a eutrophied boreal lake.* Chemosphere 50: 247–50.

Huttunen, J. T., T. Hammar, J. Alm, J. Silvola, and P. J. Martikainen. 2001a. *Greenhouse Gases in Non-Oxygenated and Artificially Oxygenated Eutrophied Lakes during Winter Stratification.* Journal of Environmental Quality J Environ Qual 30: 387–94.

Huttunen, J. T., K. M. Lappalainen, E. Saarijärvi, T. Väisänen, and P. J. Martikainen. 2001b. *A novel sediment gas sampler and a subsurface gas collector used for measurement of the ebullition of methane and carbon dioxide from a eutrophied lake.* The Science of the Total Environment 266: 153–58.

Huttunen, J. T. and others. 2002. *Fluxes of CH_4, CO_2, and N_2O in hydroelectric reservoirs Lokka and Porttipahta in the northern boreal zone in Finland.* Global Biogeochem. Cycles (16), http://dx.doi.org/10.1029/2000GB001316.

Jones, G. J., and B. S. Sherman. 1999. *Hinze Dam Water Quality 1988-1998: A Limnological Overview*. CSIRO Land and Water.

Kelly, C. A., and D. P. Chynoweth. 1981. *The Contributions of Temperature and of the Input of Organic-matter in Controlling Rates of Sediment Methanogenesis. Limnology and Oceanography* 26: 891–97.

Lima, I. B. T., and E. M. M. L. Novo. 1999. *Carbon flows in the Tucuruí reservoir*. p. 78–84. In Rosa, L. P., and M. A. dos Santos [eds.] Dams and Climate Change. COPPE.

McGinnis, D. F., Greinert, J., Artemov, Y., Beaubien, S. E., & Wuest, A. (2006). *Fate of rising methane bubbles in stratified waters: How much methane reaches the atmosphere?* Journal of Geophysical Research-Oceans, 111(C9), C09007.

MacIntyre, S. (1998). *Turbulent Mixing and Resource Supply to Phytoplankton*. In J. Imberger (Ed.), Physical Processes in Lakes and Oceans (pp. 561-590). Washington, DC: American Geophysical Union.

Mengis, M., Gächter, R., & Wehrli, B. 1996. *Nitrous oxide emissions to the atmosphere from an artificially oxygenated lake*. Limnol. Oceanogr., 41(3), 548-553.

Rosa, L. P., S. Dos, Marco Aurélio, J. G. Tundisi, and B. M. Sikar. 1997a. *Measurements of greenhouse gas emissions in Samuel, Tucuruí and Balbina dams - Brazil*. p. 41–55. In Rosa, L. P., AND M. A. dos Santos [eds.] Hydropower Plants and Greenhouse Gas Emissions. COPPE.

Rosa, L. P., B. M. Sikar, E. M. Sikar, and S. Dos, Marco Aurélio. 1997b. *A model for CH_4 and CO_2 emission mean life in reservoir based on data from an Amazonian hydroplant.* p. 102–11. In Rosa, L. P., AND M. A. dos Santos [eds.] Hydropower Plants and Greenhouse Gas Emissions. COPPE.

Schladow, S. G., Lee, M., Hurzeler, B. E., & Kelly, P. B. (2002). *Oxygen transfer across the air-water interface by natural convection in lakes*. Limnology and Oceanography **47**(5):1394-1404.

Schmidt, U., and R. Conrad. (1993). *Hydrogen, carbon monoxide, and methane dynamics in Lake Constance.* Limnol. Oceanogr, 38(6), 1214-1226.

Sherman, B. S., I. T. Webster, G. J. Jones, and R. L. Oliver. 1998. *Transitions between Aulacoseira and Anabaena dominance in a turbid river weir pool*. Limnol. Oceanogr. **43**: 1902–15.

Sherman, B. S., J. Whittington, and R. L. Oliver. 2000. *The impact of artificial destratification on water quality in Chaffey Reservoir*. Arch. Hydrobiol. Spec. Issues Advanc. Limnol. Limnology and Lake Management 2000+ **55**: 15–29.

Sherman, B. S., P. Ford, A. Mitchell, and G. Hancock. 2001. *Greenhouse gas emissions from reservoirs - is Australian hydropower environmentally friendly?* p. 1–10. In Grimston, J. [ed.] Proc. NZSOLD/ANCOLD 2001 Conference on Dams: Dams - Development, Sustainability and Performance. ANCOLD.

Shindell D.T., Faluvegi G, Koch D.M., Schmidt G.A., Unger N, and Bauer S.E. (2009) *Improved attribution of climate forcing to emissions*. Science 326:716–718

Solomon, S., Qin, D., Manning, M., Chen, Z., Marquis, M., Averyt, K. B. *et al*. (2009). *Climate change 2007: the physical science basis: contribution of Working Group I to the Fourth Assessment Report of the Intergovernmental Panel on Climate Change*. Cambridge Univ Press.

Tranvik, L. J., Downing, J. A., Cotner, J. B., Loiselle, S. A., Striegl, R. G., Ballatore, T. J. *et al*. (2009). *Lakes and reservoirs as regulators of carbon cycling and climate*. Limnology and Oceanography, 54(6), 2298-2314.

Vachon, D., Y. Prairie, T., and J. Cole, J. 2010. *The relationship between near-surface turbulence and gas transfer velocity in freshwater systems and its implications for floating chamber measurements of gas exchange*. Limnology and Oceanography **55**: 1723–32.

Tremblay, A., L. Varfalvy, G. Roehm, and M. Garneau. 2005. *Greenhouse Gas Emissions - Fluxes and Processes: Hydroelectric Reservoirs and Natural Environments*. Springer.

WCD, S. 2000. *Dams and Global Climate Change, Thematic Review II.2 prepared as an input to the World Commission on Dams*. World Commission on Dams.